THE REACTIONS OF RUTHENIUM (II) POLYPYRIDYL COMPLEXES

By

Sipeng Zheng

Submitted in fulfilment of the requirements for the degree of Magister Scientiae at the Nelson Mandela Metropolitan University

December 2009

Supervisor: **Prof. H. E. Rohwer**

Acknowledgements

I am deeply grateful to my supervisor, Prof. H. E. Rohwer for his encouragement, guidance and thoughtful discussions towards my work, and patience with my mistakes.

I am immensely grateful to Dr. Eric Hosten, for his instrumental and general expertise and whose dedication to this project has gone above and beyond the call of duty. Thank you for your guidance and assistance, for sacrificing your time, your diligent editing and your infinite patience.

I offer my heartiest gratitude to my parents for their love and everything they have done for me. They always share within my interests and extend help to my problems. Without them this uphill task and my stay in South Africa both were impossible.

I would hereby like to express my sincere thanks to:

Anglo Platinum Research Centre, the Nelson Mandela Metropolitan University and the Inorganic Chemistry Department for financial assistance.

My fellow colleagues in the Inorganic Department for their support and kindness.

Henk Schalekamp, Vida Maqoko, and Phindele Gaika for all their behind-the-scenes support.

Junli for all her love, infinite patience and endless support.

Table of Contents

List of Figures and Diagrams

Chapter 4

Chapter 5

List of Tables

Chapter 5

Abbreviations

AN	acetonitrile
AzIII	arsenazo III
bpy	bipyridine
CV	cyclic voltammetry
HCl	hydrochloric acid
HP H_2O	high purity distilled water
H_2SO_4	sulphuric acid
ICP-MS	inductively coupled plasma mass spectrometry
M	mol per litre
MO	molecular orbital
mL	mililitre
MLCT	metal-to-ligand charge transfer
NMR	nuclear magnetic resonance
PGMs	the platinum group metals
$Ru(bpy)_3^{2+}$	tris(2,2'-bipyridyl) ruthenium (II)
TBAP	tetrabutylammonium perchlorate
tert-BuOK	potassium *tert*-butoxide
TsOH	*p*-toluenesulfonic acid
UV-Vis	ultraviolet – visible
v/v	volume per volume

Summary

Ruthenium (II) polypyridine complexes in general have been extensively studied because of their unique redox and photochemical properties. A typical example of such complexes is tris(2,2'-bipyridyl) ruthenium (II). In this study, this complex was synthesized and then characterized using electronic spectroscopy and cyclic voltammetry. It was also shown that the ruthenium concentration could be accurately determined using ICP-MS. It was found that the complex is very stable in various chemical environments.

It was observed from spectrophotometric investigations that persulphate and lead dioxide easily oxidize $Ru(bpy)_3^{2+}$ to $Ru(bpy)_3^{3+}$ in the presence of heat and H_2SO_4, respectively. It was also observed that the oxidation between $Ru(bpy)_3^{2+}$ and cerium (IV) occurred at approximately 3:2 [Ce(IV)]/[Ru(II)] mole ratio. The resultant $Ru(bpy)_3^{3+}$ solution was unstable in the presence of light and recovery of $Ru(bpy)_3^{2+}$ occurred gradually. The regeneration of $Ru(bpy)_3^{2+}$ from $Ru(bpy)_3^{3+}$ was found to be a multistep process, which appears to involve the formation of an intermediate species. The following reaction model was found to best explain the kinetic data obtained:

$$Ru(bpy)_3^{2+} + Ce(IV) \rightarrow Ru(bpy)_3^{3+}$$

$$Ru(bpy)_3^{3+} \rightarrow Ru(bpy)_3^{2+}$$

$$Ru(bpy)_3^{3+} \rightarrow Ru^* \text{ intermediate}$$

$$Ru^* \text{ intermediate} \rightarrow Ru(bpy)_3^{2+}$$

Theoretical rate constants were also calculated for the same process under the experimental conditions. The comparison between the experimental and theoretical results gave good agreement. In addition, the factors that influence the rate of the regeneration of $Ru(bpy)_3^{2+}$ from $Ru(bpy)_3^{3+}$ were also discussed.

Key words: Oxidation, redox potential, regeneration, ruthenium (III), ruthenium (II) polypyridine complexes, spectrophotometric techniques

Chapter 1

Introduction

1.1 Motivation for this study

The platinum-group metals (PGMs) constitute a family of six chemically related elements which can be divided into the denser platinum, iridium and osmium, and the lighter palladium, rhodium and ruthenium. Amongst the characteristics which have been the reasons for their investigations at the NMMU, are their catalytic activities, resistance to corrosion, chemical inertness and high melting points. These render them most suitable for a number of specialist applications [1]. In this postgraduate project, the focus lies on the element ruthenium which has rather unique chemical characteristics. This thesis presents the photochemical and kinetic properties, and general synthesis of ruthenium (II) complexes based on 2,2'-bipyridyl ligand.

1.2 Aims and objectives

The primary aim of this study is to investigate selected reactions and associated kinetics of ruthenium complexes which have recently been noticed. This pertains mainly to the lower oxidation state species of ruthenium. The ruthenium (II) polypyridyl complexes fall into this category and these have low lying electronically excited states which make them amenable for possible uses for a number of important applications such as photosensitizers [2(i)].

1.3 Introduction to ruthenium

1.3.1 Overview of ruthenium [3]

Ruthenium is a greyish-white metallic element that resembles platinum in lustre and colour, but is much harder (Mohs's scale 6.5) and more brittle. It has a very high melting point (2334 ^{o}C), and only osmium is more infusible. Because of its high melting point, ruthenium is not easy to process, and because of its brittleness, it is extremely difficult to roll or draw into wire, even at white heat. Ruthenium has a high resistance to corrosion and chemical attack by acids (including *aqua regia*) and other metals. However, the metal can be easily dissolved in solutions of hypochlorites.

The name of ruthenium was selected in honour of the old Latin name for the former Ruthenia district (Little Russia, now Ukraine) of greater Russia. Ruthenium was observed by G. E. Osann in 1828, when he made a premature announcement of the discovery of the metal in platinum ores from the Ural Mountains. It was recognized as a separate element by the German Estonian, Carl Ernst Claus (also known as Karl Karlovich Claus), at the university of Kazan in 1845, who retained the name given by Osann. The metal was also isolated by the Polish chemist J. Sniadecki, who called it Vestium, but did nothing further with it.

Ruthenium is popularly known as the 'Cinderella' of the Platinum Group Metals (PGMs), not only because it is the cheapest, but probably also since its limited demand fails to satisfy its level of supply. There are three main industrial uses of ruthenium consumption worldwide: electrical and electronic uses. For example, ruthenium dioxide is used in resistor pastes for printed resistive circuits and for chip resistors used in hybrid integrated circuits; electrochemical and chemical uses. For example, a ruthenium compound is essential for the active component of anodes used in the electrochemical production of chlorine; and lastly, catalytic and pharmaceutical uses. Ruthenium is essential for the manufacture of a wide variety of special and pharmaceutical chemicals.

1.3.2 Occurrence

Ruthenium is as rare as osmium with its abundance in the earth's crust probably 0.0004 ppm [4]. The main sources of the element are the same as for osmium-laurite (essentially ruthenium disulphide with some osmium disulphide), osmiridium and

platinum concentrates. The proportion of ruthenium in the minerals is highly variable [4].

1.3.3 The coordination chemistry of ruthenium

1.3.3.1 Background

The density of ruthenium at 20 ^{o}C is 12.45 g/cm^3 [3]. Apart from osmium, ruthenium is the only metal that has a closely-packed hexagonal crystal structure, with the following lattice constants: a = 2.7056 Å and c/a = 1.5825 Å [3]. Its outer electron configuration is $4d^7 5s^1$ and its valence states are 2, 3, 4, and 8, like those of osmium [3]. Ruthenium has seven stable isotopes (percentage abundance shown in parentheses): 96 (5.7 percent); 98 (2.2 percent); 99 (12.8 percent); 100 (12.7 percent); 101 (17.0 percent); 102 (31.3 percent) and 104 (18.3 percent) [3].

1.3.3.2 The common oxidation states of Ruthenium [5]

For ruthenium, the principal lower oxidation states are (0), (II), and (III).

The Ru (0) State, d^8.

The chemistry in this state is primarily one of the metal carbonyls; mononuclear and polynuclear carbonyls are known for the element. Both types undergo substitution reactions, and in the polynuclear species the clusters are often retained. They also undergo protonation reactions, and a variety of hydrido species are known.

The Ru (II) State, d^6.

All Ru(II) complexes are octahedral and diamagnetic for the t_{2g}^6 configuration. An enormous number of Ru complexes with CO, PR_3, and similar π-acid ligands are known. For other ligands, the main chemistry is that of chloro, ammonia, and other amine ligands. The aqua ion $[Ru(H_2O)_6]^{2+}$ has been prepared, but it is readily oxidized to $[Ru(H_2O)_6]^{3+}$.

The Ru (III) State, d^5.

There is an extensive chemistry with both π-acid and σ-donor ligands. All the complexes are of low-spin type with one unpaired electron and are octahedral.

The Ru (IV) State, d^4.

In this state most complexes are neutral or anionic. They all have octahedral or distorted octahedral structures, thus should have t_{2g}^4 electron configuration.

Ruthenium in high oxidation states.

There are a wide range of oxo-compounds of ruthenium in oxidation (VI), (VII), and (VIII). Ruthenium tetroxides and oxo anions provide some of the more unusual and useful features of the chemistry. The major compounds or ions are shown in Table 1.1.

Table 1.1: Some oxo compounds and ions of ruthenium and the comparison with osmium [5].

VIII	VII	VI
RuO_4	RuO_4^-	RuO_4^{2-}
		$RuO_2Cl_4^{2-}$
OsO_4		
OsO_3N^-		$[OsO_2X_4]^{2-\ a}$, $[OsO_2en_2]^{2+}$
$OsO_4X_2^{2-\ a}$	$OsOF_5$	$[OsO_2(OH)_2X_2]^{2-\ b}$

[a] X = F or OH.
[b] X = Cl, CN, etc.

Ruthium tetroxide RuO_4.

Since ruthenium is recovered and separated from the rest of the PGMs by utilizing the high volatility of its tetroxide, it is important to understand the chemistry of this oxo compound. The ruthenium tetroxide is highly volatile and toxic. It can be obtained when acidic ruthenium solutions are treated with oxidizing agents such as MnO_4^-, AuO_4^-, BrO_3^-, or Cl_2; the oxide can be distilled from the solutions or swept out by a gas stream. The compound has a tetrahedral structure. It is extremely soluble in CCl_4 and can be extracted from aqueous solutions. RuO_4 is quite soluble in dilute sulphuric acid giving golden-yellow solutions. It is also soluble in alkali hydroxide solutions; RuO_4 is reduced by hydroxide first to perruthenate (VII), which in turn is further reduced to ruthenate (VI), the reaction equations [5] are shown in page 5.

$$4RuO_4 + 4OH^- \longrightarrow 4RuO_4^- + 2H_2O + O_2$$

$$4RuO_4^- + 4OH^- \longrightarrow 4RuO_4^{2-} + 2H_2O + O_2$$

The ruthenium tetroxide is a powerful oxidizing agent, and it is slowly decomposed by light.

1.3.3.3 Coordination numbers [5]

Table 1.2 illustrates the oxidation states and stereochemistry of ruthenium. The majority of the ruthenium complexes exhibit octahedral geometries. In addition to certain complexes that exhibit geometries ranging from tetrahedral (displayed by higher oxidation state ruthenium ions) to trigonal bipyramidal (displayed by lower oxidation state ruthenium ions) geometries.

Table 1.2: Oxidation states and stereochemistry of ruthenium [5].

Oxidation state	Coordination number	Geometry	Examples
Ru^{-II}	4	Tetrahedral	$[Ru(diphos)_2]^{2-}$
Ru^{0}	5	*Tbp*	$Ru(CO)_5$
Ru^{II}	5	*Tbp*	$RuHCl(PPH_3)_3$
	6	Octahedral	$[Ru(bpy)_3]^{2+}$
Ru^{III}	6	Octahedral	$[RuCl_5H_2O]^{2-}$
Ru^{IV}	6	Octahedral	K_2RuCl_6
Ru^{V}	6	Octahedral	$KRuF_6$
Ru^{VI}	4	Tetrahedral	RuO_4^{2-}
	6	Octahedral	RuF_6
Ru^{VII}	4	Tetrahedral	RuO_4^-
Ru^{VIII}	4	Tetrahedral	RuO_4

1.4 Ruthenium complexes with nitrogen donor atoms

1.4.1 General description

These complexes are largely formed by the ruthenium in the (II) and (III) oxidation states, which include ammonia complexes, aromatic amine complexes and nitrosyl complexes according to their ligand types. However, in this study the focus will be on ruthenium (II) with aromatic amine ligands since they have π systems, which have

distinctly different features of interest from the ammine complexes. The most important species are those containing 2,2'-bipyridyl (bpy), which form tris-chelates [5].

1.4.2 Polypyridine as a ligand

Polypyridine complexes are compounds in which a polypyridine ligand, such as 2,2'-bipyridine coordinates to the metal ion. Polypyridine compounds are multidentate ligands which have characteristic properties, such as photosensitization. The complexes are very stable to light, electricity, and heat because the bonds between the central metal ion and polypyridine ligands are usually very strong. The polypyridine itself is generally very stable [6(i)].

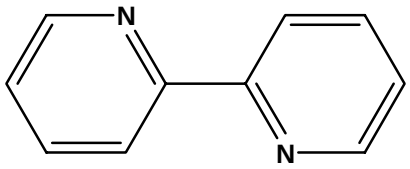

bipyridine

All nitrogen heterocyclics with a delocalized π or aromatic ring system are capable of complexing with a whole variety of metal ions [2(ii)]. The bench-mark systems for polypyridines are complexes based on Ru(II), for example, ruthenium (II) trisbipyridyl complexes.

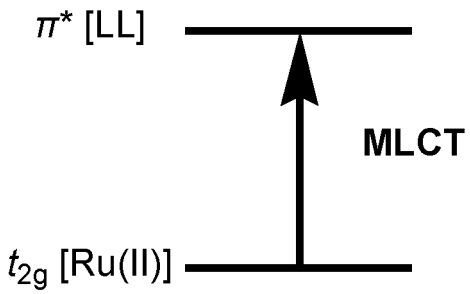

Figure 1.1: Illustration of metal-to-ligand charge transfer (MLCT) in polypyridine complexes of Ru(II). LL refers to bidentate polypyridine ligands [2(ii)].

Figure 1.1 above illustrates that in polypyridine complexes of Ru(II), they exhibit a strong absorption band in the visible light region, which is called metal-to-ligand charge transfer (MLCT) [2(ii)]. The MLCT transition corresponds to promotion of an electron from a molecular orbital (MO) that is largely Ru (II) based (filled t_{2g} level) to a MO that is largely ligand based (empty π* orbital of the ligand).

1.5 Introduction to tris(2,2'-bipyridyl) ruthenium (II)

1.5.1 General description

Ruthenium (II) trisbipyridyl complexes have been thoroughly studied because of a unique combination of chemical stability, redox potentials, light absorption, luminescence emission, excited-state energy, and excited-state lifetime. Studies concerning this and other ruthenium (II) polypyridine complexes have made an important contribution to the growth of several branches of chemistry, including photochemistry, photophysics, photocatalysts, electrochemistry, chemiluminescence, and to a better understanding of fundamental chemical processes [7]. The use of these complexes has resulted in wide applications in different areas, from solar energy related research to molecular wires, sensors and switches, machines, and also as therapeutic agents [8].

1.5.2 Photophysical properties

This section provides an overview on the photophysical properties of the ruthenium (II) trisbipyridyl complexes. The $Ru(bpy)_3^{2+}$ complex has octahedral geometry of D_3 symmetry. The absorption spectrum in the visible region is dominated by an intense metal-to-ligand charge transfer (MLCT) band at 450 nm, caused by the transition from a dπ metal orbital to a ligand based orbital as shown in Figure 1.1. The singlet MLCT excited state rapidly decays via intersystem crossing (isc) to a lower triplet MLCT excited state, which has a relatively long life time for the excited state of $Ru(bpy)_3^{2+}$ to efficiently transfer its energy to another molecule (a quencher), either by energy transfer or electron transfer. In the absence of a quencher, the excited state undergoes deactivation through both nonradiative and radiative decay pathways [8]. The process is illustrated in Figure 1.2 (page 8). The quenching reactions and associated quenching kinetics are discussed in details in Chapter 3 (see Section 3.5.2).

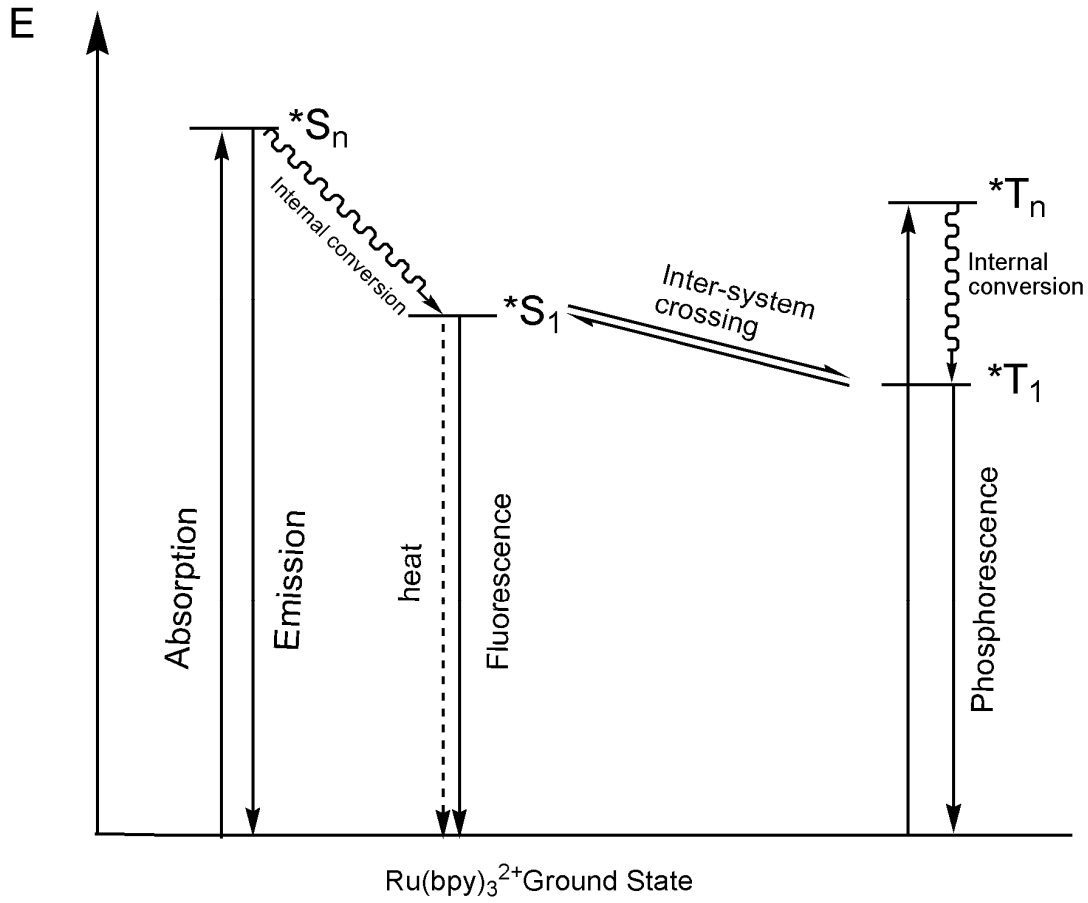

Figure 1.2: The simplified schematic presentation of relaxation pathways of photoexcited $Ru(bpy)_3^{2+}$. Symbol $*S_n$ represents the upper singlet excited state, while $*S_1$ represents the lowest excited state. The excited singlet state can decay either by spin allowed radiative transition fluorescence or in competitive pathways such as non-radiative decay to the ground state or inter-system crossing to the triplet state ($*T_1$).

1.6 Specific objectives

This study is the first ruthenium (II) trisbipyridyl complexes investigation undertaken at the Nelson Mandela Metropolitan University and can, therefore, be considered to be the preliminary study in order to gain access to and be able to appreciate the current chemical models in the literature. Once confidence in the existing or subsequently modified models is justified, possible improvements and suggestions will follow to benefit possible future applications in this field.

The specific objectives of this study are:

1. The characterisation of ruthenium (II) polypyridyl complexes

The ruthenium (II) polypyridyl complexes were characterized by various techniques including UV-Vis spectroscopy and cyclic voltammetry.

2. The reactions and photochemical properties of tris(2,2’-bipyridyl) ruthenium (II)

The reactions of tris(2,2’-bipyridyl) ruthenium (II) with different oxidizing agents were investigated, the factors that affected the rates of reactions were discussed for gaining in depth understanding of photochemical properties of tris(2,2’-bipyridyl) ruthenium (II).

3. The kinetic characteristics associated with the abovementioned changes are of interest for applications in the photochemical domain and were investigated as such with the aid of computational models.

Chapter 2

Experimental

2.1 Apparatus

2.1.1 Ultraviolet and visible spectra

UV-Visible absorption is a powerful tool to monitor the reaction kinetics. All the spectra used in this study were recorded either on a Perkin-Elmer Lambda 12 UV/VIS spectrophotometer or a Shimadzu UV-3100 UV-VIS-NIR spectrometer. Quartz cuvettes with a 1 cm path length were used throughout. For the Perkin-Elmer spectrophotometer, the UV WinLab Version 1.22 software package was used for instrument control. Scan speed of 240 nm/min was employed with a slit width of 1 nm. For the Shimadzu spectrometer, a medium or slow scan speed was used with a slit width of 2 nm. The spectra were recorded in the range of 200 nm to 700 nm. High purity distilled water was used as the reference solution unless otherwise specified.

For the kinetic studies which require precise temperature control, a Grant KD100 circulating thermostat controller was connected to the Perkin-Elmer spectrophotometer cuvette holder. The controller was mounted onto a Grant W6 water bath equipped with a Grant CZ1 cooling system. The setup was used to maintain various required temperatures of the spectrophotometer cuvette holder. A Samsung SH 122KG external air-conditioning unit was employed in order to maintain a constant room temperature. Also a Gibson dehumidifier 1600 was used to try to minimize water condensation on the cuvettes at lower temperatures by reducing the room humidity.

2.1.2 Photometric titrations

The absorbance measurements for photometric titrations were recorded with Metrohm 662 photometer. This photometer consists of a probe connected to the main unit with two light guides. The first light guide passes the light from a source in the main unit to the probe. At the probe the light passes through the solution and is reflected back to the second light guide and detector. Absorbance is measured by first dipping the probe into the solvent, zero the meter and then immerse the probe into the solution to be measured. The light path length through the solution is 1 cm. The photometer can also be connected via RS232 analogue connector to a titroprocessor. For titrations where spectra were recorded, a computer program namely PhotoMet titrator (Version 2.3) special designed by Dr. E. C. Hosten, was employed with the titroprocessor. This enables photometric titrations to be performed automatically, making it possible to record titrations with a large number of points.

2.1.3 Kinetic data recording using photometer

The kinetic data associated with the photosensitive reduction of the reagents was recorded with the similar setup used for photometric titrations as mentioned above. An OSRAM 120 W drying lamp was placed 55 cm away from the reaction vessel, the light intensity was measured at 6720 lux/m^2 (room light and lamp light) and 174 lux/m^2 (room light only) using a TopTronic T630 Lightmeter. In order to maintain a constant reaction temperature for kinetic studies, a Julabo heating immersion circulator equipped with Julabo 5A water bath was employed. The setup is illustrated in Figure 2.1 (page 12).

Figure 2.1: Picture illustrates the experimental system employed to record kinetic data during a photosensitive reduction.

2.1.4 Potentiometric titrations

Potentiometric titrations can be performed simultaneously with the photometric titrations by using the PhotoMet titrator (Version 2.3) computer program. All the potentiometric titrations were performed and recorded using the same setup as in photometric titrations. A Metrohm 6.0402.100 combined platinum-wire electrode was used. Potentiometric standardization titrations were performed with a Metrohm 716 DMS Titrino with Metrohm 728 stirrer.

2.1.5 pH measurements

pH measurements were performed with a Metrohm 691 pH meter using a Metrohm 6.0232.100 combined pH glass electrode. Calibration was performed with pH 4.00 (Merck) and pH 7.00 (Merck) buffer solutions.

2.1.6 Fluorescence spectra

Fluorescence spectra were recorded in a 1-cm path length quartz cell on a Shimadzu RF-150X spectrofluorometer.

2.1.7 Cyclic voltammetry

Electrochemical measurements were carried out using a cyclic voltammetric technique. The measurements were recorded with a BAS Epsilon system and C3 cell stand. All measurements were carried out at room temperature with a conventional three-electrode configuration consisting of platinum working (1.6 mm in diameter) and auxiliary electrodes and a non-aqueous $Ag/AgNO_3$ reference electrode. Ferrocene was added as an internal standard to the electrochemical cell. The supporting electrolyte was tetrabutylammonium perchlorate (TBAP) in acetonitrile.

2.1.7.1 Silver/Silver ion (Non-aqueous) reference electrodes

The salt solution required for a reference electrode must be separated from the analyte solution by a frit that allows ionic conduction between the two solutions, but does not allow appreciable contamination of the analyte solution by the reference electrode solution. Typically, the solutions separated by the frit do not contain the same ions and the different rates of diffusion across the frit by the different ions gives rise to a potential across the frit – the junction potential [9].

In this study, to prevent junction potential, a suitable non-aqueous reference electrode was used. The Ag/Ag^+ reference electrode was made by placing a clean silver wire into an electrolyte containing silver ion. The electrolyte in the reference compartment was the same as the solution electrolyte. The salt used in this study was tetrabutylammonium perchlorate (TBAP) at approximately 0.1 M concentration. Polar solvent used was acetonitrile (A.N). Silver ion was formed by dissolving 0.01 M $AgNO_3$ in the chosen electrolyte. The non-aqueous reference electrode consists of 0.01 M $AgNO_3$, 0.1 M TBAP and A.N. The solution electrolyte consists of 0.1 M TBAP and A.N and appropriate concentration of analyte. A typical cyclic voltammogram recorded is shown in Figure 2.2 (page 14).

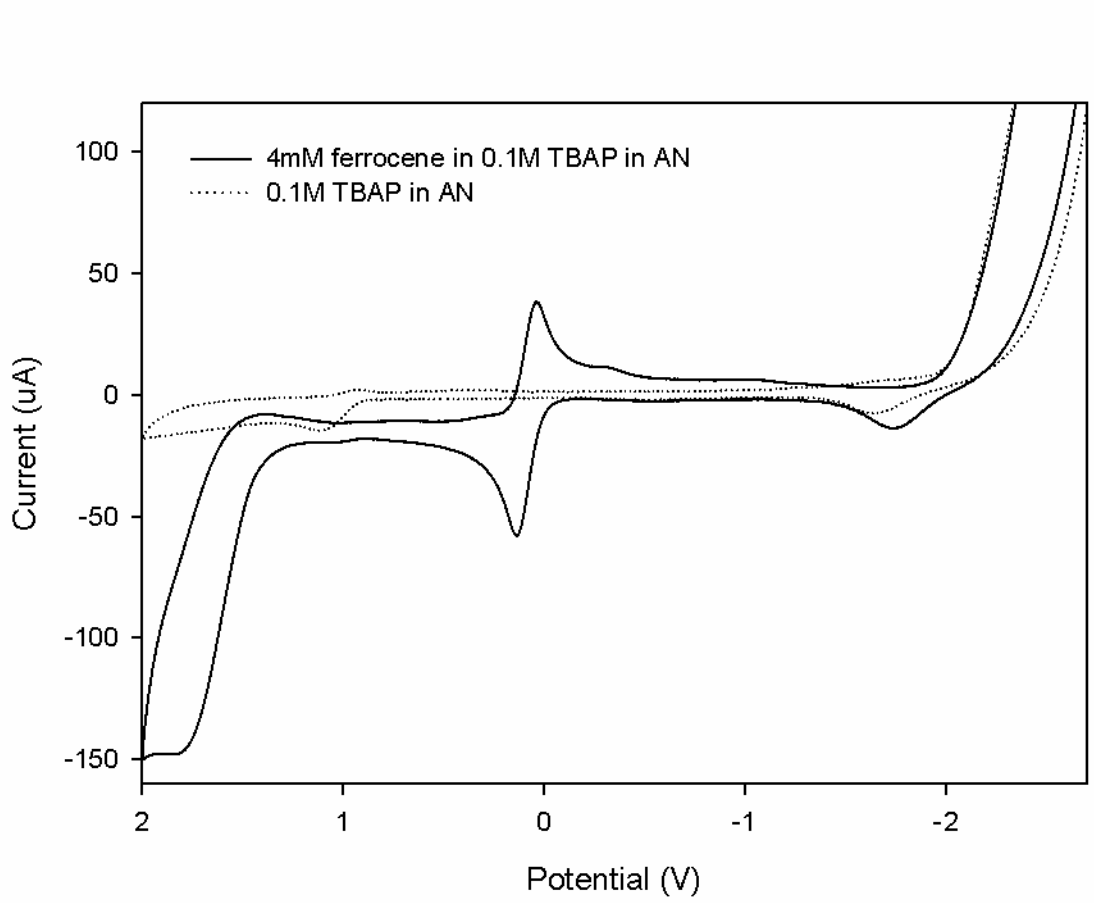

Figure 2.2: The cyclic voltammogram of 4 mM ferrocene in 0.1 M TBAP in acetonitrile. Scan initiated at -2.7 V versus non-aqueous Ag/$AgNO_3$ reference electrode in positive direction at 100 mV/s. The ferrocene exhibits a reversible metal to ligand charge transfer oxidation, which is suitable for an internal standard.

2.1.7.2 Internal standard

The potential of the non-aqueous reference electrode depends on the solvent, the electrolyte, and the concentrations of silver nitrate and the salt. Since the potential of a non-aqueous reference electrode can vary among different electrodes, redox potentials measured using such a reference electrode was quoted relative to an internal reference compound, Ferrocene. All the redox potentials in this study are reported relative to the ferrocenium / ferrocene couple, $E_{1/2}$ = 0 V, ΔE = 52 mV for the $Fc^{+/0}$ redox couple.

2.1.8 Inductively-Coupled Plasma Mass Spectrometer (ICP-MS)

Ruthenium concentration was determined with a Perkin-Elmer *Sciex Elan 6100* ICP-MS spectrometer with version 2.3.2 software. The general ICP-MS operating conditions used are listed in Table 2.1. A Perkin-Elmer AS-90 auto sampler was

used for automated sampling. The ICP-MS room temperature was regulated at 25.0±0.5 ^{o}C using an LG (SK Series) air conditioning unit.

Table 2.1: General ICP-MS operating conditions.

Nebuliser gas flow (L.min^{-1})	ICP RF-Power (W)	Nebulizer Type	Detector Mode	Gas Type
0.97	1400	cross flow	analog	argon

Standards in the concentration range from 5 µg/L to 1000 µg/L were prepared with Spectrascan certified Multi-element PGM standard No. 8313. All standards were prepared in 1 % HCl (v/v). All the samples for analysis were diluted to fall into this range and the matrix was kept the same in all cases.

2.1.9 Elemental analysis

The elemental analysis for carbon, hydrogen, and nitrogen of the reagent was carried out by the Department of Chemistry at the University of the Western Cape in Cape Town.

2.1.10 NMR spectroscopy

The ^{1}H NMR spectra were recorded at 300K using a Bruker 300MHz spectrometer. The peak positions are relative to SiMe4 as reference. Deuterated DMSO was used as the reference solvent.

2.1.11 Preparation of solutions

All the aqueous stock solutions were prepared using ultrahigh purity water unless notified, while the non-aqueous stock solutions were prepared using UV grade acetonitrile. In order to obtain the ultrahigh purity water, a Millipore Simplicity water purification system (18.2 MΩ.cm) was employed.

2.1.12 Computer hardware and software used

Table 2.2: Computer system used for kinetic calculations.

CPU	Inter ® Pentium ® Dual Core E5200 Wolfdale 2.5 GHz
Motherboard	MSI Intel G31M3-F
Memory module	2 GB DDR2 240-pin DIMM
Processing platform	64 bit

All apparatus utilized their own software packages as detailed above. The Windows XP compatible software used during this study include:

- Microsoft Office Word 2007
- Microsoft Office Excel 2007
- SigmaPlot 11
- ChemDraw Version 8
- SimpleGraph (Author: Dr E C Hosten)
- SPC-V-MR (Author: Dr E C Hosten) [10]
- DynaFit 3 (Auther: Dr P. Kuzmic) [11]

The SPC-V-MR program was written by Dr E. Hosten using Borland Turbo Pascal V 6.0 [10], which was used to simulate mole ratio titrations where the mole ratios between various reagents change. The program uses an iterative Gauss-Newton algorithm to calculate the free reagent (unreacted) concentrations. Together with the free reagent concentrations, the estimated formation constants and the molar extinction values, the program can then calculate the total absorbance. By comparing the calculated absorbance with the experimental absorbance, the program uses another iterative Gauss-Newton algorithm to calculate better estimates for reagent concentrations, formation constants and molar extinction values. These iterative cycles then continue until the changes to all the constants become statistically insignificant. During all the calculations the change in volume during the titrations due to the addition of titrant, is taken into account. This program simulates the following type of equilibria:

$$aA + bB + cC \xleftrightarrow{\beta} A_aB_bC_c$$

$$\beta = \frac{[A_aB_bC_c]}{[A]^a[B]^b[C]^c}$$

This program was used to simulate the redox reactions between $Ru(bpy)_3^{2+}$ and Ce(IV). Although the type of equilibrium modeled is not a redox equilibrium, it does enable one to test various models to determine the stoichiometry at the photometric endpoints.

The program DynaFit 3 [11] written by Dr. P. Kuzmic was employed for the simulation of experimental kinetic data of the oxidation-light reduction reaction between

$Ru(bpy)_3^{2+}$ and Ce(IV). The results calculated with the program are discussed in more details later in the relevant chapters.

2.1.13 Difference between a photometer and a spectrophotometer

The absorbance measurements were recorded with both the photometer and the spectrophotometer. Although the two instruments share the same working principle, each has their own advantages and disadvantages. With photometer, the absorbance readings can be taken without disturbing the reaction solution and other measurements can be recorded simultaneously, e.g. pH measurements and potential readings. Furthermore, for photochemical studies, an adjustable light source was also applied as shown in Figure 2.1. The main disadvantage of the photometer is that the absorbance can only be measured at a single wavelength during a titration or a kinetic run, whereas with the spectrophotometer, continuous kinetic associated reactions can be monitored throughout a wide range of selected wavelengths. A discrepancy between the absorbance recorded by the photometer and spectrophotometer was found (page 18).

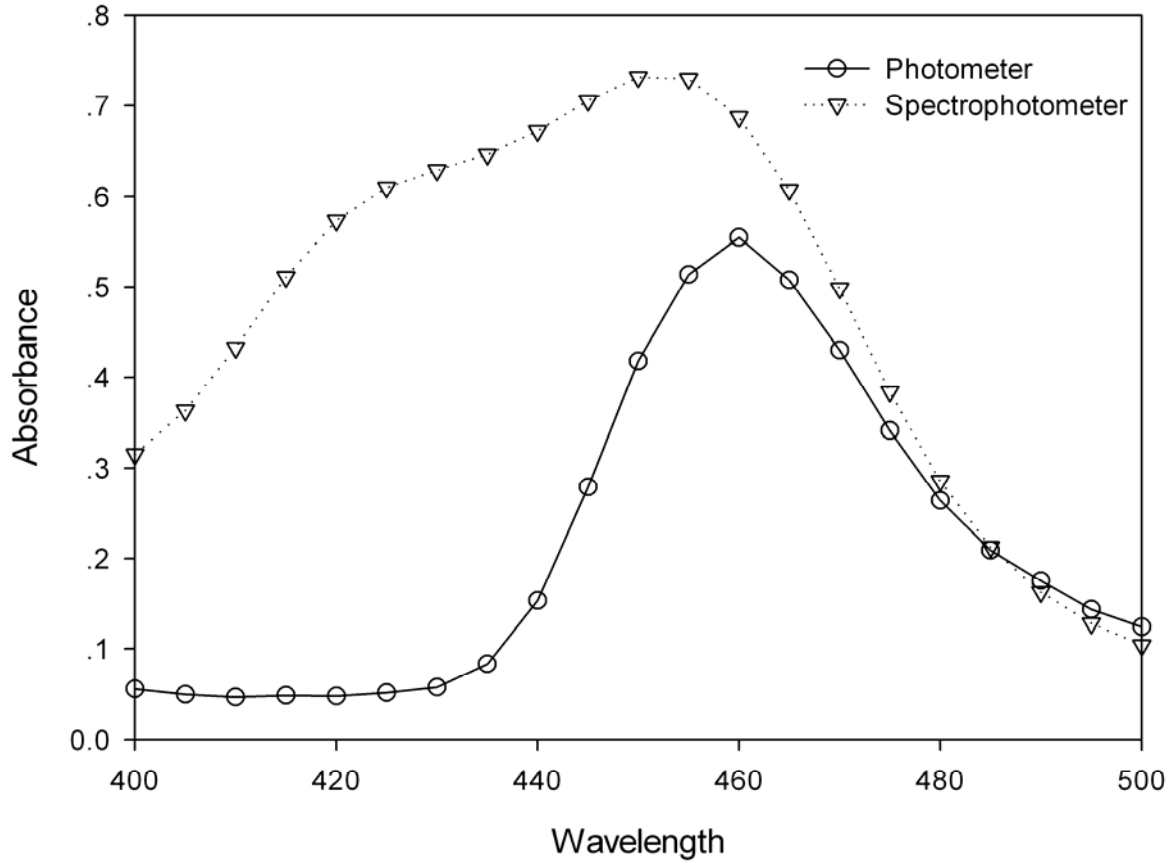

Figure 2.3: Differences between spectra of $Ru(bpy)_3^{2+}$ recorded with the spectrophotometer and photometer. $[Ru(bpy)_3^{2+}] = 5.540 \times 10^{-5}$ M.

Figure 2.3 shows the differences between spectra of $Ru(bpy)_3^{2+}$ recorded with the spectrophotometer and photometer. The spectrophotometer absorbance readings are much higher at lower wavelength compared to that the photometer. The difference in absorbance readings becomes negligible at higher wavelength region, namely 500 nm. In addition, the photometer absorbance reading is lower at the peak, and the peak is shifted about 10 nm towards a lower wavelength. This shift is most likely due to the photometer using a graduated filter for wavelength selection. Another three samples were prepared to confirm the findings. The results were recorded with both spectrophotometer and photometer.

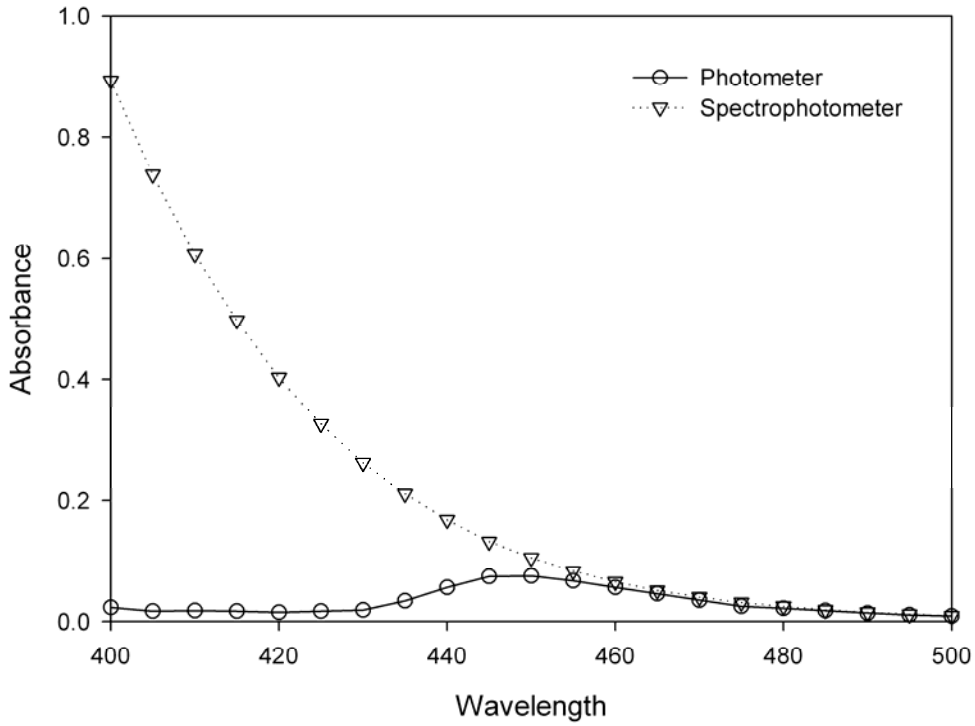

Figure 2.4: Differences between spectra of Ce(IV) solution recorded with the spectrophotometer and photometer. [Ce(IV)] = 1.250 x 10^{-3} M.

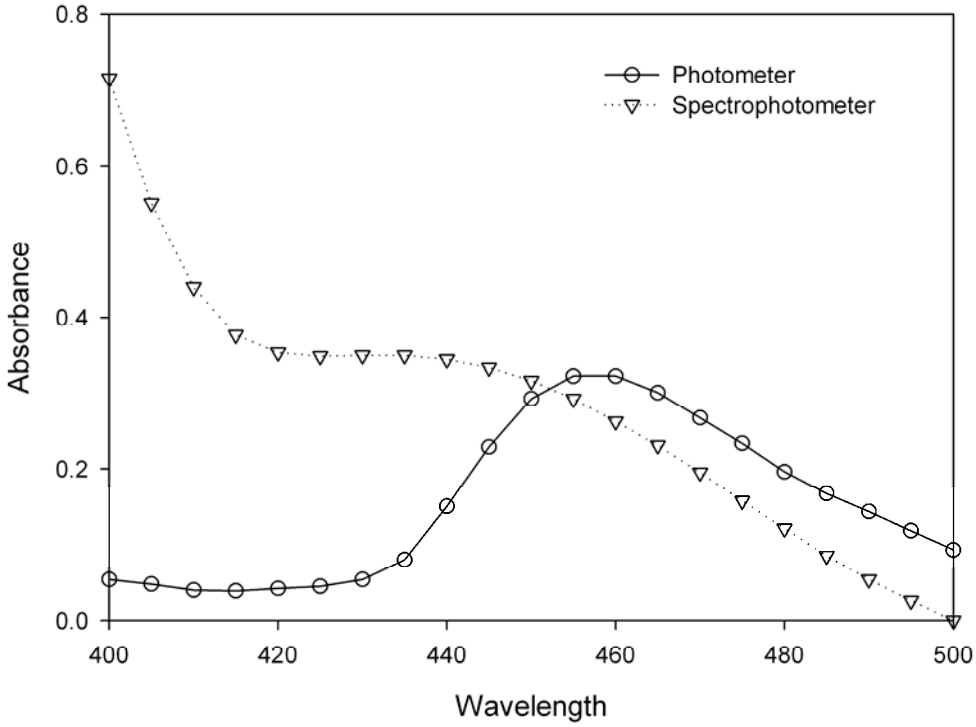

Figure 2.5: Differences between spectra of dichromate solution recorded with the spectrophotometer and photometer. [$Cr_2O_7^{2-}$] = 1.000 x 10^{-3} M.

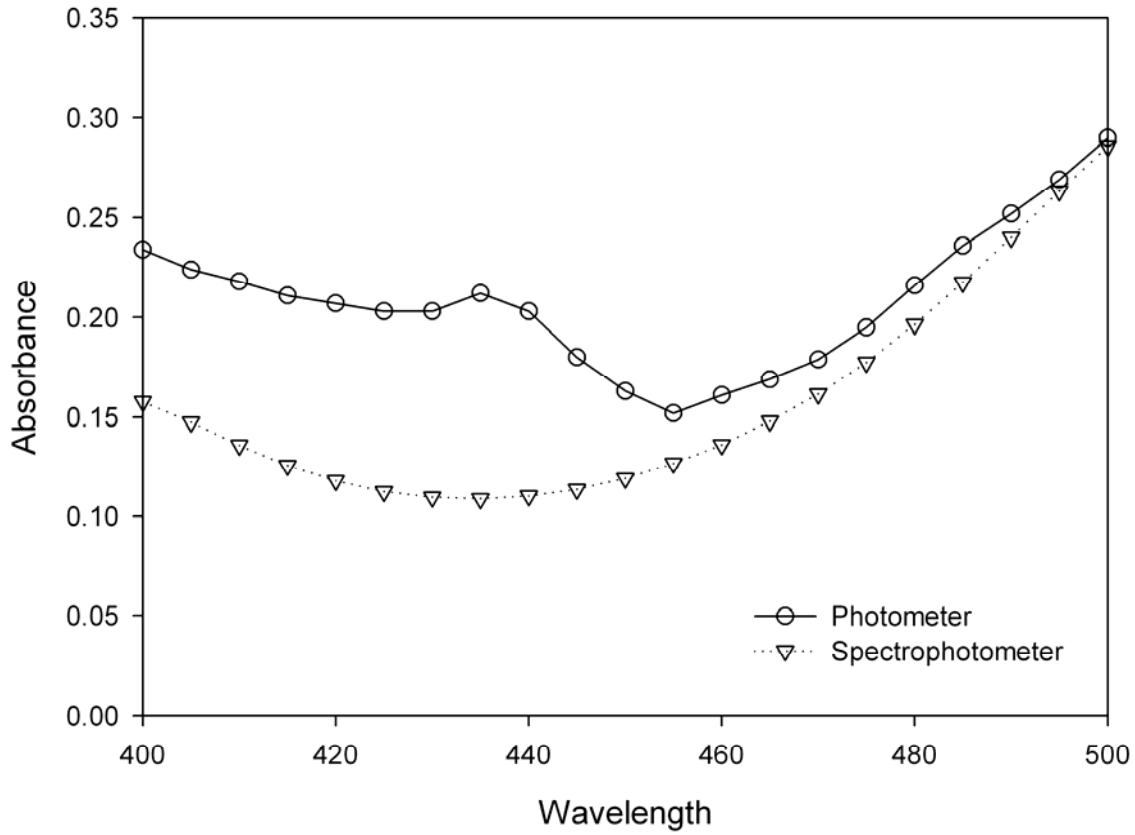

Figure 2.6: Differences between spectra of arsenazo III solution recorded with the spectrophotometer and photometer. [AzIII] = 1.00 x 10^{-5} M.

Figure 2.6 shows the differences between spectra of arsenazo III solution recorded with the spectrophotometer and photometer. The photometer absorbance readings are higher than those spectrophotometer absorbance readings at lower wavelength, and as shown before the differences in absorbance readings become negligible at higher wavelength region.

In summary, Figures 2.3, 2.4 and 2.5 show the spectrophotometer absorbance readings are much higher at lower wavelength compared to that the photometer absorbance readings. Interestingly, all these three samples are in yellowish colour, whereas the arsenazo III solution is purple in colour. Therefore the discrepancy between the spectra recorded by the photometer and spectrophotometer is likely due to the fact that the photometer uses a graduated filter that might have faded with time, whereas the spectrophotometer uses a holographic grating in the monochromator.

For this matter, the photometer absorbance readings could not be used for the kinetic simulations, and more detailed discussions on the differences between the spectrophotometer and photometer are presented in Chapter 5.

Table 2.3: The calculated molar absorption coefficients of $Ru(bpy)_3^{2+}$, Ce(IV), dichromate and arsenazo III solutions recorded from different instruments at different wavelengths.

Solution	Molar absorption coefficient ε		Molar absorption coefficient ε	
	450 nm Photo.	450 nm Spectro.	425 nm Photo.	425 nm Spectro.
$Ru(bpy)_3^{2+}$	7524	13170	918	10986
Ce(IV)	60	84	13.6	260.8
Dichromate $Cr_2O_7^{2-}$	293	317	45	349
Arsenazo III	16300	11920	20300	11240

2.2 Reagents used

Ultra pure distilled water was used in all aqueous solution preparations. For non-aqueous solution preparations, UV grade acetonitrile was used unless specified.

Table 2.4: Reagents used in this study.

Reagent	Chemical formula	Percentage purity	Supplier
Ruthenium (III) chloride hydrated	$RuCl_3.xH_2O$	41.12	Alfa Aesar
2,2'-bipyridine	$C_{10}H_8N_2$ Mr = 156.19 $g.mol^{-1}$	99.5	Riedel-de Haën
Di-sodium hydrogen phosphate	Na_2HPO_4 Mr = 141.96 $g.mol^{-1}$	-	Merck

Phenothiazine	$C_{12}H_9NS$ Mr = 199.28 g.mol^{-1}	98	Aldrich
Ammonium ceric sulphate	$(NH_4)_4Ce(SO_4)_4.2H_2O$ Mr = 632.55 g.mol^{-1}	94	Merck
Di-Ammonium iron (II) sulphate 6-hydrate	$(NH_4)_2SO_4.FeSO_4.6H_2O$ Mr = 392.13 g.mol^{-1}	99.0	BDH
Potassium dichromate	$K_2Cr_2O_7$ Mr = 294.22 g.mol^{-1}	99.5	Merck
Ruthenium trichloride trihydrate	$RuCl_3.3H_2O$ Mr = 261.60 g.mol^{-1}	-	Hopkin & Williams
Di-sodium tetraborate (Borax)	$Na_2B_4O_7.10H_2O$ Mr = 381.37 g.mol^{-1}	99.5	Merck
Potassium persulphate	$K_2S_2O_8$ Mr = 270.33 g.mol^{-1}	98	Saarchem
Lead dioxide	PbO_2 Mr = 239.20 g.mol^{-1}	93	Minema
Cerous trichloride	$CeCl_3.6H_2O$ Mr = 354.60 g.mol^{-1}	94.7	Schuchardt München
Arsenazo (III) acid	$C_{22}H_{18}As_2N_4O_{14}S_2$ Mr = 776.24 g.mol^{-1}	-	Aldrich
Tetrabutylammonium perchlorate	$C_{16}H_{36}ClNO_4$ Mr = 341.92 g.mol^{-1}	98	Fluka
Silver nitrate	$AgNO_3$ Mr = 169.87 g.mol^{-1}	99.2	Merck
Potassium hydrogen phthalate	$HO.CO.C_6H_4.COOK$ Mr = 204.23 g.mol^{-1}	99.5	Hopkin & Williams

Organic reagents			
Tert-butanol	$C_4H_{10}O$ Mr = 74.12 g.mol^{-1}	99	Fluka
Oxalic acid	$H_2C_2O_4.2H_2O$ Mr = 126.07 g.mol^{-1}	99.5	Saarchem
Trichloroacetic acid	CCl_3COOH Mr = 163.39 g.mol^{-1}	99.0	BDH
Acetonitrile	CH_3CN Mr = 41.05 g.mol^{-1}	99.9	BDH
Trifluoroacetic acid	$C_2HF_3O_2$ Mr = 114.02 g.mol^{-1}	99	Sigma-Aldrich
Toluene-4-sulphonic acid	$CH_3.C_4H_4.SO_3H.H_2O$ Mr = 190.22 g.mol^{-1}	99	Saarchem
Acids and bases			
Sulphuric acid	H_2SO_4	99	Merck
Nitric acid	HNO_3	65	Merck
Phosphoric acid	H_3PO_4	85	Associated Chemical
Sodium hydroxide pellets	NaOH	99.9	Minema

2.3 Standardization of reagents

2.3.1 Standardization of acids and bases

Sulphuric acid solutions were standardised with freshly prepared borax solutions. Sodium hydroxide solutions were standardised with the standardized sulphuric acid solutions.

2.3.2 Standardization of Ce(IV) solution

A standardization method used in previous study [10] was employed, the procedure is the following: A dichromate solution, with concentration of 5 x 10^{-3} M, was prepared from primary standard grade potassium dichromate dried in an oven at 100 ^{o}C for an hour. A Fe(II) solution of concentration 1.8 x 10^{-2} M was prepared in 1.0 M H_2SO_4. A Ce(IV) solution of concentration of 1.2 x 10^{-2} M was prepared in 1.0 M H_2SO_4. The Fe(II) and Ce(IV) solutions were prepared just before the titrations were performed in order to minimize the air oxidation of Fe(II), and the reduction of Ce(IV).

The standardization of the Fe(II) solution was performed as follows: 25 mL of the Fe(II) solution was pipetted into a beaker with 5 mL H_3PO_4 (concentrated) and 25 mL H_2SO_4 (2.0 M). The dichromate solution was then titrated into the beaker using a Metrohm 716 DMS Titrino resulting in an endpoint at approximately 15 mL. Table 2.5 below shows an example of the results obtained.

Table 2.5: Results obtained from the standardization of a Fe(II) solution using potentiometric titrations with dichromate.

$[K_2Cr_2O_7]$ = 5.000 x 10^{-3} M		
Vol. Fe (II) = 25.00 ml		
Titration number	**Vol. CrO_7^{2-} ml**	**[Fe(II)] 10^{-2} M**
1	14.973	1.797
2	14.986	1.798
3	14.977	1.797
Results: **[Fe(II)] = 1.797 x 10^{-2} M**		
Mean Relative Deviation: 0.333ppt		

The Ce(IV) solution was standardized as follows: 10 mL of the Fe(II) solution was pipetted into a beaker with 25 mL 2.0 M H_2SO_4. The H_3PO_4 is not required since Ce(IV) is a strong oxidizing agent, and the presence of PO_4^{3-} results in a precipitate. The Ce(IV) was then titrated into the beaker and the endpoint was obtained at approximately 15 ml. Results from such a titration are shown in Table 2.6 (page 25).

Table 2.6: Results obtained from the standardization of a Ce(IV) solution using potentiometric titrations with Fe(II).

[Fe(II)] = 1.797 x 10^{-2} M		
Vol. Fe (II) = 10.00 ml		
Titration number	**Vol. Ce(IV) ml**	**[Ce(IV)] 10^{-2} M**
1	15.326	1.173
2	15.325	1.173
3	15.308	1.174
4	15.336	1.172
5	15.302	1.174
Results: **[Ce(IV)] = 1.173 x 10^{-2} M**		
Mean Relative Deviation: 0.6ppt		

Different concentrations of standardised Ce (IV) solutions were prepared by diluting the stock Ce(IV) solution in 500 ml volumetric flasks, and to keep the sulphuric acid concentration constant, different volumes of 1.0 M H_2SO_4 solution were added. The results are shown below in Table 2.7.

Table 2.7: Examples of dilutions of standard Ce(IV) stock solution.

$[Ce(IV)]_{stock}$ = 1.173 x 10^{-2} M			
$[H_2SO_4]_{stock}$ = 1.0 M			
Vol. of $Ce(IV)_{stock}$ added (ml)	**Vol. of 1.0 M H_2SO_4 added (ml)**	**Resultant [Ce(IV)] in mol.L^{-1}**	**Resultant [H_2SO_4] in mol.L^{-1}**
10.656	39.344	2.500 x 10^{-4}	0.1
42.626	7.374	1.000 x 10^{-3}	0.1

2.4 Experimental procedures for spectrophotometric titrations

A reaction solution of the reagent with appropriate concentration was prepared, and 25 ml of this solution was transferred quantitatively into the reaction vessel, a measured volume of known concentration of oxidant was then added. After the

reaction had settled sufficiently, usually about 2 minutes, a 3-ml sample was pipetted into a cuvette and the spectrum was recorded. The content of the cuvette was then emptied back into the reaction flask before the addition of the next amount of oxidant. The oxidant was added with a Metrohm 765 dosimat, and the reaction solution was under continuous gentle stirring.

2.5 Procedure for spectrophotometric kinetic studies

A 3-ml reaction solution of the complex with appropriate concentration was pipetted into a cuvette. The initial spectrum of the solution was recorded as the first scan. A measured volume of known concentration of reagent was then added into the cuvette immediately prior to the start of the second scan. The reaction time was started at the time of addition of the reagent. The progress of the reaction was followed using spectrophotometer.

2.6 Volume correction

The addition of titrant to the reaction solution causes the volume of the reaction solution to increase. However, this causes the absorbance of the solution to decrease since the concentration of the initial reagent decreases. It is necessary to correct the absorbance for volume changes, the observed absorbance values are multiplied by (V + *v*)/V, where V is the original volume of the solution, and *v* is the volume of added titrant.

All spectra and absorbance curves shown in this study are volume corrected unless specified.

Chapter 3

Synthesis and characterization of ruthenium (II) polypyridine complexes

3.1 Introduction

Ruthenium (II) complexes of polypyridines, typified by $Ru(bpy)_3^{2+}$ (where bpy is 2,2'-bipyridine) have been the subject of much study, particularly for their redox and photophysical properties. From reports in the literature it can be seen that the synthesis of $[Ru(bpy)_3](PF_6)_2$ is normally attempted in two ways: refluxing $RuCl_3.3H_2O$ in ethylene glycol [12] or using the convenient intermediate $Ru(DMSO)_4Cl_2$ [13] where the synthesis is performed under less vigorous conditions.

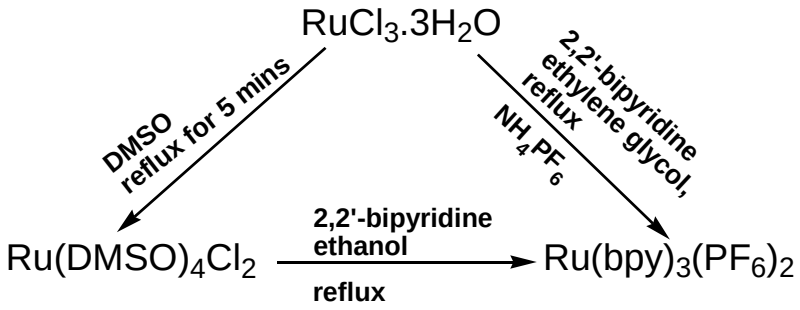

Scheme 3.1: Synthetic routes of $[Ru(bpy)_3](PF_6)_2$

3.2 Experimental

3.2.1 Synthesis of $Ru(DMSO)_4Cl_2$

The compound was synthesized by a variation of a published method [13]. A suspension of 0.30 g of $RuCl_3.3H_2O$ in degassed DMSO (3 ml) was heated under reflux with continuous stirring. After 5 minutes reflux a brown-orange colour appears. A yellow precipitate formed which was filtered, washed successively with acetone and diethyl ether, and dried overnight under vacuum. Yield = 75 %. m.p. 120 ^oC. IR(KBr) (cm^{-1}): v(S-O) 1114; v(C-S) 717; v(Ru-S) 482, v(Ru-Cl) 352.

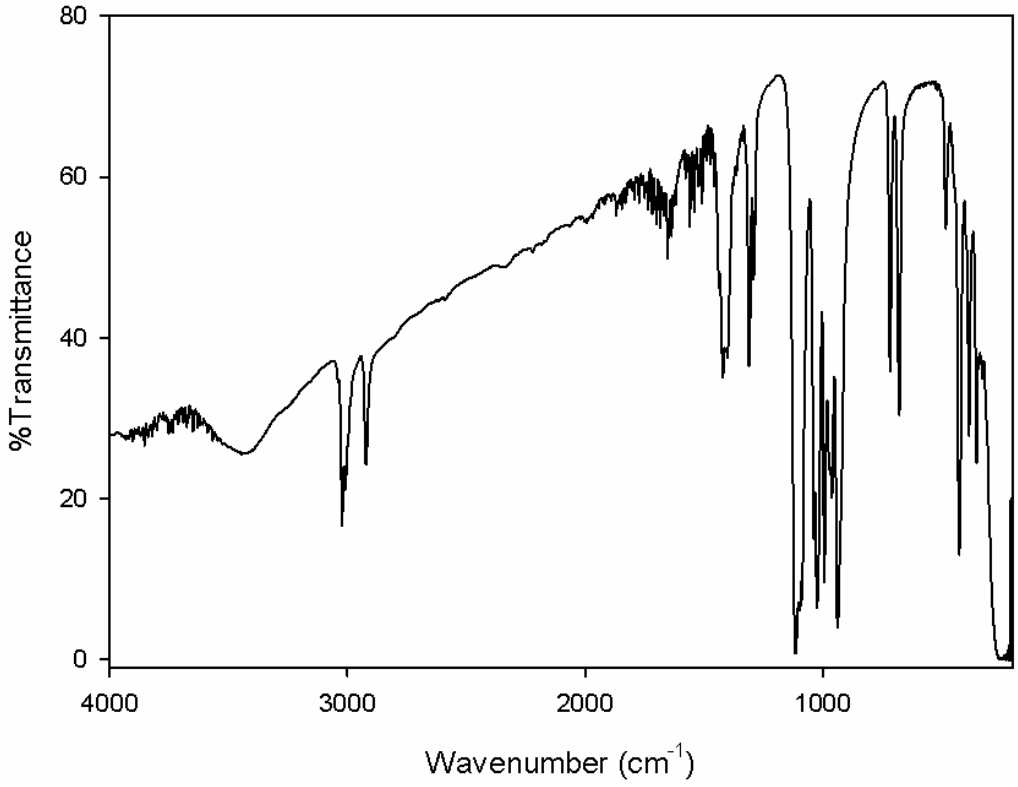

Figure 3.1: IR spectrum of $Ru(DMSO)_4Cl_2$.

3.2.2 Synthesis of $[Ru(bpy)_3](PF_6)_2$

The $[Ru(bpy)_3](PF_6)_2$ [12] used for this study was prepared by refluxing for 3 hours a suspension of $RuCl_3.3H_2O$ (0.5097 g) and 2,2'-bipyridine (1.6012 g) in ethylene glycol (7.5 ml, degassed). After heating was stopped, the hot solution was left to cool to room temperature. A 10 ml of saturated aqueous solution of NH_4PF_6 was then added and an orange precipitate was formed immediately. The product was filtered and left to dry under vacuum. Yield = 68 %.

Anal. Calcd. for $C_{30}H_{24}F_{12}N_6P_2Ru$ (mol.wt. = 859.55 g/mol) (%): C, 41.92; H, 2.81; N, 9.78. Found: C, 41.18; H, 2.88; N, 10.21. ^{1}H NMR (ppm, DMSO): δ 8.17 (t, 1H, *H*(1)), 7.72 (d, 1H, *H*(2)), 7.51 (t, 1H, *H*(3)), 8.83 (d, 1H, *H*(4)).

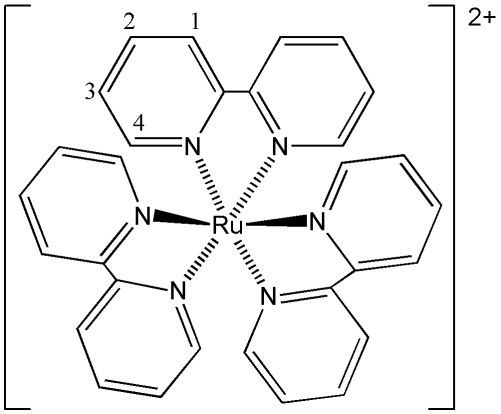

Figure 3.2: Structure of *tris(2,2'-bipyridyl) ruthenium (II).*

3.2.3 Results and discussions

The preparation of $[Ru(bpy)_3](PF_6)_2$ from $RuCl_3.3H_2O$ in ethylene glycol resulted in a 68 % yield with a pure product that did not need purification before use. Its ^{1}H NMR spectral data were consistent with the calculated values. The elemental analysis was performed and also consistent with the structure. When compared to the ^{1}H NMR signals from 2,2'-bipyridine, the pyridine signals from the complex all shifted downfield by 0.2 ppm.

3.3 Electronic spectroscopy

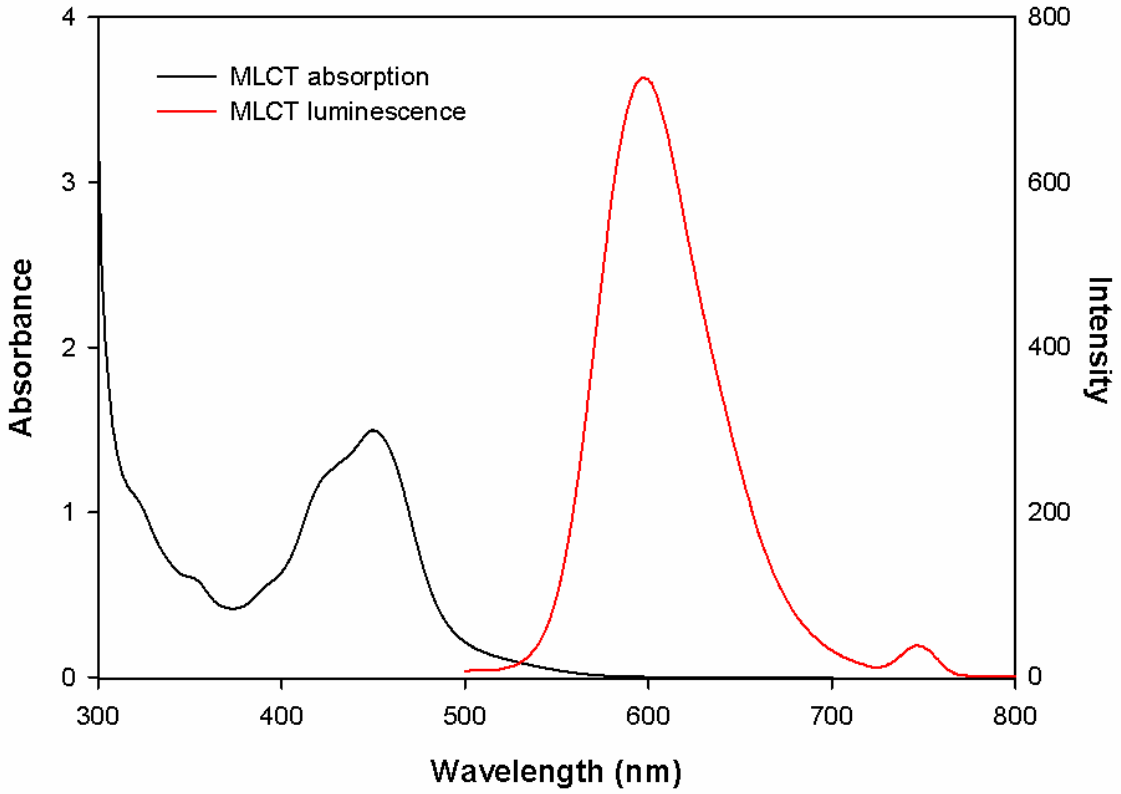

Figure 3.3: MLCT absorption and emission spectra of $Ru(bpy)_3^{2+}$ in acetonitrile. $[Ru(bpy)_3^{2+}]$ = 0.1 mM.

The electronic absorption and emission spectra of $Ru(bpy)_3^{2+}$ in acetonitrile are shown in Figure 3.3. Upon excitation at 453 nm, the complex emits intense luminescence with emission maximum at about 600 nm, which is characteristic MLCT luminescence from the triplet MLCT Ru(dπ) to ligand (π*) state.

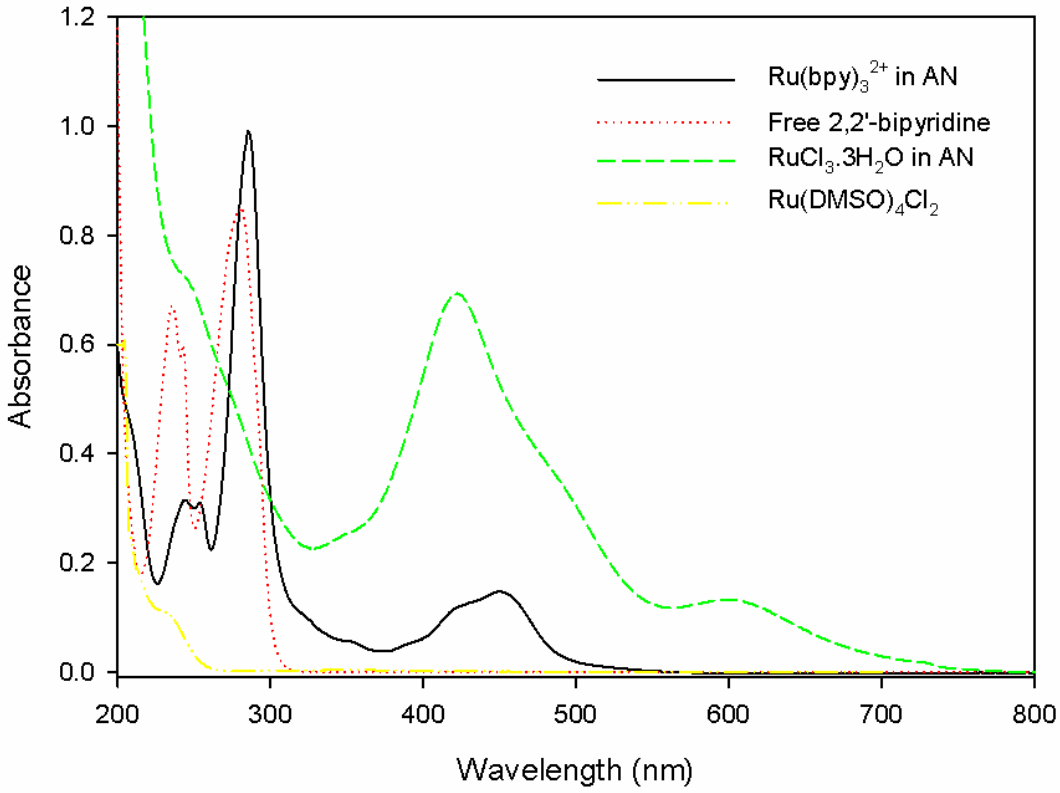

Figure 3.4: Comparison of UV-Vis spectra of $Ru(bpy)_3^{2+}$, free 2,2'-bipyridine and $RuCl_3.3H_2O$ in acetonitrile. $[Ru(bpy)_3^{2+}]$ = 1.108 x 10^{-5} M, [2,2'-bipyridine] = 1.0 x 10^{-3} M, $[Ru(DMSO)_4Cl_2]$ = 1.0 x 10^{-5} M, $[RuCl_3.3H_2O]$ = 1.0 x 10^{-4} M. $RuCl_3.3H_2O$ was freshly prepared in acetonitrile.

Figure 3.4 compares the UV-Vis spectra of $Ru(bpy)_3^{2+}$ with the free 2,2'-bipyridine in acetonitrile. The $Ru(bpy)_3^{2+}$ shows an intra-ligand π to π* transition at 286 nm, while the metal-to-ligand charge transfer (MLCT) transition takes place at 453 nm. The relative spectral data for $Ru(bpy)_3^{2+}$ are summarized in Table 3.1 below.

Table 3.1: Absorption data for $Ru(bpy)_3^{2+}$ in acetonitrile at 298 K.

λ_{max} (nm)	ε (M^{-1} cm^{-1})
244	28420
254	28042
286	89296
453	13131

3.4 Concentration determination using ICP-MS

With an ICP-MS the total Ru(II) concentration can be accurately measured (see Section 2.3.4.3 - Chapter 2 for detailed operating conditions). The standardisation of tris(2,2'-bipyridyl) ruthenium (II) was performed as follows: the calculated amount of orange colour $[Ru(bpy)_3](PF_6)_2$ powder was firstly dissolved in 5 ml of acetonitrile due to its insolubility in water, and then transferred quantitatively into a 500 ml volumetric flask filled up to the mark with ultra high purity water. The approximate Ru(II) concentration of 1.1 x 10^{-5} M was prepared. The reason for preparing the sample in aqueous medium is that the ICP-MS response to an introduction of organic solvents (e.g. acetonitrile) is unpredictable and more often than not extinguishes the plasma. In order to overcome such instrumental difficulties organic solvent should be avoided altogether in this analysis method.

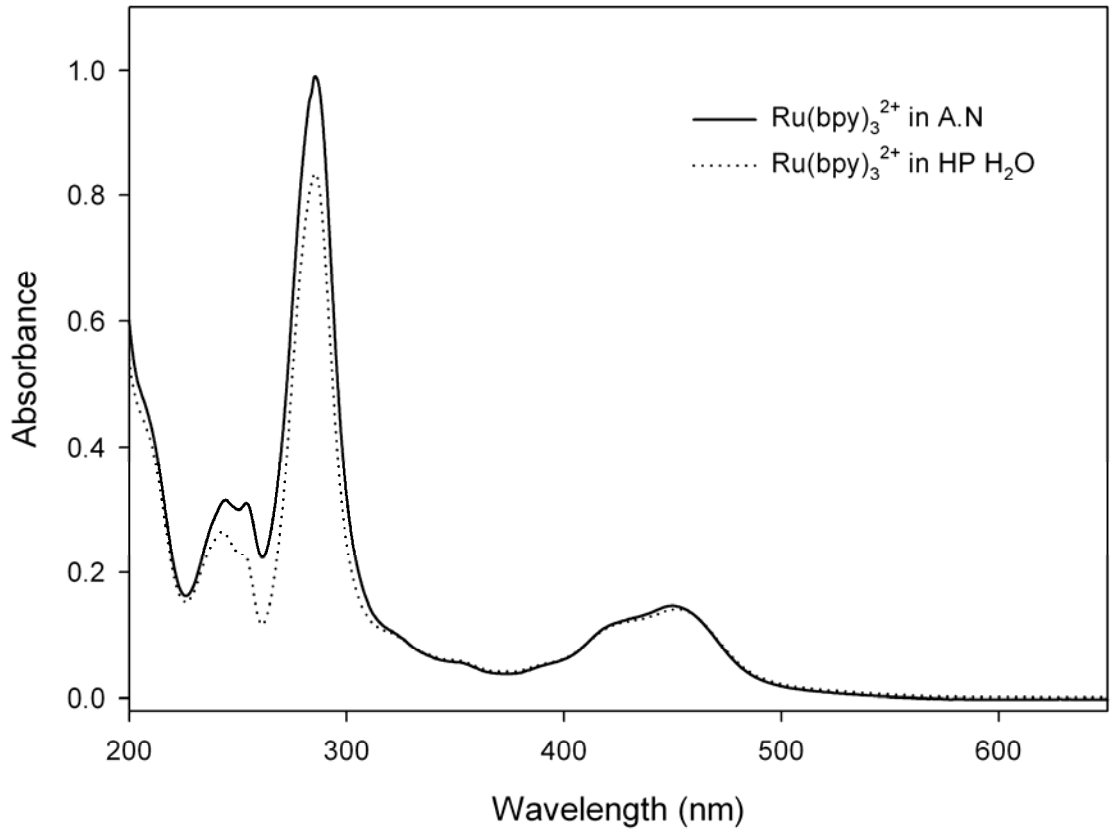

Figure 3.5: Comparison of UV-Vis spectra of $Ru(bpy)_3^{2+}$ in high purity water and acetonitrile (AN). The volume ratio between the amount of acetonitrile to dissolve $Ru(bpy)_3^{2+}$ powder and the water to prepare the solution was 1:100. The spectra were recorded after the solutions reached equilibrium. $[Ru(bpy)_3^{2+}] = 1.108 \times 10^{-5}$ M.

Figure 3.5 shows the UV-Vis spectra of $Ru(bpy)_3^{2+}$ in aqueous and non-aqueous (AN) media. Small differences in absorbance can be observed in the lower wavelength region. The intensity of the 2,2'-bipyridine characteristic peak at 286 nm decreases. However, at 453 nm the Ru(II) keeps consistency as an intense broad peak in both media, which shows the solution is suitable for concentration determination by ICP-MS. In addition, the resultant solution of $Ru(bpy)_3^{2+}$ in water is very stable, no spectral changes could be observed even after 80 days. Because of the stability and easy to work with the aqueous medium, the $Ru(bpy)_3^{2+}$ stock solutions used in this study were prepared following the above mentioned method unless specified.

Table 3.2: Examples of results obtained from the analysis of tris(2,2'-bipyridyl) ruthenium (II) using ICP-MS. The tris(2,2'-bipyridyl) ruthenium (II) solutions of approximate concentration of 1.1 x 10^{-5} M were prepared in distilled water. The sample solution was diluted to bring it into the optimum operating range of the ICP-MS.

Run #	Diluted [Ru] µg/L	Con. RSD	Without Dilution µg/L	[Ru] mol/L
1	566.220	0.683	1132.440	$1.120x10^{-5}$
2	553.416	1.828	1106.831	$1.095x10^{-5}$
3	560.499	1.061	1120.997	$1.109x10^{-5}$
			Average:	$1.108x10^{-5}$

Comparing the values in Table 3.2 with the previously calculated $Ru(bpy)_3^{2+}$ concentration (1.1 x 10^{-5} M), it appears that the differences are negligible between experimental calculated and ICP-MS analyzed values. This result confirms that an ICP-MS can be used to accurately measure Ru(II) concentration. The concentrations of the ruthenium stock solutions used in this study were therefore determined using this technique.

3.5 Characterization of tris(2,2'-bipyridyl) ruthenium (II)

3.5.1 Introduction

Tris(2,2'-bipyridyl) ruthenium (II) has been widely studied because of its unique characteristic chemistry and applications based on its chemistry. Up to today, the tris(2,2'-bipyridyl) ruthenium (II) continues to attract attention in several branches of

chemistry [7]. In this section, the properties of the complex including redox potentials, light absorption, luminescence emission have been investigated and compared to previous studies [14-15].

3.5.2 Fluorescence spectrophotochemistry

3.5.2.1 Literature review [16-17]

After the absorption of a photon, $Ru(bpy)_3^{2+}$ will emit light in the visible region of the spectrum (see Figure 3.3, page 30). This emission is termed luminescence. If the emission occurs from an excited state that has the same spin multiplicity as the ground state, then the emission is called fluorescence. Phosphorescence occurs when the excited state is of different multiplicity than the ground state (see Figure 1.2, page 8). In the presence of other chemical species, the emission of an excited state may decrease or be eliminated completely; it is then said that the emission has been quenched. Quenching is a bimolecular process and involves energy transfer between the excited state of one molecule (the donor, *D*) and the ground state of another molecule (the quencher, *Q*). The quenching process can lead to a chemical reaction between the donor and quencher, or it can involve energy transfer between them with no new products formed.

The fundamental equation of luminescence spectroscopy is shown below:

$$O(\lambda) = K\, I(\lambda)\, \Phi(\lambda)\, F(\lambda) \qquad \ldots 3.1$$

where O(λ) is the observed luminescence intensity when the sample is irradiated at wavelength λ with an incident intensity (quanta/sec) of $I(\lambda)$. The luminescence quantum yield, Φ(λ) is the probability that once a molecule has absorbed a photon it will emit a photon. F(λ) is the fraction of incident light absorbed by the sample, and K is proportionality constant. For most pure substances the emission spectrum is independent of the exciting radiation. K is then usually constant as long as the detector wavelength, system gain, and geometry do not change. The fraction of radiation absorbed, F(λ), is given by Beer's Law.

$$F(\lambda) = 1 - e^{-2.303\, \varepsilon(\lambda)\, l\, C} \qquad \ldots 3.2$$

where ε(λ) is the molar absorptivity at wavelength λ; *C* is the concentration in moles/liter; and l is the optical path length. If ε(λ) l *C* << 1, the exponential part of Equation 3.2 can be expanded as a power series, keeping only the first two terms, which produces Equation 3.3 shown below:

$$F(\lambda) = 2.303\ \varepsilon(\lambda)\ l\ C \qquad \ldots 3.3$$

for optically dilute solutions, where ε(λ) l C < 0.05. Substitution of Equation 3.3 into Equation 3.1 yields;

$$O(\lambda) = 2.303\ K\ I(\lambda)\ \Phi(\lambda)\ \varepsilon(\lambda)\ l\ C \qquad \ldots 3.4$$

The Equation 3.4 is for an optically dilute sample, where the emission intensity depends linearly on the concentration. This result is routinely used in analytical determinations.

Furthermore, as mentioned before, quenching is the process of removal of energy from an excited state of a substance by a different chemical species. If a quencher (*Q*) is added to a solution of a luminescent material (*D*), then the following processes can occur:

D ⟶	D*	I	excitation	…3.5
D* ⟶	D + $h\nu$	k_e	emission	…3.6
D* ⟶	D + heat	k_{vr}	relaxation	…3.7
D* + Q ⟶	D + Q*	k_q	quenching	…3.8

As shown in Equation 3.5, the molecule *D* is excited by absorbing radiation of energy $h\nu$ and intensity I. The excited state of this molecule, *D**, can be deactivated by the processes in Equations 3.6 – 3.8. k_e is the rate constant for emission, and k_{vr} is the rate constant for vibrational deactivation paths. The bimolecular quenching constant is k_q. If the steady state approximation is made for the excited state of *D* in Equations 3.5 – 3.8, and the resultant equation substituted into Equation 3.4, Equation 3.9 is then obtained.

$$\Phi_0 / \Phi = 1 + \frac{k_q[Q]}{(k_e + k_{vr})} \qquad \ldots 3.9$$

Where Φ is the measured emission of D and the subscript "0" denotes the emission without quencher.

By taking the ratio of the emission in the absence of quencher to that in the presence of a quencher, Equation 3.9 was obtained, which contains only fundamental rate constants and measurable quantities. Equation 3.9 is called the Stern-Volmer equation, and it is one of the fundamental equations of photophysics. Equation 3.9 is normally written as:

$$\Phi_0 / \Phi = 1 + K_{SV}[Q] \qquad \ldots 3.10$$

with

$$K_{SV} = \frac{k_q}{(k_e + k_{vr})}$$

where K_{SV} is the Stern-Volmer quenching constant.

The lifetime of an excited state is defined as the reciprocal of a rate constant: $\tau = 1/k$. In the absence of a quencher, the donor can lose energy only by emission and vibrational relaxation, so the total rate constant is $k_e + k_{vr}$; therefore, the lifetime of the excited state in the absence of quencher is: $\tau_o = 1/(k_e + k_{vr})$. Substituting into the Stern-Volmer constant produces:

$$K_{SV} = k_q \tau_o \qquad \ldots 3.11$$

K_{SV} can be determined by plotting the observed ratio of emission intensities versus quencher concentration (Equation 3.10). If τ_o is known, the bimolecular quenching constant k_q can be obtained using Equation 3.11. The bimolecular rate constant is the constant for the actual reaction between the donor and quencher.

3.5.2.2 Experimental

The following procedure adapted from another study was used [12]: a calculated amount of $[Ru(bpy)_3](PF_6)_2$ powder was dissolved in acetonitrile to make a concentration of 1.0×10^{-3} M, the UV-Vis spectrum of this stock solution was recorded. As shown in Figure 3.1, the spectrum determines the λ_{max} in the MLCT region (453 nm). The stock solution was then diluted to make five different solutions, 25 ml each. Each solution contained the same concentration of 1.0×10^{-4} M of $Ru(bpy)_3^{2+}$ but with different amount of phenothiazine added. In order to achieve this

into each of five 25 ml volumetric flasks, a certain volume of 1.0 x 10^{-3} M of phenothiazine stock solution was pipetted, 0, 5, 10, 15 and 20 ml. Phenothiazine acts as a quencher in this case. Acetonitrile was also added to make all the solution volumes the same.

A fluorescence spectrum was obtained for each of the five solutions. The results are shown in the next section.

3.5.2.3 Results and discussions

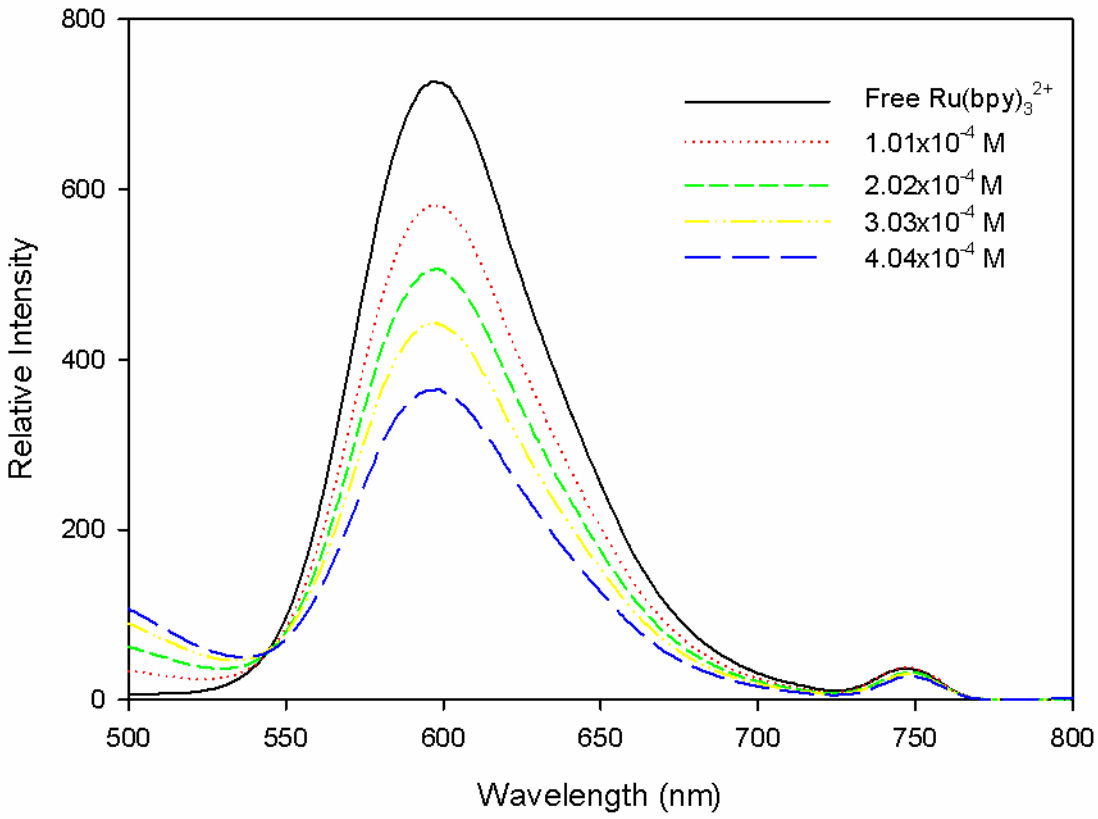

Figure 3.6: Emission spectra of $Ru(bpy)_3^{2+}$ in acetonitrile at 298 K. $[Ru(bpy)_3^{2+}] = 1.0 \times 10^{-4}$ M; Phenothiazine concentrations are denoted in the legend.

Figure 3.6 shows the emission spectra of $Ru(bpy)_3^{2+}$ in acetonitrile in the presence of phenothiazine as a quencher. As the phenothiazine concentration increases, the emission intensity decreases. This is evidence that the excited state of $Ru(bpy)_3^{2+}$ has been quenched by phenothiazine and energy has been transferred between the excited state of $Ru(bpy)_3^{2+}$ and the ground state of phenothiazine. At 750 nm, a small peak can be observed in the spectra caused by scattered light. This scattered light is associated with the scattering of the excitation light by the solvent molecule.

Figure 3.6 shows the emission intensities with respect of different phenothiazine concentrations. As mentioned in Section 3.5.2.1, and according to Equation 3.10, the Stern-Volmer constant K_{SV} can be determined by plotting the observed ratio of emission intensities versus quencher concentration.

The area of each of the five peaks was calculated using trapezoid method and the results are shown in Table 3.3. These values were used for the ratio Φ_0/Φ, with the sample in the absence of quencher as the numerator.

Table 3.3: Examples of results obtained from emission spectra of $Ru(bpy)_3^{2+}$ in acetonitrile in the presence of phenothiazine.

[Phenothiazine]x10^{-4} M	Emission peak area	Φ_0/Φ
0	55221	1
1.01	44657	1.23
2.02	39003	1.41
3.03	34538	1.59
4.04	28754	1.92

The curve of ratio of emission intensities Φ_0/Φ versus [phenothiazine] was then plotted as shown below in Figure 3.7.

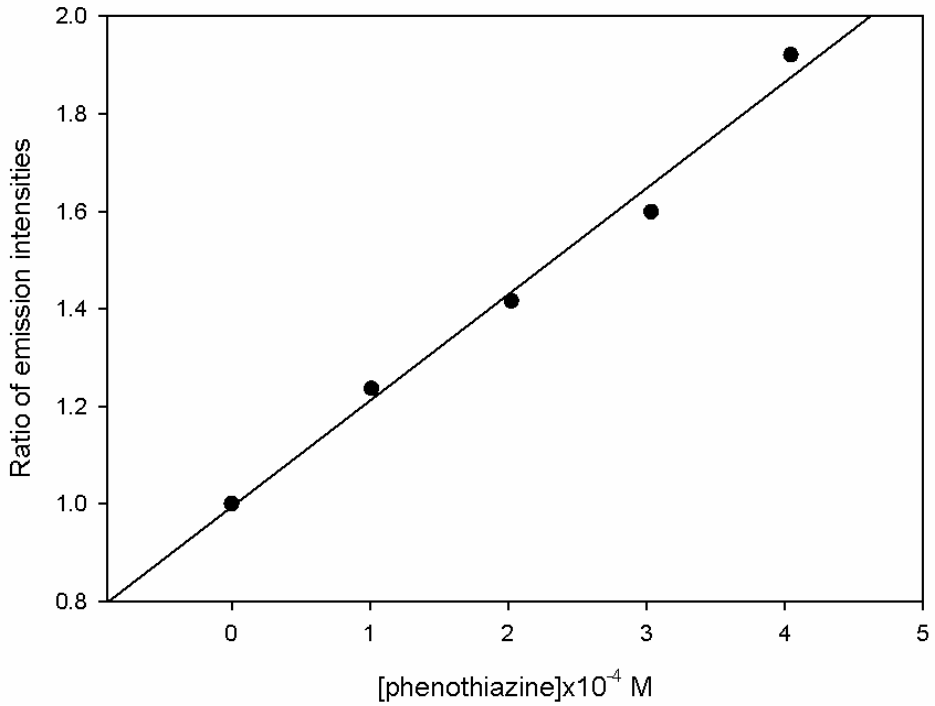

Figure 3.7: The ratio of emission intensities Φ_0/Φ against phenothiazine concentration plot. A least square fit of 0.987 was obtained for the curve.

The line with best fit obtained was y = 0.217 x + 0.993. Using the literature value for τ_o [18], the experimental value of k_q was calculated. Table 3.4 below shows the comparison of experimental values obtained with the literature values.

Table 3.4: The quenching rate constant for phenothiazine in acetonitrile with $Ru(bpy)_3^{2+}$ at 298 K.

K_{SV} x 10^3 M^{-1}	τ_o [18] x 10^{-7} s	k_q experimental x 10^9 $M^{-1}s^{-1}$	k_q literature x 10^9 $M^{-1}s^{-1}$
2.178	8.7	2.503	2.5 [19] or 1.3 [20]

Table 3.4 compares the experimental k_q value determined here with values found in the literature. Variation in k_q values can be due to various factors such as: fluorescence from impurities and effects of scattered light. Also oxygen dissolved in a solvent exerts a marked fluorescence extinction therefore solvent degassing is required. In addition, exposures to excitation light might cause the $Ru(bpy)_3^{2+}$ sample to produce a photochemical reaction, which results in a change in fluorescence intensity. The spectrum scan speed can be increased to minimize this effect.

The Stern-Volmer analysis yielded a quenching rate constant (k_q) of 2.503 x 10^9 $M^{-1}s^{-1}$. This indicates that the electron-transfer quencher, phenothiazine is a very efficient electron acceptor for quenching the $Ru(bpy)_3^{2+}$ excited state.

3.5.3 Redox potential

3.5.3.1 Introduction

Because of the redox properties of $Ru(bpy)_3^{2+}$, the complex plays an important role in a number of applications, for example it can function as a photocatalyst for the decomposition of water into hydrogen and oxygen [21]. In this section, the redox behavior of the compound in acetonitrile was examined using cyclic voltammetry with a platinum disk as a working electrode.

3.5.3.2 Results and discussions

The potentials are reported with reference to the ferrocene couple ($E_{1/2}$ = 0 V, ΔE = 52 mV, see Figure 2.2, page 14). In addition, $E_{1/2}$ value was calculated from the average of the anodic and cathodic peak potentials at scan rate of 100 mV/s. The cyclic voltammogram of $Ru(bpy)_3^{2+}$ obtained is shown below in Figure 3.8.

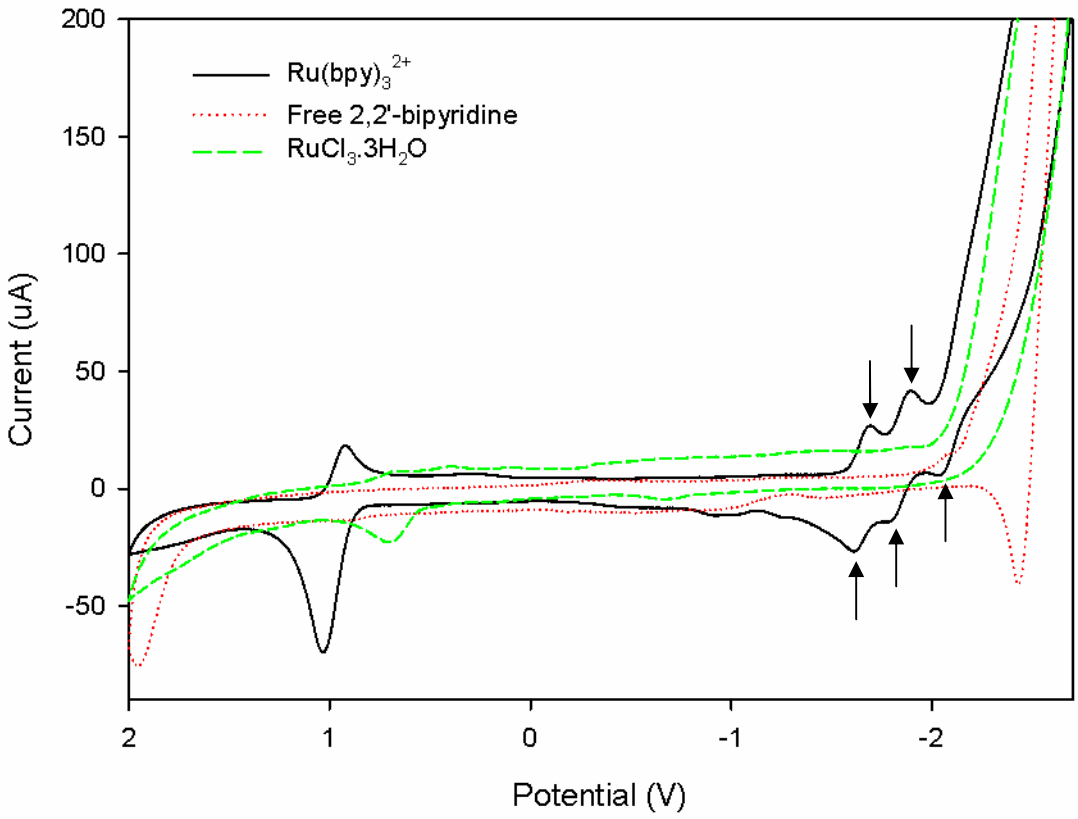

Figure 3.8: Comparison of cyclic voltammograms of 3.2 mM $Ru(bpy)_3^{2+}$ with 2,2'-bipyridine and $RuCl_3.3H_2O$ in 0.1 M TBAP in acetonitrile. Scan initiated at -2.7 V versus non-aqueous Ag/AgNO3 reference electrode in positive direction at 100 mV/s. Platinum working electrode (1.6 mm in diameter). Ferrocene in 0.1 M TBAP in acetonitrile was recorded as internal reference ($E_{1/2}$ = 0 V).

After having verified a flat background of 0.1 M tetrabutylammonium phosphate (TBAP) supporting electrolyte in acetonitrile in the range of -2.7 to 2.0 V vs. Ag/Ag^+, the cyclic voltammogram of 3.2 mM $Ru(bpy)_3^{2+}$ was recorded. The $Ru(bpy)_3^{2+}$ exhibits a reversible metal to ligand charge transfer oxidation at 0.963 V; E_{pc} = 922 mV and E_{pa} = 1004 mV. $E_{1/2} = (E_{pc} + E_{pa})/2$ = 0.963 V. A separation of 82 mV between anodic and cathodic peaks indicates a one-electron couple, this redox process is assigned to the Ru(II)/Ru(III) couple. The difference between the

cathodic and anodic currents to the Ru(II)/Ru(III) couple indicates the redox ability of the species. For example, larger anodic current shows Ru(III) species can be easily reduced to Ru(II), while the slightly reduced cathodic current illustrates that the oxidation of Ru(II) to Ru(III) is more difficult. The arrows in Figure 3.8 indicate the three closely spaced ligand-localized redox reactions at -1.65, -1.83, -2.07 V, where each added electron is localized on a single ligand.

In addition, different scan rates were applied to the electrochemical cell to examine the redox behavior of the Ru(II)/Ru(III) couple. The disproportion disappears if the scan window is narrowed, the cyclic voltammograms obtained are shown in Figure 3.9.

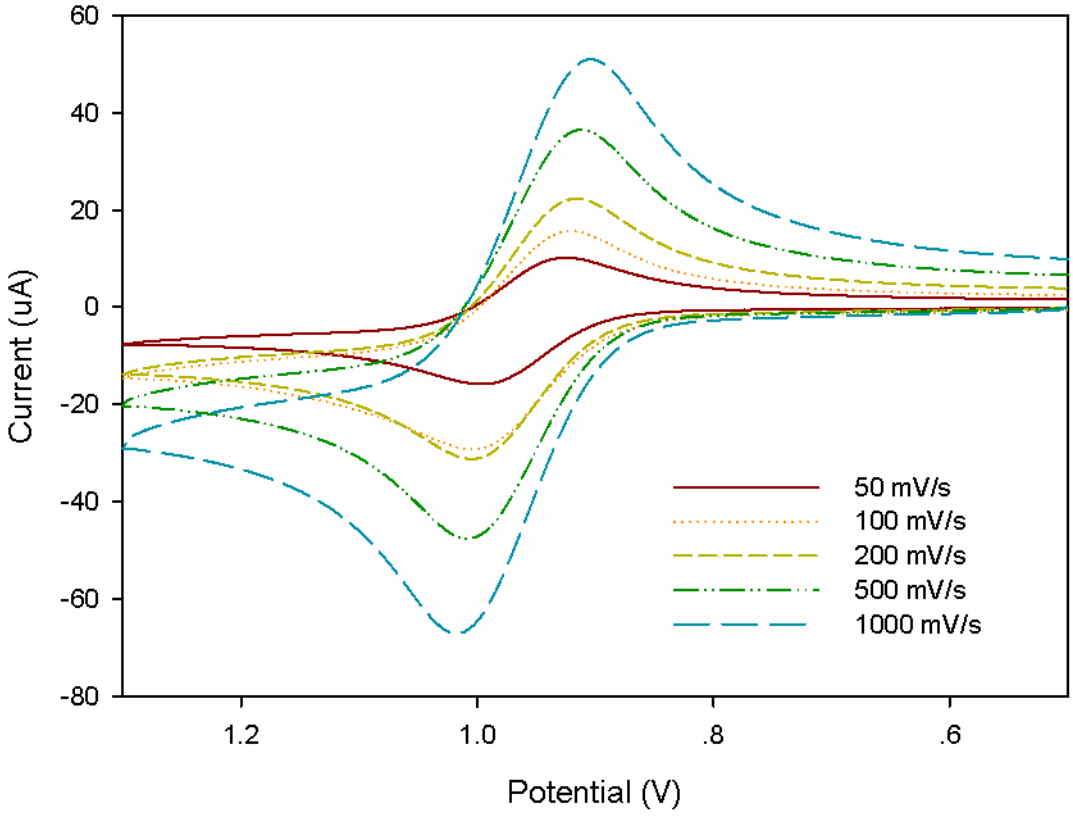

Figure 3.9: Cyclic voltammograms of quasi-reversible couples of Ru(II/III) scanned at various rates. Scan was initiated at 0.5 V versus non-aqueous Ag/AgNO3 reference electrode in positive direction. [$Ru(bpy)_3^{2+}$] = 3.2 mM. The different scan rates are denoted in the legend.

Table 3.5 (page 42) shows the data obtained at different scan rates according to Figure 3.9. It can be observed that ΔE_p appears greater than 0.0591 V at higher scan rates. Therefore the experimental ΔE_p values demonstrate that the $Ru(bpy)_3^{2+}$

oxidation actually is not completely reversible under the conditions employed even at the slowest scan rate used. For a typical reversible couple, the separation between anodic and cathodic potentials of $\Delta E_p = E_{pa} - E_{pc} = 0.0591/n$ V should be obtained, where n is the number of electrons transferred in the electrode reaction. For the Ru(II)/Ru(III) couple, $\Delta E_p = 0.0591$ V was expected. However, the unexpected experimental values illustrate that the chemical reversibility ($I_{pc}/I_{pa} = 1$) is not synonymous with electrochemical reversibility ($\Delta E_p = 0.0591$ V), the $Ru(bpy)_3^{2+}$ oxidation is actually quasi-reversible.

Table 3.5: Experimental results obtained for quasi-reversible couples of Ru(II/III) scanned at various rates.

Scan Rate (mV/s)	E_{pa} (V)	E_{pc} (V)	$E_{1/2}$ (V)	ΔE_p (V)	E_{pa}-$E_{1/2}$ (V)	I_{pa} (uA)	I_{pc} (uA)	I_{pc}/I_{pa}
50	0.997	0.924	0.961	0.073	0.036	14.29	13.48	1.06
100	1.004	0.922	0.963	0.082	0.041	23.92	21.45	1.11
200	1.004	0.915	0.960	0.089	0.044	27.57	27.05	1.02
500	1.009	0.911	0.960	0.098	0.049	41.93	42.65	0.98
1000	1.018	0.904	0.961	0.114	0.057	58.33	57.03	1.02

The potential difference $E_{pa} - E_{1/2}$ is a convenient indication for "Nernst behaviour" [22]. The values shown in Table 3.5 are very close to the expected values for a reversible one-electron transfer process where $E_{pa} - E_{1/2} = 0.0565$ V at 25°C [23].

In addition, according to the Randles-Sevcik equation shown below for a reversible system [24]:

$$I_p = (2.69 \times 10^5)\, n^{3/2}\, A\, D^{1/2}\, C\, v^{1/2} \qquad 3.12$$

where I_p is the peak current (A), n is the electron stoichiometry, A is the electrode area ($A = 0.0201$ cm^2), C is concentration (mol/cm^3), and *v* is scan rate (V/s). The diffusion coefficient D (cm^2/s) of $Ru(bpy)_3^{2+}$ in acetonitrile at 298 K was determined by a plot of I_{pc} *vs*. $v^{1/2}$ as shown in Figure 3.10 (page 43)

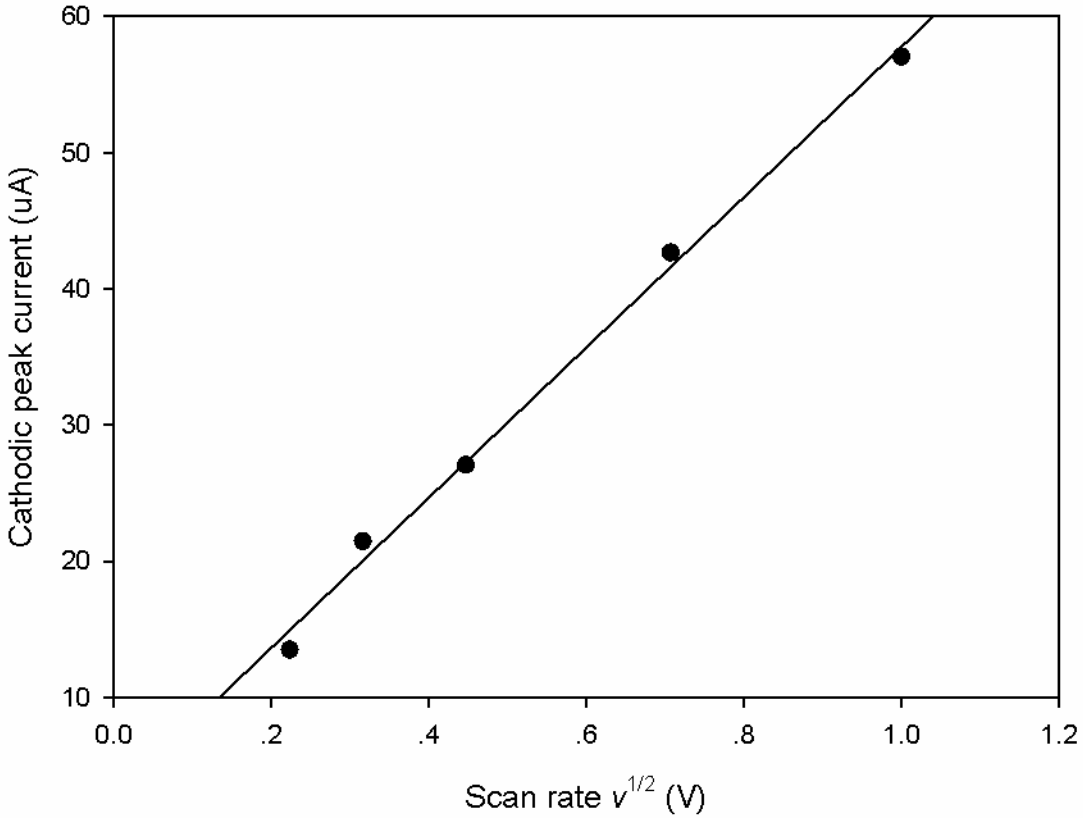

Figure 3.10: The I_{pc} vs. $v^{1/2}$ plot according to the Randles-Sevcik equation. After unify all the units a linear equation was obtained with a least square fit yield 0.995: $y = 5.517 \times 10^{-5} x + 2.604 \times 10^{-6}$.

The Figure 3.10 shows a plot of I_{pc} *vs*. $v^{1/2}$ which yields a straight line according to Equation 3.12. The slope of the line was used to determine the diffusion coefficient, since n, A and C are known.

By adjusting the potential scan rate, the heterogeneous electron-transfer rate constants k_s (cm/s) could also be calculated, based on the relation [25]:

$$\psi = f\left(n\Delta E_p\right) = \frac{\gamma^{\alpha/2} k_s}{\sqrt{\pi a D}} \qquad 3.13$$

where α is the transfer coefficient for the electron transfer, γ is the ratio of the diffusion coefficients of the reactant and product species. a = nF*v*/RT, where *v* is the scan rate (mV/s). ψ is a tabulated function whose values are provided in Table 3.6 (page 44).

If γ = 1, the Equation 3.13 can be written as,

$$k_s = \psi\left[\pi D\frac{nFv}{RT}\right]^{1/2} \qquad 3.14$$

At 298 K, k_s can therefore be determined from Equation 3.14. The calculated results are summarised in Table 3.7

Table 3.6: Variation of tabulated parameter ψ with peak potential separation [25].

ψ	**ΔE_p (mV)**
2.00	72
1.00	84
0.75	92
0.50	105
0.35	121

Table 3.7: The calculated results from Randles-Sevcik equation at 298 K.

n=1

A=0.0201 cm^2

$[Ru(bpy)_3^{2+}]=3.2x10^{-6}$ mol/cm^3

$D=1.02x10^{-5}$ cm^2/s

Scan Rate (mV/s)	**ΔE_p (mV)**	***k_s* (cm/s)**
50	0.073	0.0158
100	0.082	0.0112
200	0.089	0.0118
500	0.098	0.0125
1000	0.114	0.0124
	Average:	0.0127

At equilibrium, the forward and reverse rate constants are equal when the applied potential is equal to the E^o of the redox couple. The standard heterogeneous rate constant k_s is defined for these conditions [26]. Large values for k_s indicate that following the application of an applied potential, equilibrium between oxidized and reduced species will be re-established quickly. Small values for k_s indicate slow kinetics and longer time requirement for equilibrium. The commonly accepted ranges [26] for k_s are:

$k_s > 0.020$ cm/s	Reversible
$0.020 > k_s > 5.0 \times 10^{-5}$ cm/s	Quasi-reversible
$k_s < 5.0 \times 10^{-5}$ cm/s	Irreversible

According to the experimental values obtained in Table 3.6, clearly, the $Ru(bpy)_3^{2+}$ oxidation is quasi-reversible.

In summary, the diffusion coefficient of $Ru(bpy)_3^{2+}$ in acetonitrile at 298 K was determined as 1.02×10^{-5} cm^2/s. The estimation of the heterogeneous electron transfer rate constant (k_s) leads to an average value of 0.0127 cm/s, which is confirmed with k_s reported for the quasi-reversible reaction.

Chapter 4

Reactions of tris(2,2'-bipyridyl) ruthenium (II)

4.1 Introduction

This chapter gives an overview of the reactions and properties of $Ru(bpy)_3^{2+}$ before its reactions with Ce(IV) are discussed in detail. There is fairly extensive literature on the use of the chemiluminescence reagent $Ru(bpy)_3^{3+}$ in a number of important applications [27-29]. However, many of the reports in the literature on the generation of $Ru(bpy)_3^{3+}$ from oxidation of $Ru(bpy)_3^{2+}$ are out-dated. This fact, together with the interesting nature of some of the preliminary data obtained in this study prompted a fresh look at the oxidation of $Ru(bpy)_3^{2+}$ by different oxidizing agents. In addition, the reaction between Ru(III) and arsenazo III was also investigated in the hope of developing a new analytical method so that the ruthenium concentration could be accurately determined as an alternative to ICP-MS analysis.

4.2 Influence with acids and bases in non-aqueous medium

4.2.1 Introduction

In this section, the $Ru(bpy)_3^{2+}$ stability studies were conducted in a non-aqueous medium with the presence of acids and a base. Johansson [8] showed that for certain polypyridyl ruthenium (II) complexes, the UV-Vis spectra showed isosbestic points at 350, 425, and 500 nm under the influence of a base (*tert*-BuOK). Most importantly, it was shown that the process was fully reversible and the starting spectrum was recovered instantaneously upon addition of an acid (TsOH).

Three strong organic acids were used in this study: *p*-toluenesulfonic acid (TsOH) is a strong organic acid and is non-oxidizing unlike some of the strong mineral acids, for example nitric acid, sulphuric acid, and perchloric acid [6(ii)]. Oxalic acid is another organic acid used, it is a relatively strong carboxylic acid, about 3,000 times stronger than acetic acid. The dianion, known as oxalate, is a reducing agent as well as a ligand for metal cations [6(iii)] which has been extensively studied for its chemiluminescent reactions with $Ru(bpy)_3^{2+}$ [29]. Lastly the trifluoroacetic acid is a strong carboxylic acid due to the influence of the electronegative trifluoromethyl group. It is almost 100,000-fold more acidic than acetic acid [6(iv)].

For the base, potassium *tert*-butoxide (*tert*-BuOK) was used considering its properties which include serving as a base and a nucleophile [6(v)]. The influence of acids (oxalic acid, trifluoroacetic acid, TsOH) and a base (*tert*-BuOK) on the tris(2,2'-bipyridyl) ruthenium (II) complex in a non-aqueous medium was investigated by observing the spectral changes of the reaction solution.

4.2.2 Experimental

A 1.0×10^{-3} M *tert*-BuOK solution was freshly prepared through the addition of 0.0098 g potassium to a *tert*-BuOH solution (250 ml). 0.1 M oxalic acid stock solution was prepared by dissolving a calculated amount of oxalic acid in the acetonitrile. A concentration of 0.1 M trifluoroacetic acid was achieved by adding a measured volume of 12.98 M acid stock solution supplied from Merck to the volumetric flask (250 ml) and filled up to the mark with acetonitrile. A 0.1 M TsOH solution was prepared by dissolving the TsOH solid in an acetonitrile solution.

The reaction spectra were recorded using acetonitrile as a reference solution. The reaction progress was followed in one of two ways: for kinetic observations the experimental procedures followed are as described in Chapter 2 (Section 2.5, page 26); in the case of a titration with trifluoroacetic acid, the procedure from Chapter 2 (Section 2.4, page 25) was followed. All the spectra obtained were volume corrected. The results are shown in the next section.

4.2.3 Results and discussions

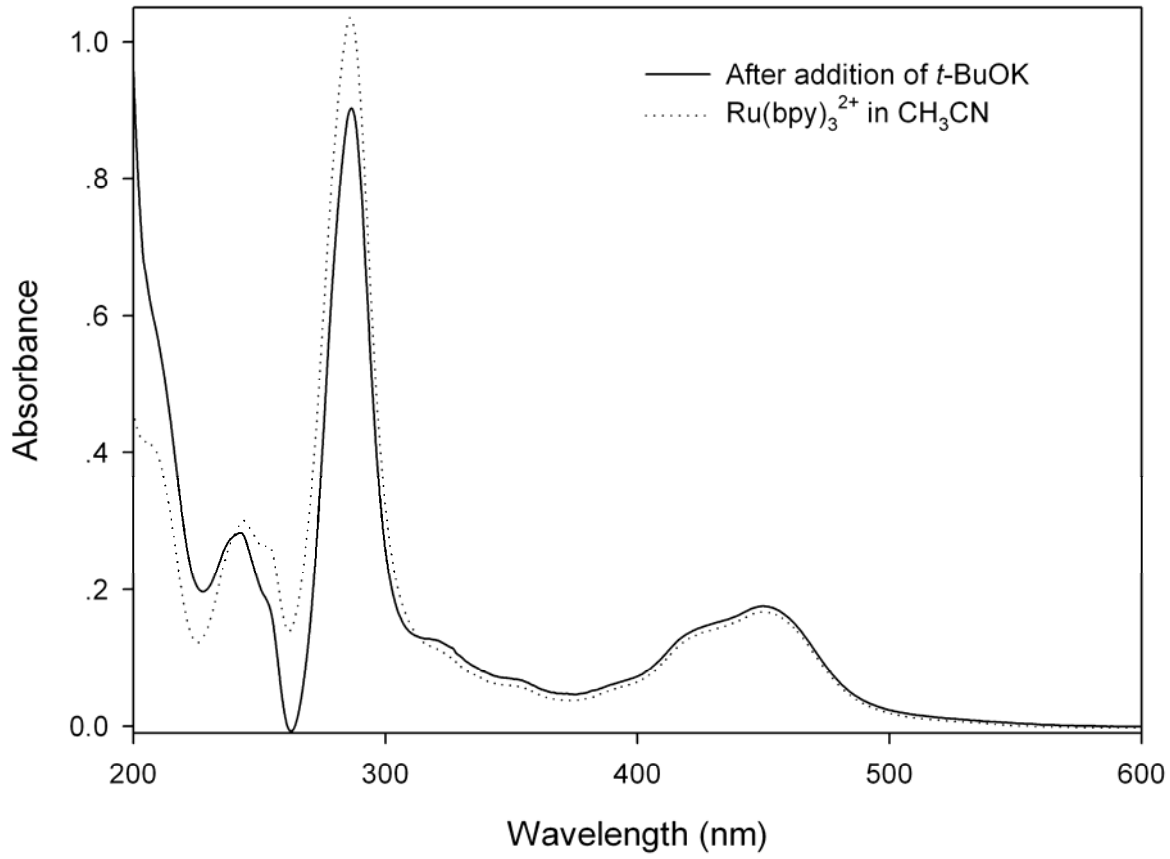

Figure 4.1: UV-Vis spectra of $Ru(bpy)_3^{2+}$ obtained before and after the addition of *tert*-BuOK at 298 K. The resultant solution is very stable, no spectral changes were observed even after 15 hours. Reagent concentration $[Ru(bpy)_3^{2+}] = 1.108 \times 10^{-5}$ M. [*t*-BuOK]/[Ru(II)] mole ratio = 1.84.

Figure 4.1 illustrates the UV-Vis spectrum of $Ru(bpy)_3^{2+}$ obtained after the addition of *t*-BuOK (±2 equivalents). The spectrum of the resultant solution was monitored over a 15 hour's period, and no changes were observed. Compared with the spectrum for $Ru(bpy)_3^{2+}$ in acetonitrile, one can see that there is no significant changes for the broad band, the metal-to-ligand charge transfer (MLCT) transition with maximum at 453 nm. Spectral changes can be observed in the UV region: there are decreases in the absorbance at 261 nm and 286 nm, the wavelengths which have been typically indicated for representing the 2,2'-bipyridine ligand-based π to π* transition.

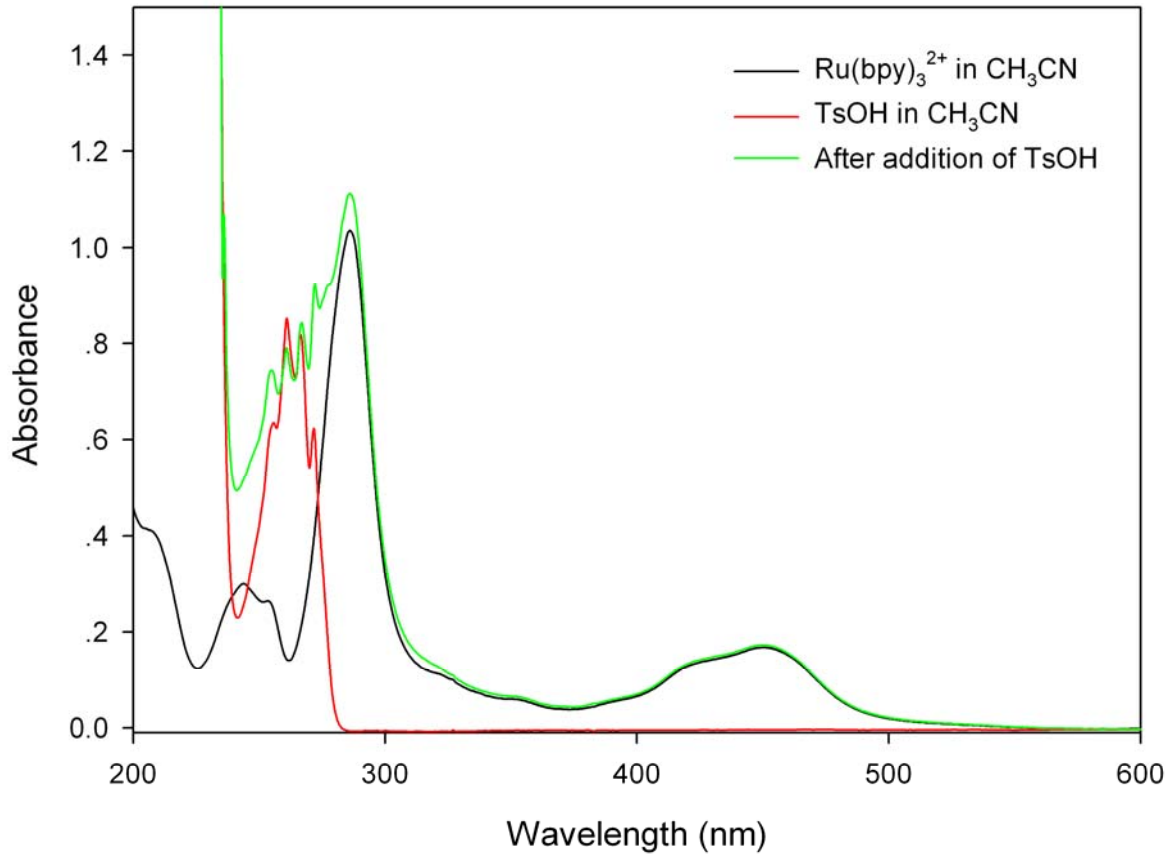

Figure 4.2: The changes in the UV-Vis spectra of $Ru(bpy)_3^{2+}$ obtained after the addition of TsOH at 298 K. Reagent Concentration: $[Ru(bpy)_3^{2+}] = 1.108 \times 10^{-5}$ M; $[TsOH]/[Ru(bpy)_3^{2+}]$ mole ratio = 60.2.

It can be seen from Figure 4.2 that the UV-Vis spectrum of the resultant $Ru(bpy)_3^{2+}$ solution after the addition of TsOH, consists of a series of absorption peaks overlay on each other in the range 250 to 312 nm. However, in comparison with the individual spectra obtained for $Ru(bpy)_3^{2+}$ and TsOH in CH_3CN, respectively, it appears that the UV-Vis spectrum of the resultant solution is a combination of the two abovementioned spectra. This indicates that the same species were present in the resultant solution and implies that there is no reaction between $Ru(bpy)_3^{2+}$ and TsOH in CH_3CN at 298 K under the conditions investigated.

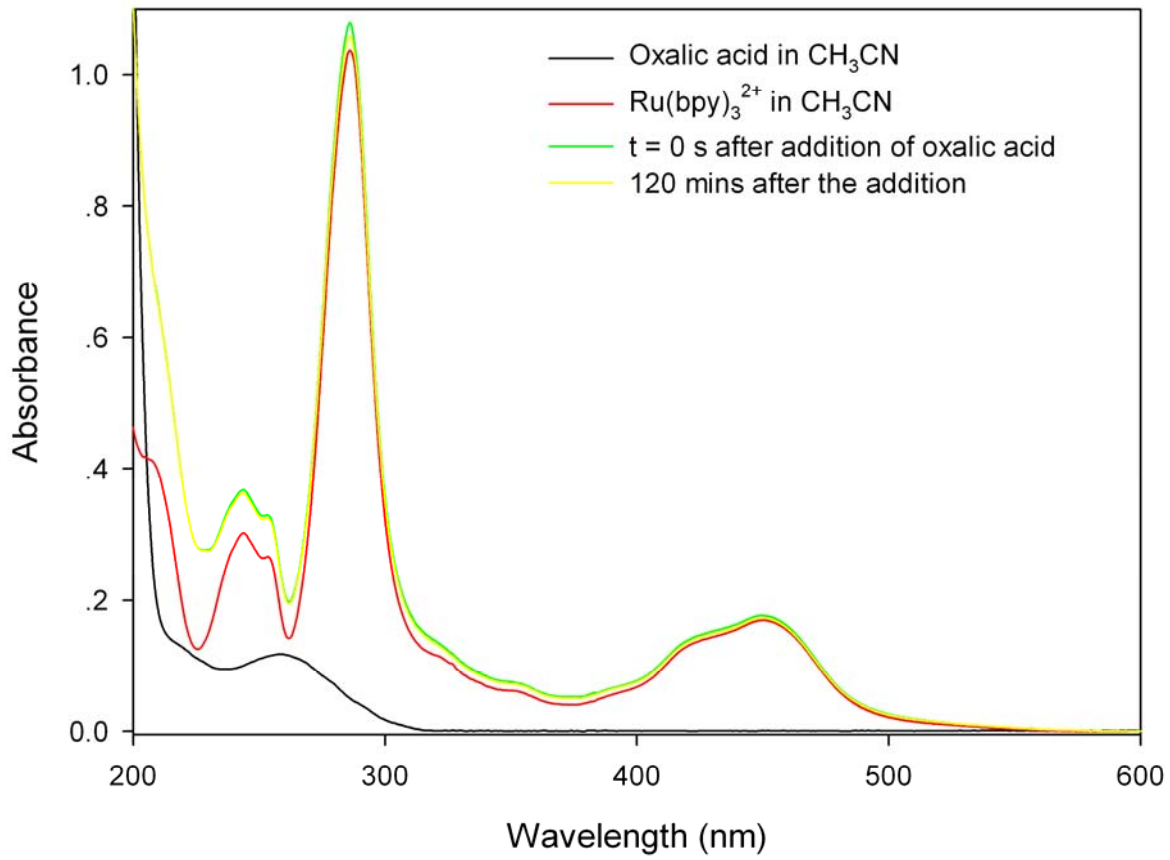

Figure 4.3: Comparison of UV-Vis spectra of $Ru(bpy)_3^{2+}$ obtained in CH_3CN before and after the addition of oxalic acid at 298 K. Only minor spectral changes observed 120 minutes after the addition of acid. Reagent Concentration: $[Ru(bpy)_3^{2+}] = 1.108 \times 10^{-5}$ M. [Oxalic acid]/$[Ru(bpy)_3^{2+}]$ mole ratio = 150.4.

Figure 4.3 shows the change in the UV-Vis spectrum of $Ru(bpy)_3^{2+}$ in CH_3CN at 298 K upon an addition of oxalic acid. Compared with the spectrum obtained for free $Ru(bpy)_3^{2+}$ under the same reaction conditions, one can see that with the addition of oxalic acid, the ligand-centered π to π* transition at 286 nm increases in intensity while there is only a minor change in the intensity of the MLCT transition at 453 nm. The increase in intensity below 300 nm is expected since the oxalic acid exhibits a broad absorption peak in this region. The absorbance of the resultant solution is lifted as a result of the combination of absorptions occurring for both species in the UV region. Furthermore, no further spectral changes were observed during a 120-minute period after the addition of the acid (Figure 4.3). It appears that oxalic acid does not react with $Ru(bpy)_3^{2+}$ under the conditions tested.

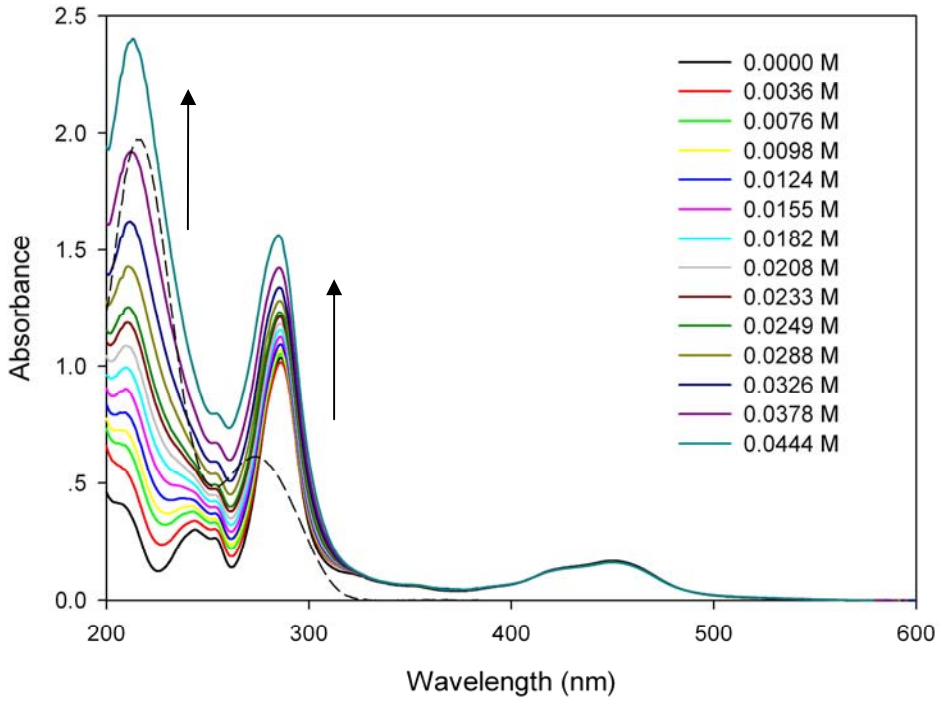

Figure 4.4: UV-Vis spectra illustrating the titration of trifluoroacetic acid with $Ru(bpy)_3^{2+}$ in CH_3CN at 298 K as a function of acid concentration. The direction of the solid arrows indicates the direction of spectrum change with increasing of acid concentration. The dash line shows the UV-Vis spectrum of 0.0444 M trifluoroacetic acid in acetonitrile. $[Ru(bpy)_3^{2+}]$ = 1.108 × 10^{-5} M; trifluoroacetic acid concentration ranges from 0.0000 M to 0.0444 M as denoted by the legend.

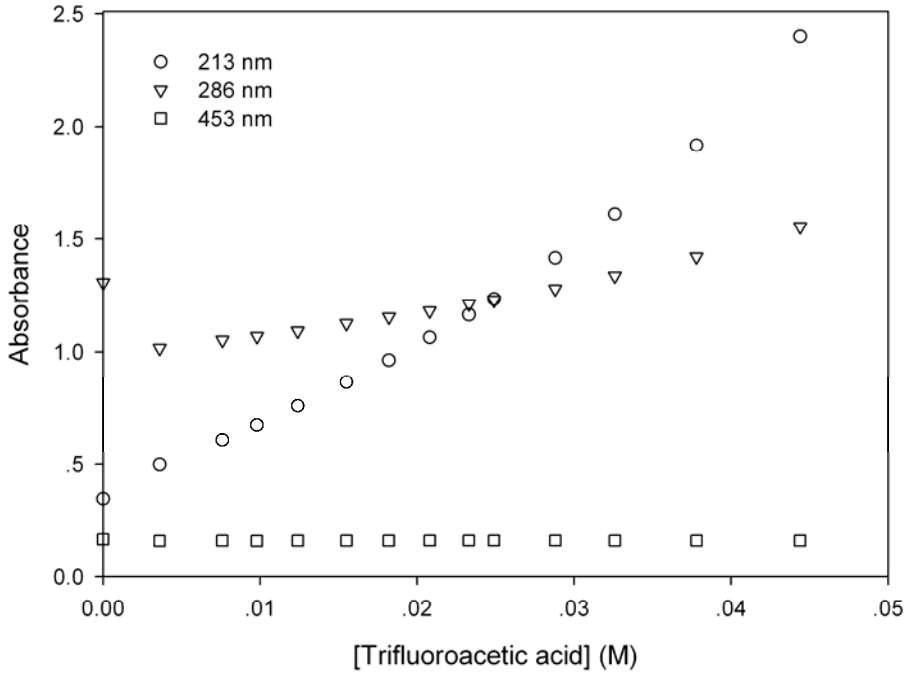

Figure 4.5: The change in absorbance at selected wavelengths as a function of trifluoroacetic acid concentration.

The reactions between $Ru(bpy)_3^{2+}$ and trifluoroacetic acid exhibit a significant increase in absorbance in the UV region between UV-Vis spectra obtained over the range of trifluoroacetic acid concentrations investigated, as illustrated in Figure 4.4. In addition, Figure 4.5 shows the changes in absorbance at 213, 286, and 453 nm, respectively, as a function of trifluoroacetic acid concentration. Notably the broad band with maximum at 453 nm remains relatively constant, irrespective of the trifluoroacetic acid concentration. It appears that the increase in absorbance in the range between 200 and 312 nm is mainly due to the increase of acid concentration. The spectrum of 0.0444 M trifluoroacetic acid in CH_3CN at 298 K (Figure 4.4) shows a broad peak between 254 and 312 nm, and a strong absorption peak in the lower UV region, with a maximum at 213 nm. These two absorption peaks are responsible for the abovementioned spectral changes.

In conclusion, $Ru(bpy)_3^{2+}$ is very stable in non-aqueous media at room temperature and does not easily react with strong organic acids and base. This is confirmed by the spectra of the MLCT band which remained relatively constant under the various reaction conditions.

4.3 Reactions with oxidants

4.3.1 Introduction

In 1966, Hercules and Lytle [30] observed a bright orange emission when an acidic solution of tris(2,2'-bipyridyl) ruthenium (II) was oxidized by solid lead dioxide and subsequently reacted with either concentrated sodium hydroxide or hydrazine. Since then, $Ru(bpy)_3^{3+}$ chemiluminescence has emerged as a versatile detection method for both flow injection analysis and liquid chromatography [28]. Common to all such analytical applications is the generation of $Ru(bpy)_3^{3+}$. There have been a variety of methods employed to obtain the $Ru(bpy)_3^{3+}$ from oxidation of $Ru(bpy)_3^{2+}$ [27, 28, 30, 33]. This section discusses previous studies in this field as well as related studies into the oxidation of $Ru(bpy)_3^{2+}$ by various oxidants, including dichromate, concentrated nitric acid, persulphate, lead dioxide, and cerium (IV).

In order to confirm the redox ability of the oxidants, a table which summarises the redox potentials of the selected oxidants at 298 K, is shown in page 53.

Table 4.1: Half-reactions and standard reduction potentials of the selected oxidants at 298 K [31].

Half-reaction	Standard reduction potential (V)
$Cr_2O_7^{2-}{}_{(aq)} + 14\ H^+{}_{(aq)} + 6\ e^- \text{-----> } 2\ Cr^{3+}{}_{(aq)} + 7\ H_2O$	+1.33
$NO_3^-{}_{(aq)} + 4\ H^+{}_{(aq)} + 3\ e^- \text{-----> } NO_{(g)} + 2\ H_2O$	+0.96
$S_2O_8^{2-} + 2H^+ + 2e^- \text{-----> } 2\ HSO_4^-$ [32]	+2.10 [32]
$PbO_{2(s)} + 4\ H^+{}_{(aq)} + SO_4^{2-}{}_{(aq)} + 2\ e^- \text{-----> } PbSO_{4(s)} + 2\ H_2O$	+1.70
$Ce^{4+}{}_{(aq)} + e^- \text{-----> } Ce^{3+}{}_{(aq)}$	+1.61

Table 4.1 shows the half reactions and standard redox potentials for the oxidants used in this study. From Chapter 3 (page 40) the redox potential for Ru(II)/Ru(III) couple is E = 0.96 V. Technically all the above-mentioned oxidants are capable of oxidizing $Ru(bpy)_3^{2+}$ to $Ru(bpy)_3^{3+}$, since the Ru(II)/Ru(III) couple has lower redox potential.

4.3.2 Experimental

In this section, high purity distilled water (HP H_2O) was used as the reaction medium. The preparation of the $Ru(bpy)_3^{2+}$ stock in aqueous medium is discussed in Chapter 3 (Section 3.4, page 32). High purity distilled water was used as reference for recording the UV-Vis spectra. The reaction vessel was kept in the dark throughout the titrations to prevent the photo-reduction of the resultant $Ru(bpy)_3^{3+}$.

4.3.2.1 Oxidizing agent: dichromate

The dichromate solution was prepared and standardised according to the method in Chapter 2 (Section 2.3.2, page 24). For the $Ru(bpy)_3^{2+}$ stock solution, a ruthenium concentration of 1.108×10^{-5} M was determined by the ICP-MS analysis, which is described in more detail in Chapter 3 (Section 3.4, page 32).

The standardised dichromate solution was titrated with $Ru(bpy)_3^{2+}$ solution following the procedure described in Chapter 2 (Section 2.4, page 25). According to the half reactions of the redox species (page 54). A sharp break/end-point was expected in the titration plot.

$$Cr_2O_7^{2-}{}_{(aq)} + 14\ H^+{}_{(aq)} + 6\ e^- \text{-----> } 2\ Cr^{3+}{}_{(aq)} + 7\ H_2O$$

$$Ru^{2+} \text{-----> } Ru^{3+} + e^-$$

$$Cr_2O_7^{2-}{}_{(aq)} + 14\ H^+{}_{(aq)} + 6\ Ru^{2+} \text{-----> } 6\ Ru^{3+} + 2\ Cr^{3+}{}_{(aq)} + 7\ H_2O$$

The mole ratio at the end-point indicates the composition of the resultant species in the reaction solution. For example, the overall reaction equation between $Ru(bpy)_3^{2+}$ and dichromate illustrated above, shows the reaction would only occur at a $[Cr_2O_7^{2-}]/[Ru(II)]$ mole ratio equal to 0.2, therefore the amount of dichromate required to initiate the oxidation was calculated. The spectra were recorded and shown in the next section (Section 4.3.3).

4.3.2.2 Oxidizing agent: nitric acid

Nitric acid was used as received from Merck. The same titration procedure as described in Chapter 2 (Section 2.4, page 25) was performed. The UV-Vis spectrum was recorded after the addition of nitric acid.

4.3.2.3 Oxidizing agent: persulphate

Persulphate is a strong oxidant that has been widely used for initiating emulsion polymerization reactions, clarifying swimming pools, hair bleaching, and micro-etching of copper printed circuit boards [32]. In this study, a 0.01 M potassium persulphate solution was prepared by dissolving a calculated amount of potassium persulphate solids in HP H_2O. General titration procedures with $Ru(bpy)_3^{2+}$ were followed as described in Chapter 2 (page 25).

4.3.2.4 Oxidizing agent: PbO_2

For the reactions of $Ru(bpy)_3^{2+}$ with PbO_2, a 25 ml of $Ru(bpy)_3^{2+}$ solution was first pipetted into the reaction vessel, and 8.1587 mg of PbO_2 powder was added. A 10 ml sample of the mixture was then transferred and centrifuged. A 3 mL aliquot of centrifuged mixture solution was then added into the cell. The reaction progress was followed in one of two ways: firstly to observe the oxidation reaction between $Ru(bpy)_3^{2+}$ and PbO_2, the reaction progress was followed using a spectrophotometer. Secondly to observe the oxidation reaction between $Ru(bpy)_3^{2+}$ and PbO_2 in the presence of sulphuric acid, the UV-Vis spectrum of the mixture was recorded as the first scan. A measured volume of 1.0 M H_2SO_4 was then added into the cuvette

immediately prior to the start of the second scan. The reaction time was started at the time of addition of H_2SO_4. The progress of the reaction was followed using a spectrophotometer.

4.3.2.5 Oxidizing agent: Ce(IV)

The reactions between $Ru(bpy)_3^{2+}$ and Ce(IV) in aqueous medium are discussed in more detail in the next chapter.

4.3.3 Results and discussions

4.3.3.1 Reaction with dichromate

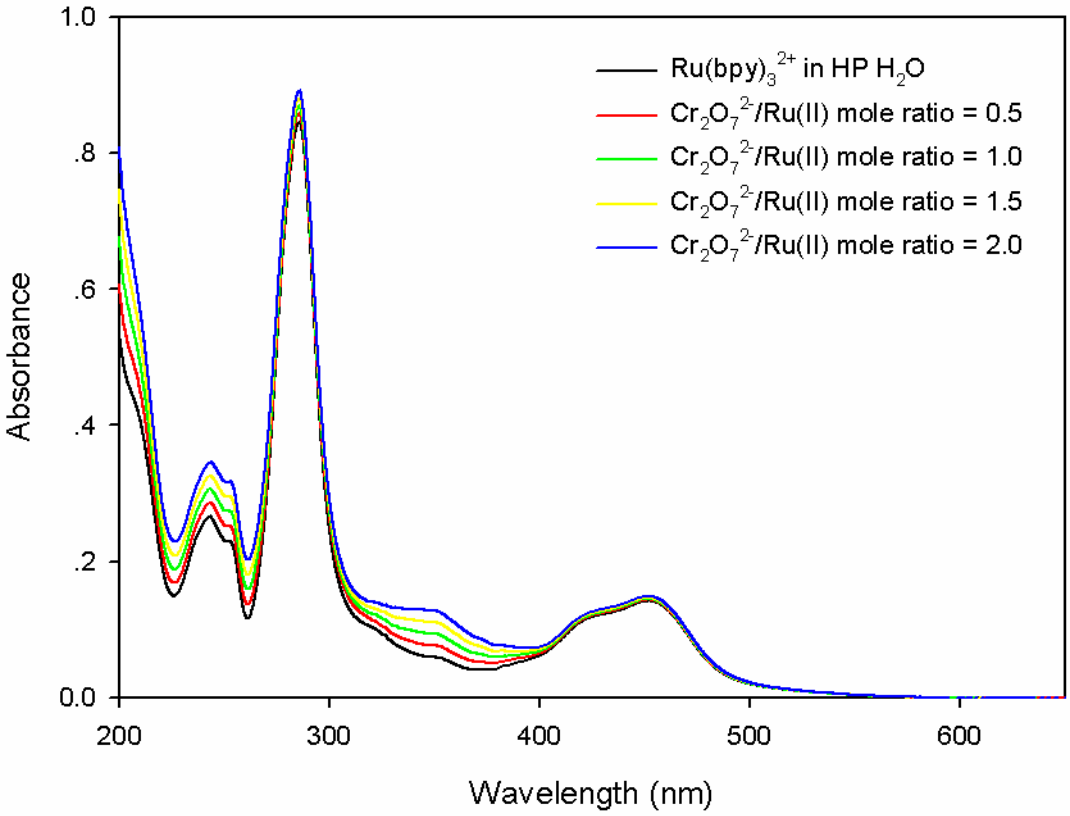

Figure 4.6: UV-Vis spectra show the oxidation of $Ru(bpy)_3^{2+}$ with dichromate as a function of $Cr_2O_7^{2-}$/Ru(II) mole ratio at 298 K. Reagent concentrations: $[Ru(bpy)_3^{2+}] = 1.108 \times 10^{-5}$ M, and $[Cr_2O_7^{2-}] = 1.000 \times 10^{-3}$ M in 0.1 M H_2SO_4. The $[Cr_2O_7^{2-}]/[Ru(II)]$ mole ratio are denoted by the legend. The spectrum of $Ru(bpy)_3^{2+}$ in HP H_2O at 298 K is included for comparison.

According to the possible half reactions between dichromate and Ru(II), a minimum $[Cr_2O_7^{2-}]/[Ru(II)]$ mole ratio of 0.2, as well as an acidic environment were required for the oxidation to take place. Figure 4.6 shows spectral changes upon the addition of $Cr_2O_7^{2-}$ to the $Ru(bpy)_3^{2+}$ solution in the presence of 0.1 M H_2SO_4 at different

$[Cr_2O_7^{2-}]$/[Ru(II)] mole ratios. No end point was observed. It appears that the oxidation reaction of $Ru(bpy)_3^{2+}$ occurs very slowly at room temperature. The rise of absorbance from 200 to 400 nm was possibly due to the increase of dichromate concentration. It appears that a stronger oxidising agent is needed for the oxidation of $Ru(bpy)_3^{2+}$ at room temperature.

4.3.3.2 Reaction with nitric acid

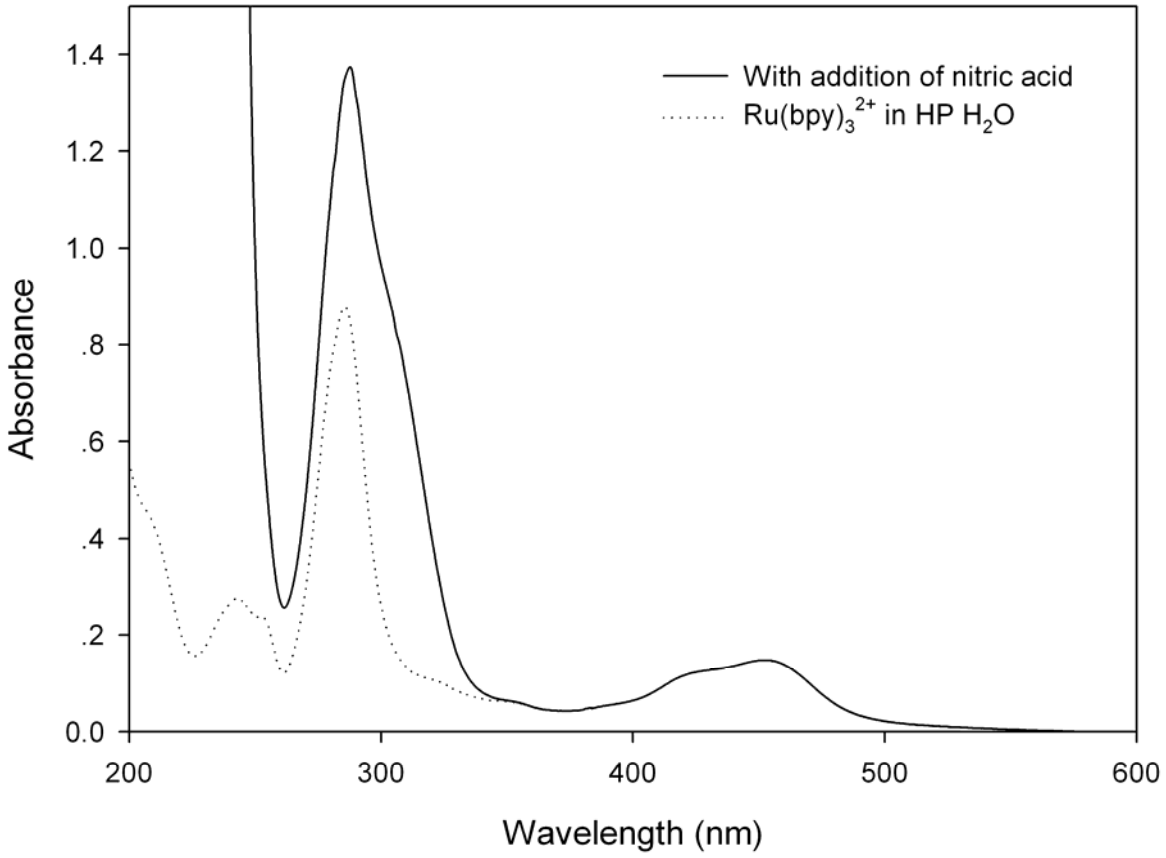

Figure 4.7: Spectral changes of a $Ru(bpy)_3^{2+}$ solution upon the addition of concentrated nitric acid at 298 K. Reagent concentrations: $[Ru(bpy)_3^{2+}]$ = 1.108 x 10^{-5} M and $[HNO_3]$ = 14.545 M. $[HNO_3]$/[Ru(II)] = 8749.3. The spectrum of pure $Ru(bpy)_3^{2+}$ in HP H_2O at 298 K is included for comparison.

Burstall [33] showed the use of concentrated nitric acid for oxidising $Ru(bpy)_3^{2+}$. However, Figure 4.7 shows the UV-Vis spectrum of the resultant solution upon the addition of concentrated nitric acid (14.545 M) at room temperature. The spectrum in the UV region is dominated by intense absorption peak from the strong acid. Comparing the spectra with that of pure $Ru(bpy)_3^{2+}$ in HP H_2O at 298 K, the intensity of the ligand-centered π to π* transition band at 286 nm increases upon the addition

of the acid. This could be explained as the overlay of the strong absorption band from nitric acid caused the increase of absorbance. The MLCT band at 453 nm remains unchanged. The oxidation of $Ru(bpy)_3^{2+}$ by nitric acid was not successful under the standard reaction conditions.

4.3.3.3 Reaction with persulphate

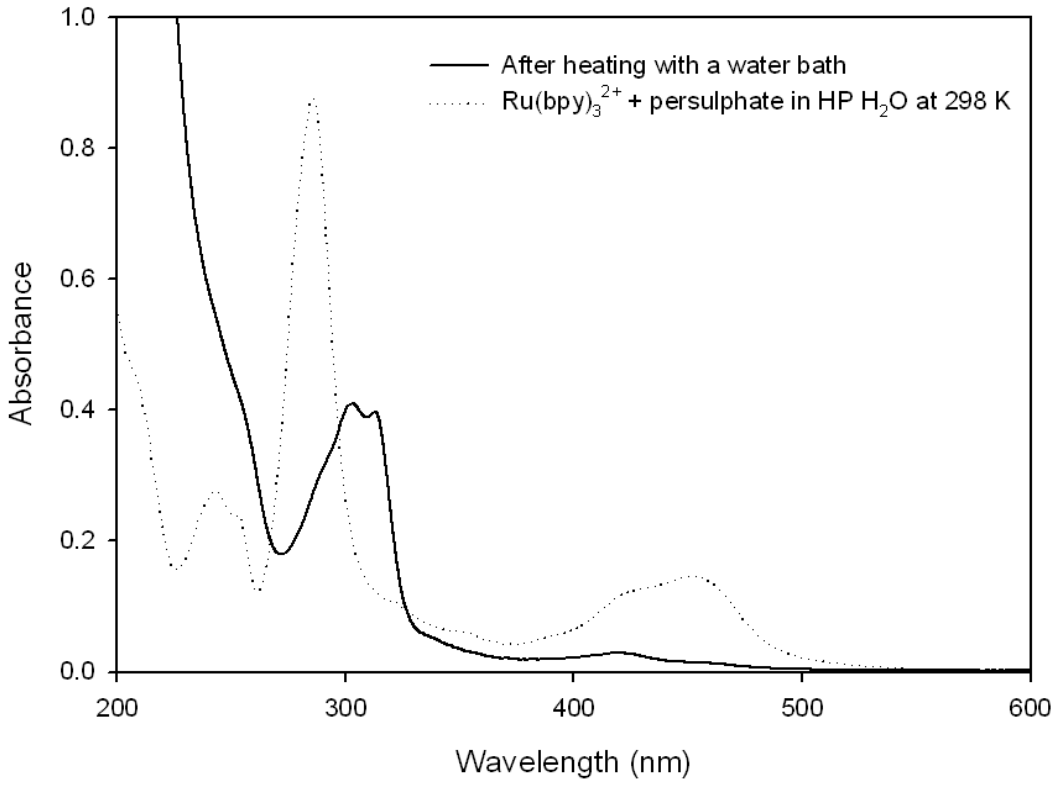

Figure 4.8: Comparison of spectral changes upon an addition of persulphate to a $Ru(bpy)_3^{2+}$ solution at 298 K and after heating the mixture with a water bath at 353 K. Reagent concentrations: $[Ru(bpy)_3^{2+}]$ = 1.108 x 10^{-5} M, $[S_2O_8^{2-}]$ = 0.01 M. $[S_2O_8^{2-}]/[Ru(II)]$ = 541.5.

Figure 4.8 illustrates the spectral changes upon an addition of persulphate to the $Ru(bpy)_3^{2+}$ solution at 353 K. No spectral changes could be observed after the addition at room temperature. According to the redox potential of $S_2O_8^{2-}/HSO_4^-$ couple (E = 2.10 V) from Table 4.1, persulphate is a very powerful oxidizing agent. In addition, the internal reorganization energy for $S_2O_8^{2-}$ is about 550 $kJ.mol^{-1}$, while this energy for ruthenium complexes is quite low (5-10 $kJ.mol^{-1}$) [34]. Consequently, oxidation of $Ru(bpy)_3^{2+}$ by $S_2O_8^{2-}$ was expected to be rapid. However, even up to a $[S_2O_8^{2-}]/[Ru(II)]$ mole ratio at 541.5, the oxidation did not take place under the standard reaction conditions. Interestingly, upon heating the solution mixture at

353 K using a water bath, the oxidation occurred rapidly. As shown in Figure 4.8, the intensity of the MLCT band at 453 nm decreases, which is evidence of Ru(II) being oxidized to Ru(III). The mechanism of the reaction can be explained as followed: with heat was applied to the system, persulphate was induced to form sulphate radicals:

$$S_2O_8^{2-} + \text{heat} \text{ -----> } SO_4^{\bullet-} + SO_4^{\bullet-}$$ [32]

The sulphate radical is one of the strongest oxidizing species with a redox potential estimated to be 2.6 V [32]. Therefore, Ru(II) was readily oxidized to form Ru(III) species sufficiently, but only when heat is applied.

4.3.3.4 Reaction with PbO_2

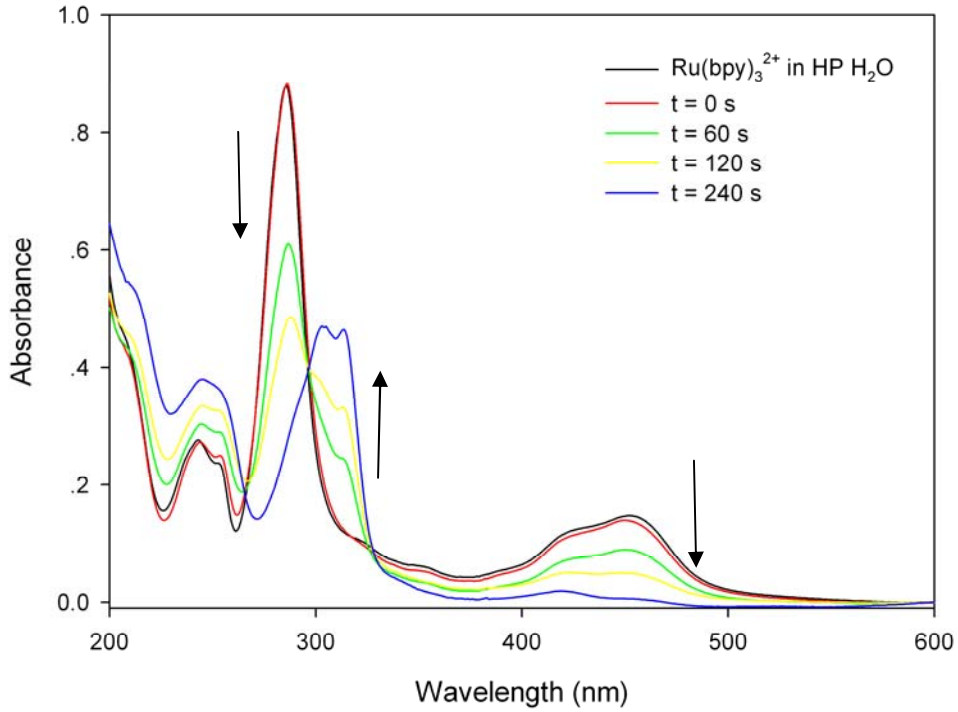

Figure 4.9: UV-Vis spectra depicting the oxidation of $Ru(bpy)_3^{2+}$ by excess PbO_2 upon the addition of sulphuric acid at 298 K. The final H_2SO_4 concentration was at 0.00332 M. The solid arrows indicate the directions of the absorbance changes as a function of time. The time intervals between each spectrum recorded are denoted by the legend, as the reaction time was started at the time of addition of H_2SO_4. $[Ru(bpy)_3^{2+}] = 1.108 \times 10^{-5}$ M. The spectrum of $Ru(bpy)_3^{2+}$ in HP H_2O at 298 K is included for comparison.

The use of PbO_2 to oxidize $Ru(bpy)_3^{2+}$ has been studied since its first discovery by Hercules and Lytle in 1966 [30]. Figure 4.9 shows the UV-Vis spectra obtained for the oxidation of $Ru(bpy)_3^{2+}$ by PbO_2 in the presence of sulphuric acid at 298 K. Notably in the absence of sulphuric acid, the oxidation develops very slowly at room temperature. After the addition of the acid, the oxidation occurs rapidly and is

completed within two minutes. The progress curve shown below (Figure 4.10) illustrates the change in absorbance at selected wavelengths as a function of time.

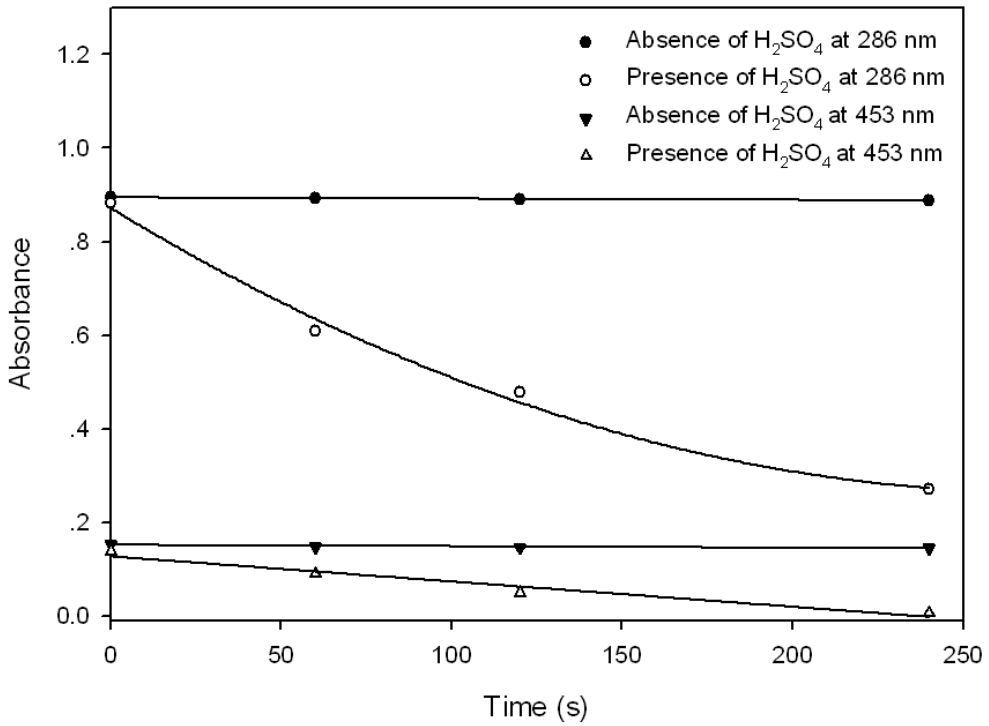

Figure 4.10: Progress curves for the oxidation of $Ru(bpy)_3^{2+}$ by excess PbO_2 in the presence and absence of sulphuric acid at 298 K as a function of time. Final $[H_2SO_4] = 0.00332$ M; $[Ru(bpy)_3^{2+}] = 1.108 \times 10^{-5}$ M.

Clearly, the H_2SO_4 acts as a catalyst in this reaction. This result obtained compare favourably with those obtained by Balcerzak [35], who showed that the ruthenium and osmium in the form of sulphate complexes were more readily oxidized to higher oxidation states.

In this reaction the amount of PbO_2 was in excess, but it is not possible in this case to determine the ratio that PbO_2 reacts with $Ru(bpy)_3^{2+}$, since PbO_2 is a solid and is effectively removed from the reaction by centrifugation. This is not a problem for Ce(IV) since the concentration of Ce(IV) can be accurately determined. For more detailed discussions see Chapter 5.

In conclusion, amongst the common oxidants in our laboratory, persulphate and lead dioxide was found to easily oxidize $Ru(bpy)_3^{2+}$ to $Ru(bpy)_3^{3+}$ in the presence of heat and H_2SO_4 respectively.

4.4 Reactions with arsenazo III

4.4.1 Introduction

The aim of this work was to try to develop a new analytical method for the determination of ruthenium concentration as an alternative to ICP-MS analysis (see Section 3.4, page 32). Arsenazo III (Figure 4.11) {3,6-bis[(2-arsonophenyl)azo]-4,5-dihydroxy-2,7-naphthalene-dissulphonic acid}, is a bisazo reagent (contains azo R-N=N-R'), and was first synthesised by Savvin in 1959 [36-39]. It is mainly used as a chromogenic reagent for photometric analysis. It can react and form very stable complexes with a variety of metal ions. Many of the complexes of arsenazo III with metal ions have high molar absorptivities, which enable even dilute solutions to be analyzed by visual methods [36-39].

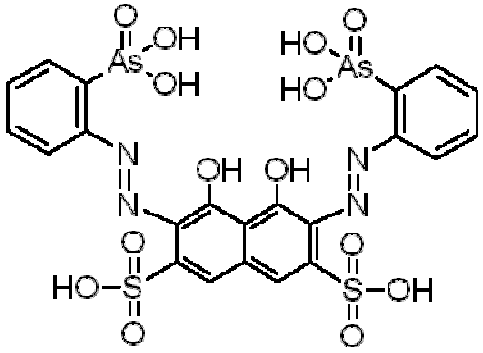

Figure 4.11: Structure of arsenazo III.

In this section, arsenazo III was used in the hope of forming complexes with ruthenium (III) metal ion, so that the ruthenium concentration can be determined using a spectrophotometric method.

4.4.2 Experimental

Arsenazo III stock solution (1.0×10^{-4} M) was prepared by dissolving an appropriate amount of the arsenazo III acid solid in high purity distilled water. A stock solution of ruthenium (III) (1.0×10^{-3} M) was freshly prepared by dissolving a calculated amount of ruthenium trichloride ($RuCl_3.3H_2O$) in high purity distilled water. The spectral changes of the arsenazo III solution upon the addition of $RuCl_3$ was monitored following the procedure described in Section 2.5 (page 26). In the case of investigating the interactions between $RuCl_3$ and water, a concentration of 1.0×10^{-4} M experimental solution was made by pipetting appropriate amounts of

freshly prepared ruthenium stock solution (1.0 x 10^{-3} M) into a 100 ml volumetric flask and filled up to the mark with HP distilled water. 3 ml of this solution was then pipetted into a cuvette; the progress of the reaction was followed using spectrophotometer.

4.4.3 Results and discussions

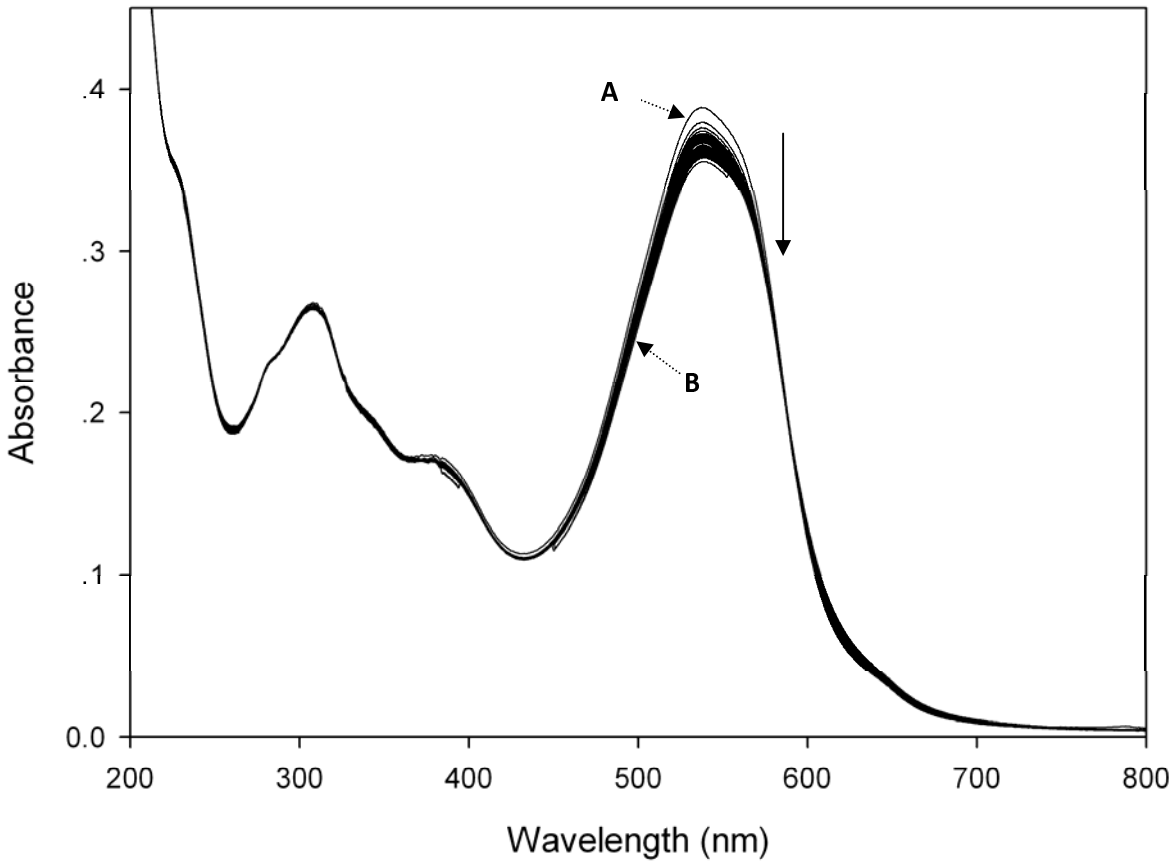

Figure 4.12: Spectral changes resulting from the initial addition of $RuCl_3.3H_2O$ to an arsenazo III solution at 318 K as a function of time. The spectra denoted by A, and B respectively refer to the spectra recorded at t = 0, and t = 168 minutes, as the reaction time was started at the time of addition of $RuCl_3.3H_2O$. [AzIII]/[Ru(III)] mole ratio = 4.82. Reagent concentrations: [$RuCl_3.3H_2O$] = 1 x 10^{-4} M, [AzIII] = 1.0 x 10^{-5} M.

Figure 4.12 shows the spectral changes upon the addition of $RuCl_3.3H_2O$ to an arsenazo III solution at 318 K. The solid arrow indicates the direction of absorbance change with time. The spectra show a small decrease in absorbance with an increasing of time. Other metal ions typically show complexation absorption bands at 605 and 652 nm [10]. In this study no absorption bands could be observed at these two wavelengths. It therefore appears that under the condition studied ruthenium

does not form a complex with arsenazo III. Interestingly, it was observed that the $RuCl_3.3H_2O$ stock solution changed its colour from dark reddish brown to light grey during the experiment. This promoted an investigation on the spectral behavior and solution stabilities of $RuCl_3.3H_2O$ at 318 K (see Figure 4.13 below).

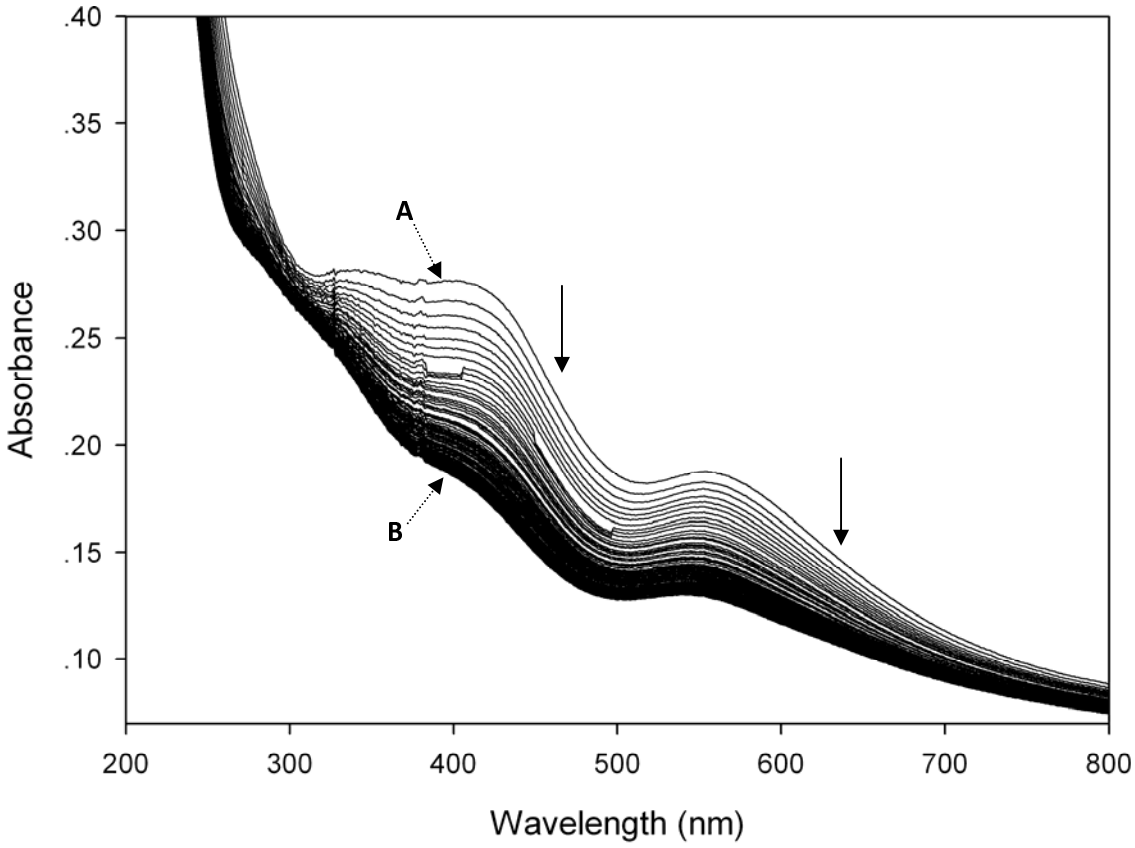

Figure 4.13: Illustration of spectra changes of $RuCl_3.3H_2O$ in solution at 318 K as a function of time. The spectra denoted by A and B respectively refer to the spectra of freshly prepared $RuCl_3.3H_2O$ in solution (A) and the spectra recorded after 258 minutes (B); the solid arrow indicates the direction of absorbance change with time. [$RuCl_3.3H_2O$] = 1.0 x 10^{-4} M.

Figure 4.13 shows the change in UV-Vis spectra upon storing $RuCl_3.3H_2O$ in solution at 318 K as a function of time. It is clear that the absorbance decreases in the range of wavelengths investigated. Compared with Figure 4.12, it appears that the decrease in absorbance in Figure 4.12 could be a result of aquation of $RuCl_3.3H_2O$ in solution. This confirms that there is no evidence depicting the complex formation between arsenazo III and Ru(III) at 318 K.

The reaction of ruthenium (III) chloride in aqueous solution is a complicated matter itself. A number of reports in the literature [40-42] are available regarding to the

aquation of $RuCl_3$. Khan and his colleagues [40] proposed a reaction mechanism that has widely gained acceptance:

$$[RuCl_3(H_2O)_3] + H_2O \longleftrightarrow [RuCl_2(H_2O)_4]^+ + Cl^-$$

$$[RuCl_2(H_2O)_4]^+ + H_2O \longleftrightarrow [RuCl(H_2O)_5]^{2+} + Cl^-$$

They indicate that $[RuCl_2(H_2O)_4]^+$ is the dominant species in the solution. However, a number of factors could influence this equilibrium, such as temperature, pH of the solution, ionic strength, etc. Since the primary focus of this section is to develop an analytical method in order to determine the ruthenium concentration, the aquation of the ruthenium (III) chloride was not considered further.

In conclusion, although arsenazo III is an excellent colour reagent for the photometric analysis of many metal ions, it was found to be unsuitable for the determination of ruthenium. However, further effort to establish a reliable method for determining ruthenium concentration using photometric analysis certainly deserves consideration.

Chapter 5

Reactions of tris(2,2'-bipyridyl) ruthenium (II) with Ce(IV)

5.1 Introduction

This chapter focuses on the oxidation reaction of $Ru(bpy)_3^{2+}$ with cerium (IV). It was found that the resultant $Ru(bpy)_3^{3+}$ gradually recovers back to $Ru(bpy)_3^{2+}$ when stored under room light. The regeneration of $Ru(bpy)_3^{2+}$ was investigated by observing the spectral changes of the reaction solution. Various reaction models were simulated and rate constants calculated. The factors that affected the regeneration of $Ru(bpy)_3^{2+}$ are also discussed.

5.2 Reaction of tris(2,2'-bipyridyl) ruthenium (II) with Ce(IV)

5.2.1 Introduction

Ce(IV) is a powerful oxidant with redox potential at +1.61 V [31]. Rubinstein and Bard [29] reported the use of Ce(IV) to effectively produce $Ru(bpy)_3^{3+}$ from $Ru(bpy)_3^{2+}$:

$$Ce^{4+} + e^- \longrightarrow Ce^{3+}$$

$$Ru^{2+} \longrightarrow Ru^{3+} + e^-$$

They also reported that Ce(IV) is a better oxidant than PbO_2 to oxidize Ru(II) since Ce(IV) is a one-electron oxidant which reacts efficiently with Ru(II). The solid PbO_2 on the other hand undergoes a direct two-electron oxidation reaction which is ineffective and slow.

In this section, the Ru(II) oxidation mechanism was studied by spectrophotometric monitoring of the changes in the solution absorbance after addition of the Ce(IV). The spectra at different [Ce(IV)]/[Ru(II)] mole ratios were recorded.

5.2.2 Experimental

A 1.108 x 10^{-5} M $Ru(bpy)_3^{2+}$ stock solution was prepared and standardized according to the methods described in Chapter 3 (see Section 3.4, page 32). The preparation and standardisation procedures for the cerium (IV) solution were explained in Chapter 2 (Section 2.3.2, page 24).

The following experimental procedure was followed: 25 ml of 1.108 x 10^{-5} M $Ru(bpy)_3^{2+}$ stock solution was transferred quantitatively into a double-walled reaction flask. A measured volume of 3.000 x 10^{-5} M Ce(IV) solution was then added with a Metrohm 765 dosimat. After the reaction had settled sufficiently, a 3-ml sample was pipetted into a cuvette and the spectrum was recorded. The content of the cuvette was then emptied back into the reaction flask before the addition of the next amount of Ce(IV) solution. The reaction solution flask was kept in dark as much as possible, to prevent any photosensitive reductions occurring during the titration. The results are shown in the next section.

The sulphuric acid concentration is very important for the stability of the Ce(IV) solution since Ce(IV) has a high charge density and is thus easily hydrolyzed. To avoid the complex hydrolysis phenomena that occurs above pH 1 [43], the experimental Ce(IV) solutions were prepared in 0.1 M H_2SO_4. It was observed that 3.000 x 10^{-5} M Ce(IV) in 0.1 M H_2SO_4 gave consistent values during titrations.

As mentioned in Chapter 4 (page 59), in the presence of sulphuric acid the ruthenium (II) is more readily oxidized to higher oxidation states with the oxidant as after each addition of Ce(IV) into the $Ru(bpy)_3^{2+}$ solution, the H_2SO_4 concentration also increases. Table 5.1 (page 66) shows some examples of addition of Ce(IV) in the mole ratio titrations and the corresponding H_2SO_4 concentrations in solution.

Table 5.1: Examples of [Ce(IV)]/[Ru(II)] mole ratio titrations data and corresponding H_2SO_4 concentrations in solution. Reagent concentration: [Ce(IV)] = 3.000 x 10^{-5} M in 0.1 M H_2SO_4.

Volume of Ce(IV) added (ml)	[Ce(IV)]/[Ru(II)] mole ratio	[H_2SO_4] (x 10^{-2} M)
1.10	0.119	0.421
4.60	0.497	1.554
7.40	0.800	2.284
9.20	0.995	2.690
12.20	1.319	3.279
15.70	1.697	3.857
18.70	2.022	4.279

Therefore, it is important to observe whether if any spectral changes of $Ru(bpy)_3^{2+}$ was caused by the increase of H_2SO_4 concentrations. The same experimental procedure was followed with 0.100 M H_2SO_4 as a titrant instead of Ce(IV). The spectra were recorded as shown in Figure 5.1 below.

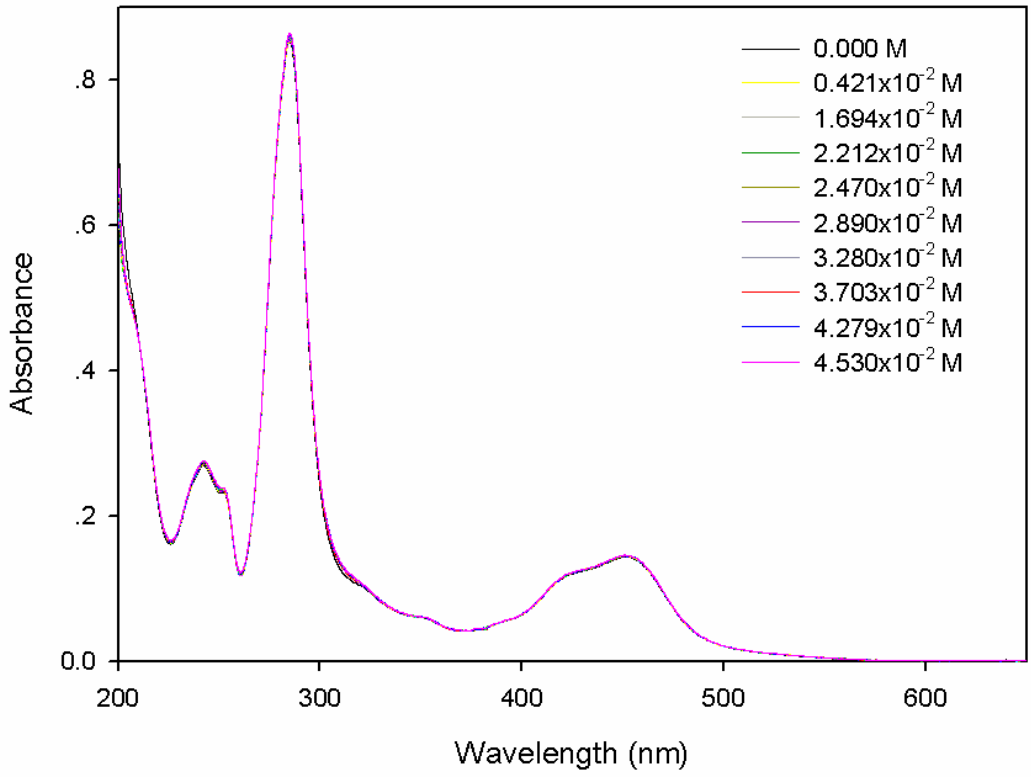

Figure 5.1: UV-Vis spectra of $Ru(bpy)_3^{2+}$ solution as a function of H_2SO_4 concentration. Reagent concentrations: [$Ru(bpy)_3^{2+}$] = 1.108 x 10^{-5} M; [H_2SO_4] = 0.100 M. Final H_2SO_4 concentrations are denoted in the legend.

Figure 5.1 shows the UV-Vis spectra of $Ru(bpy)_3^{2+}$ solutions upon the addition of H_2SO_4. It was found that there was no spectral changes of $Ru(bpy)_3^{2+}$ solution upon the increase of H_2SO_4 concentration in the titration range. The presence of H_2SO_4 provided an acidic environment for the oxidation.

5.2.3 Results and discussions

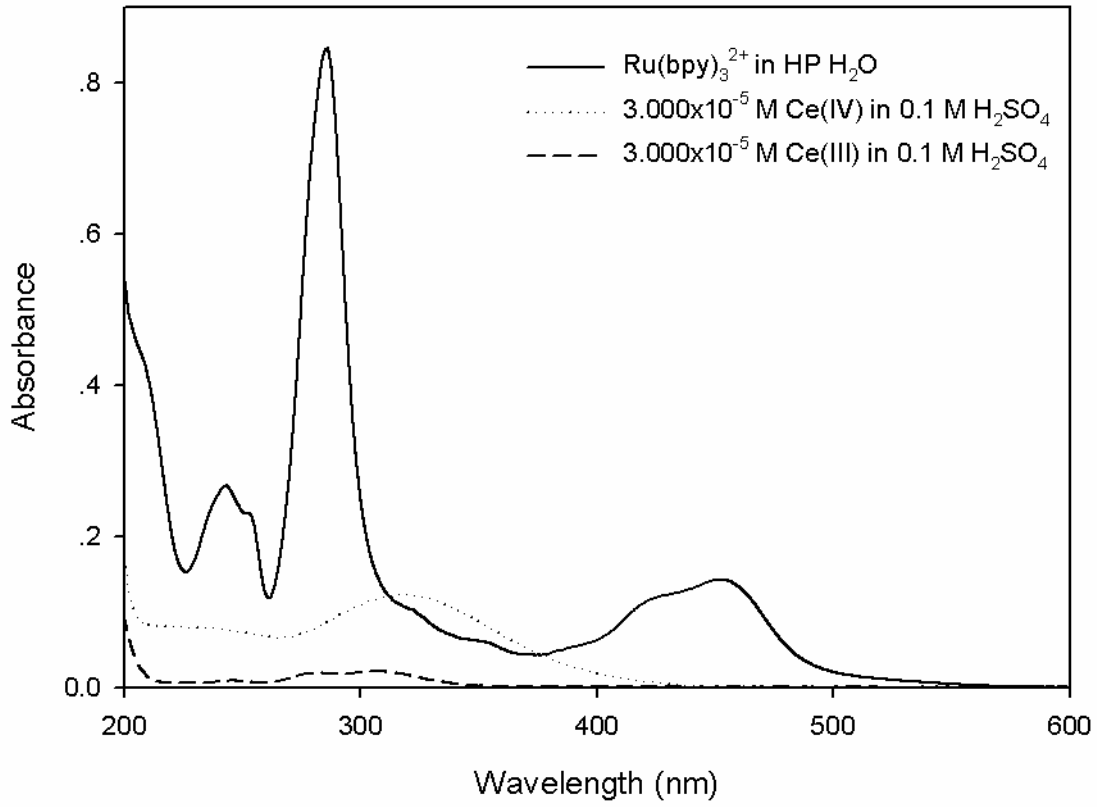

Figure 5.2: UV-Vis spectra of $Ru(bpy)_3^{2+}$ compared with Ce(IV) and Ce(III) in the wavelength region of interest. $[Ru(bpy)_3^{2+}] = 1.108 \times 10^{-5}$ M, Ce(III) and Ce(IV) concentrations are denoted in the legend.

The tris(2,2'-bipyridyl) ruthenium (II) solution on its own is yellow-orange in colour. The spectrum of such a solution is shown in Figure 5.2 above. Also for comparison the spectrum of an Ce(IV) solution is shown. It is clear that the Ce(IV) does not absorb significantly at 453 nm, but it does absorb strongly at 318 nm. After the oxidation Ce(IV) would be reduced to Ce(III), the spectrum of Ce(III) shows there is no interference in the visible region, and only absorbs slightly in the UV region.

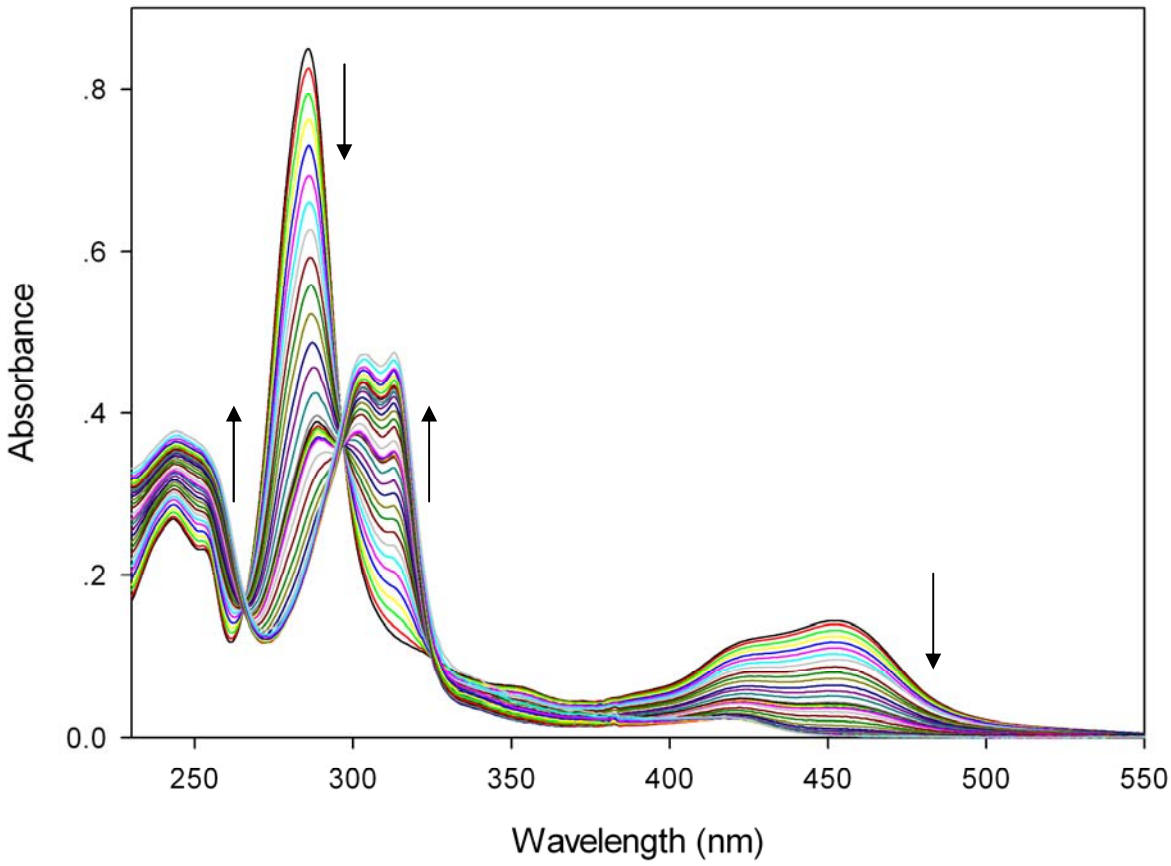

Figure 5.3: UV-Vis spectra of the $Ru(bpy)_3^{2+}$ oxidation by addition of different amounts of Ce(IV) solution. Reagent concentrations: $[Ru(bpy)_3^{2+}]$ = 1.108 x 10^{-5} M and [Ce(IV)] = 3.000 x 10^{-5} M in 0.1 M H_2SO_4. The arrows indicate the direction of the absorbance changes with an increase in the Ce(IV) concentration.

Figure 5.3 illustrates the changes in the UV-Vis spectra of $Ru(bpy)_3^{2+}$ as a function of Ce(IV) concentrations - a trend typical of the $Ru(bpy)_3^{2+}$ oxidation. Upon addition of Ce(IV) to $Ru(bpy)_3^{2+}$, a definite colour change in the solution could be noted, starting with a yellow-orange $Ru(bpy)_3^{2+}$ solution becoming light yellow and finally ending with a colourless solution.

In considering Figure 5.3 above, the absorbance peaks at 286 and 453 nm decrease upon the addition of Ce(IV) to the $Ru(bpy)_3^{2+}$ solution, while a doublet arises at 304 and 313 nm. Typically, the absorbance peak at 453 nm is due to the metal-to-ligand charge transfer (MLCT), caused by the transition from a dπ metal orbital to a ligand based orbital. The decrease of the absorbance peak at 453 nm indicates the oxidation reaction of $Ru(bpy)_3^{2+}$. Furthermore, relatively clear isosbestic points were

observed at 264, 299, and 323 nm, and these points shifted slightly upon increasing the Ce(IV) concentration.

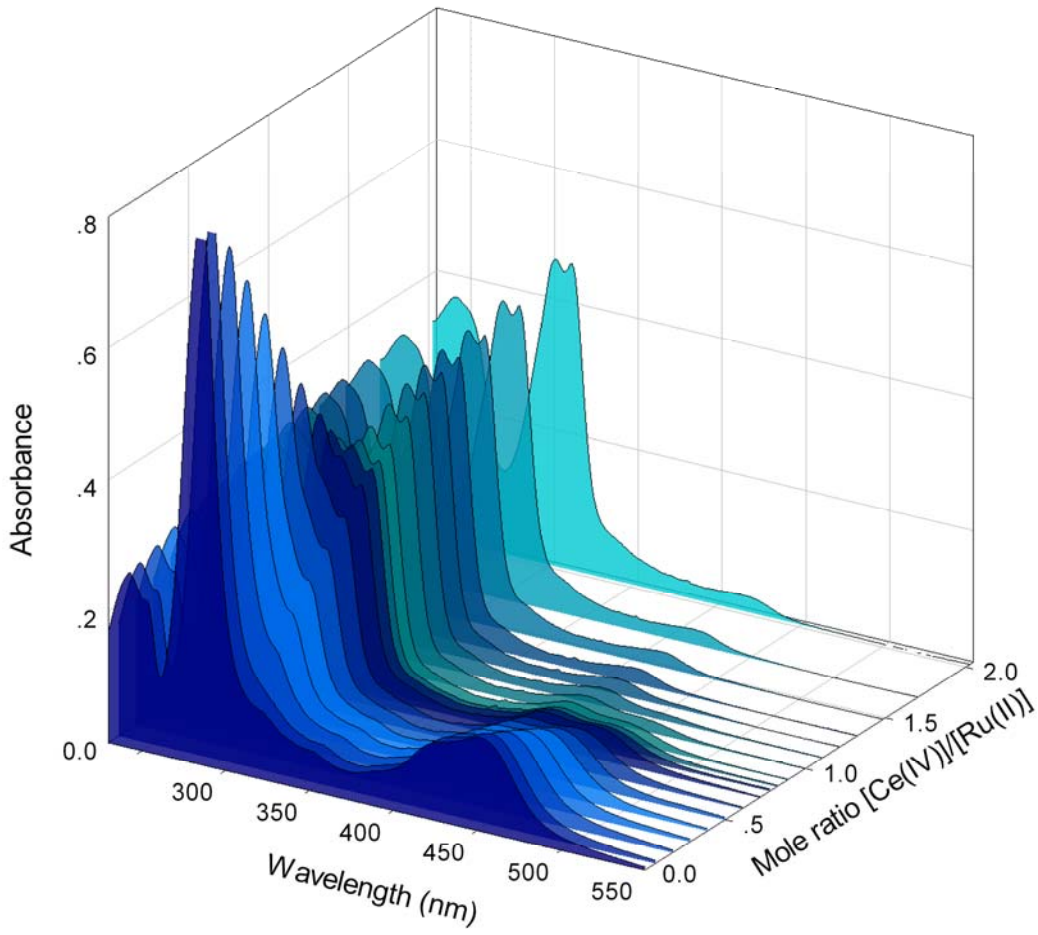

Figure 5.4: 3D plot of the spectra of $Ru(bpy)_3^{2+}$ oxidation with Ce(IV) as a function of [Ce(IV)]/[Ru(II)] mole ratio. Reagent concentrations: $[Ru(bpy)_3^{2+}] = 1.108 \times 10^{-5}$ M and $[Ce(IV)] = 3.000 \times 10^{-5}$ M in 0.1 M H_2SO_4.

Figure 5.4 shows the 3D plot of the spectra from titrations of $Ru(bpy)_3^{2+}$ with Ce(IV). The most important feature is that after a [Ce(IV)]/[Ru(II)] mole ratio of 1.0, only minor spectral changes are observed. It therefore appears that no further reaction occurs after the [Ce(IV)]/[Ru(II)] mole ratio reaches 1.0.

The program DynaFit 3 [11] was used to test the reaction model and to obtain constants from the absorbance data. It was assumed that a simple redox reaction occurred due to the addition of Ce(IV) into $Ru(bpy)_3^{2+}$:

$$Ru(II) + Ce(IV) \rightleftharpoons Ru(III) + Ce(III)$$

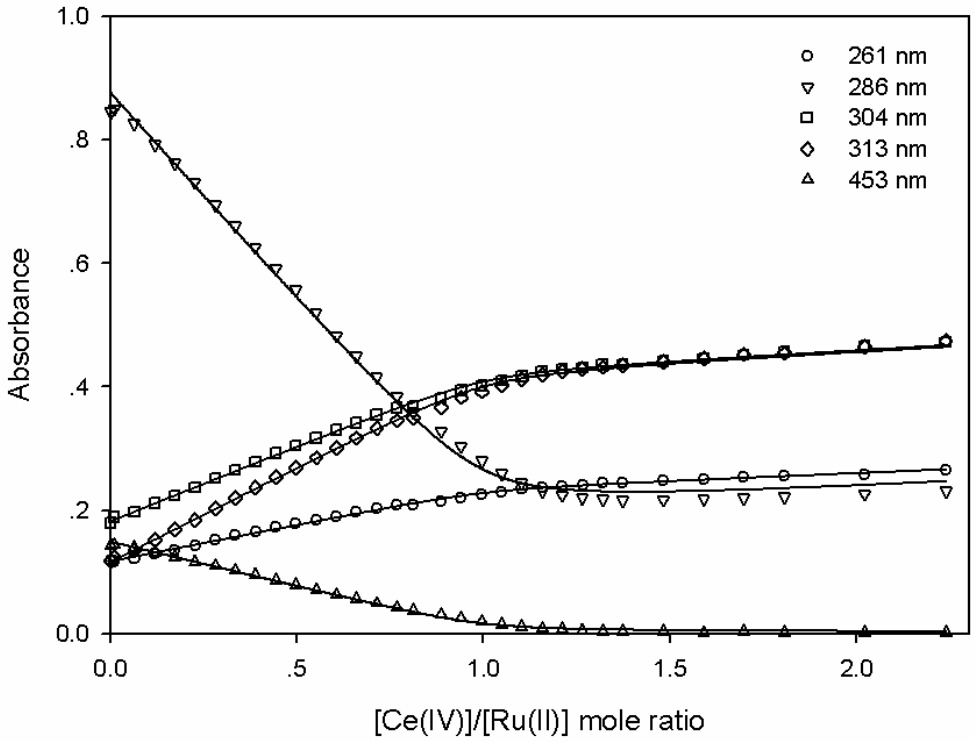

Figure 5.5: Absorbance curves of a titration of Ce(IV) into $Ru(bpy)_3^{2+}$ as a function of [Ce(IV)]/[Ru(II)] mole ratio at different wavelengths. Reagent concentrations: $[Ru(bpy)_3^{2+}] = 1.108 \times 10^{-5}$ M, $[Ce(IV)] = 3.000 \times 10^{-5}$ M; symbols – experimental points; lines – calculated curves.

Figure 5.5 illustrates the absorbance plots from mole ratio titrations of $Ru(bpy)_3^{2+}$ with Ce(IV). The calculated curves are in excellent fits at all wavelengths. The formation (β) and molar absorptivity constants (ε) calculated with data at different wavelengths from a typical titration are shown in Table 5.2 below:

$\beta = 1.06 \times 10^7$		
Wavelength (nm)	**$\varepsilon_{Ru(II)}$**	**$\varepsilon_{Ru(III)}$**
261	10583	21318
286	79121	18231
304	16447	38556
313	13443	284
453	13392	272.22

Table 5.2: Formation (β) and molar absorptivity constants (ε) calculated from an $Ru(bpy)_3^{2+}$ - Ce(IV) mole ratio titration.

5.2.4 Mole ratio titrations using photometer

5.2.4.1 Experimental procedure

In order to obtain photometric titration curves with more points, a photometer and titroprocessor setup was used to perform mole ratio titrations of $Ru(bpy)_3^{2+}$ with Ce(IV). The setup was described in Section 2.1.2.

The mole ratio titrations involve keeping the concentration of $Ru(bpy)_3^{2+}$ constant while varying the concentration of Ce(IV). The resulting absorbances at specific wavelengths are plotted against the mole ratio of the two reagents. With Ru(II) the absorbance at 453 nm was used, since at this wavelength a large change in the spectrum occurs and the absorbances of free Ce(IV) and Ce(III) are negligible (Figure 5.2). The shape of the absorbance curve at a particular wavelength depends on the values of the molar absorptivity constants of the reagents and complexes, and the value of the formation constants of the complexes.

For these titrations 25.00 ml of 1.108×10^{-5} M $Ru(bpy)_3^{2+}$ stock solution was pipetted into a reaction vessel. 3.000×10^{-5} M Ce(IV) solution in 0.1 M H_2SO_4 was then titrated into the $Ru(bpy)_3^{2+}$ solution. During the titration, the reaction solution was continuously under stirring, but not vigorously to prevent splashes and air bubbles being trapped in the light path of the photometer probe. Following each addition of Ce(IV), the reaction solution was allowed to equilibrate for 5-second time interval, after which its absorbance reading at 453 nm was recorded. Subsequent titrations were performed with different time intervals and light conditions.

The disadvantage of using the photometer is that the absorbance can only be measured at a single wavelength (453 nm) during a titration, a detailed explanation on the differences between spectrophotometer and photometer is discussed in Section 2.1.13 (page 17).

5.2.4.2 Results and discussions

The end-point of a photometric titration can be determined by means of graphical method. Two lines are drawn on the graph as shown in Figure 5.6 (page 72) and the intersection of these two lines indicates the end-point. The mole ratio of the end-point indicates the stoichiometry of the reaction.

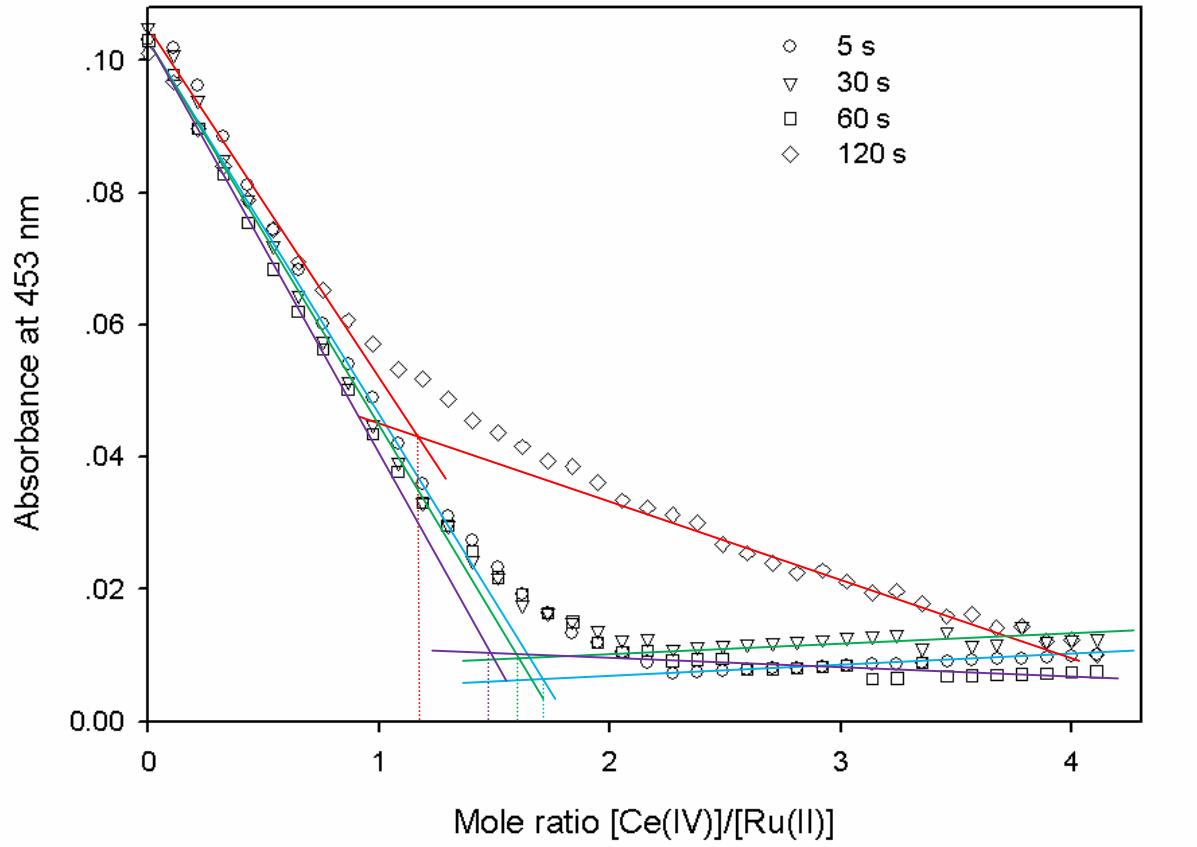

Figure 5.6: Absorbance curves of $Ru(bpy)_3^{2+}$ as a function of [Ce(IV)]/[Ru(II)] mole ratios at 453 nm. Titrations were performed under room light. $[Ru(bpy)_3^{2+}]$ = 1.108 x 10^{-5} M, [Ce(IV)] = 3.000 x 10^{-5} M. The different equilibrated time intervals are denoted in the legend. Linear regressions were drawn though the linear regions of the curves to obtain the point of intersect.

Figure 5.6 shows the absorbance curves of the automated titrations between Ru(II) and Ce(IV) at 453 nm with the reaction vessel uncovered and exposed to the room light. Using different equilibrated time intervals before each reading was taken, the absorbance curves show that with 5 s, 30 s, and 60 s pause times, only slight differences were observed. However, with a pause time of 120 s, the absorbance readings were much higher than the ones with shorter pause times. Also, the increase in absorbance readings at longer pause time, causes the point of intersection shift to a lower mole ratio region.

As mentioned previously, the lines are drawn from the experimental points before and after the endpoints. The end-point was calculated with different pause times from Figure 5.6 and the results are shown in Table 5.3.

Table 5.3: Determination of the endpoint from [Ce(IV)]/[Ru(II)] mole ratio titrations under room light using the graphical method. Reagent concentrations: $[Ru(bpy)_3^{2+}] = 1.108 \times 10^{-5}$ M, $[Ce(IV)] = 3.000 \times 10^{-5}$ M.

Pause time (s)	End-point from graph
5	1.70
30	1.60
60	1.48
120	1.17

Table 5.3 shows that the longer the pause time, the smaller the mole ratio calculated from the absorbance curves. Since the absorbance curves show that with pause time of 5 s, 30 s, and 60 s only small differences were observed, it is possible to calculate the average mole ratio at those end-points. In the case of 120 s pause time, it was suspected that a light activated reduction took place while the reaction vessel was exposed to the room light. Therefore, a separate titration was conducted in the dark. The results are discussed later (page 75).

An average mole ratio value for the above-mentioned endpoints of 1.59 (*i.e.* a 1.5:1 oxidation) was obtained. This corresponds to the reaction:

$$3\ Ce(IV) + 2\ Ru(II) \longrightarrow 2\ Ru(III)$$

In addition, The program, SPC-V-MR was used to analyze the Ce(IV) versus Ru(II) mole ratio titrations (Section 2.1.12, page 16), the results of which are illustrated in Figure 5.7 (page 74).

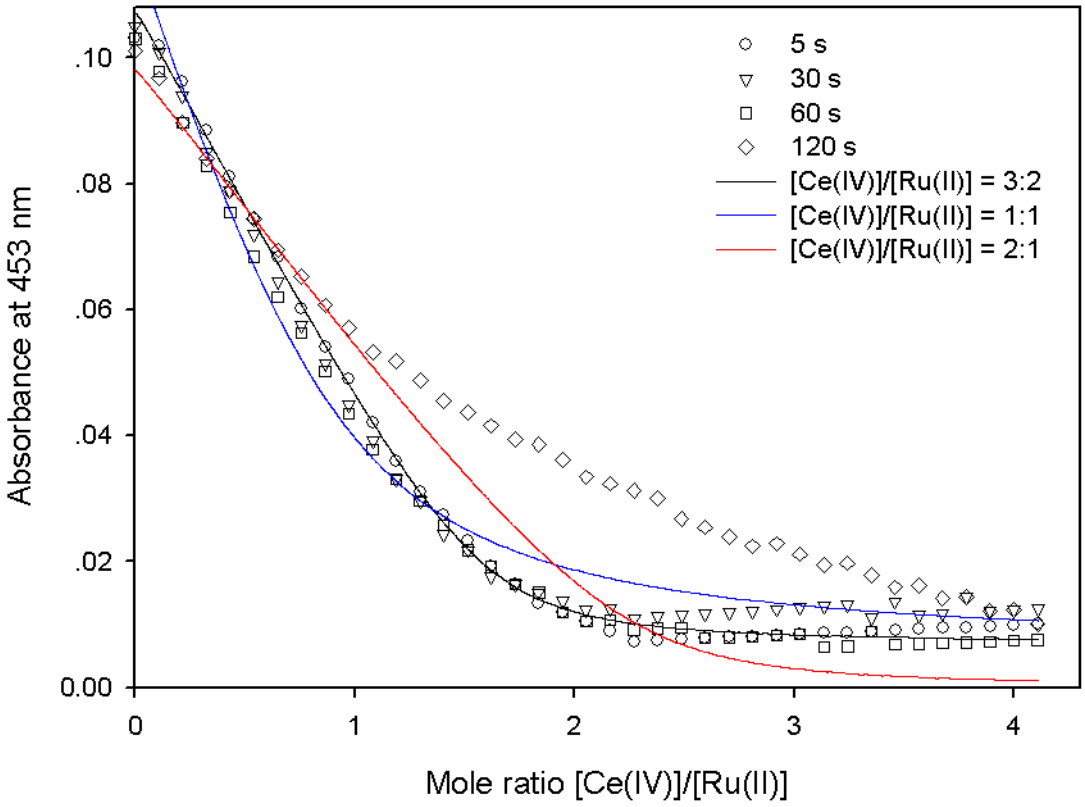

Figure 5.7: Absorbance curves of $Ru(bpy)_3^{2+}$ as a function of [Ce(IV)]/[Ru(II)] mole ratios at 453 nm. Titrations were performed under room light. The calculated curves were simulated on 1:1, 3:2 and 2:1 [Ce(IV)]/[Ru(II)] mole ratio reaction models. Symbols = experimental data; Lines = calculated fits. The different equilibrated time intervals are denoted in the legend.

The simulation of the oxidation of [Ce(IV)]/[Ru(II)] mole ratio of 3:2 results in good absorbance curve fits as shown in Figure 5.7, this confirms with the results obtained from graphical method. This is interesting since a 1:1 mole ratio reaction between Ce(IV) and Ru(II) was expected.

For comparison the same automated titrations between Ru(II) and Ce(IV) at 453 nm were performed. With same pause times, but the reaction vessel was kept in the dark. The results are shown in Figure 5.8 (page 75).

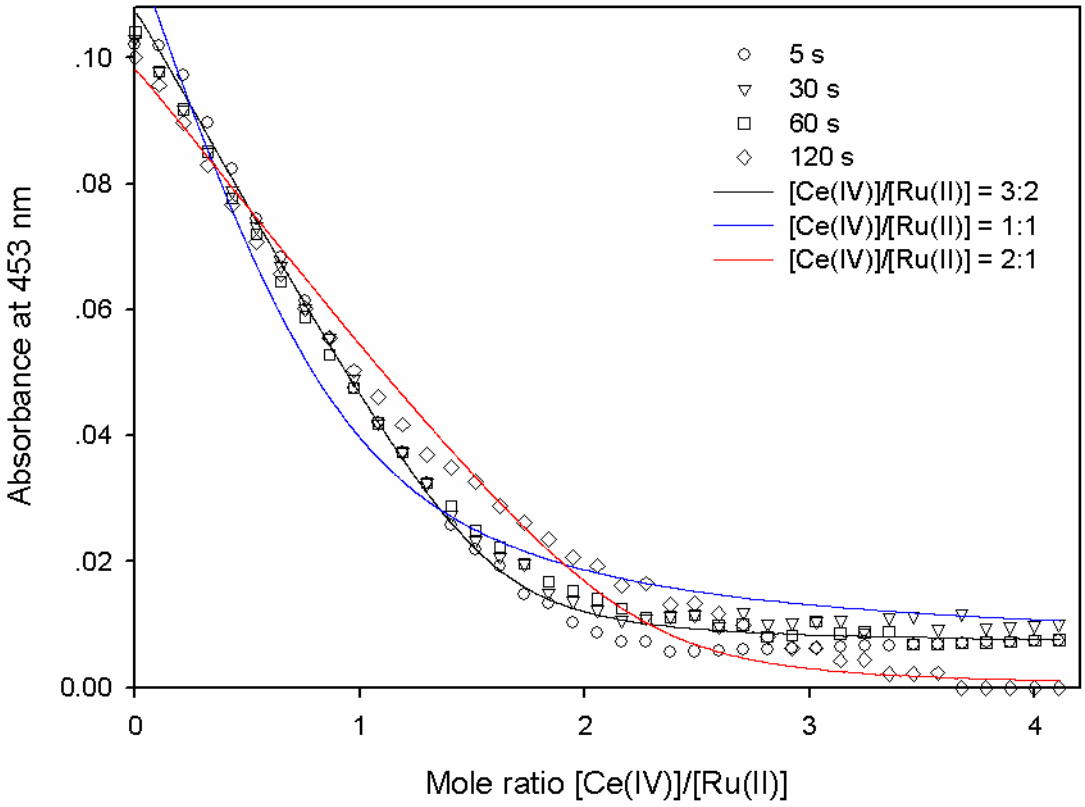

Figure 5.8: Absorbance curves of $Ru(bpy)_3^{2+}$ as a function of [Ce(IV)]/[Ru(II)] mole ratios at 453 nm. Titrations were performed in the dark. [$Ru(bpy)_3^{2+}$] = 1.108 x 10^{-5} M, [Ce(IV)] = 3.000 x 10^{-5} M. Symbols = experimental data; Lines = calculated fits. The different equilibrated time intervals are denoted in the legend.

Figure 5.8 shows very little difference in absorbance curves when different equilibrated time intervals were employed. With the pause time of 120 s before each reading, the absorbance readings are still slightly higher than the curves with shorter pause time. In this case the 120 s curve shows a much sharper endpoint than the same titration performed under light conditions. The simulations once again show good absorbance curve fits at a [Ce(IV)]/[Ru(II)] mole ratio 3:2.

In conclusion, the photometer was found to be a very convenient instrument for the mole ratio titrations between Ce(IV) and $Ru(bpy)_3^{2+}$. Both graphical and computer simulation methods were used to determine the endpoint. Consistent mole ratio values were obtained for both methods. An unexpected [Ce(IV)]/[Ru(II)] mole ratio of 3:2 indicates the following oxidation reaction occurred upon the addition of Ce(IV):

$$3\ Ce(IV) + 2\ Ru(II) \longrightarrow 2\ Ru(III)$$

This differs from the expected 1:1 reaction. A possible explanation for this discrepancy is the regeneration of $Ru(bpy)_3^{2+}$ from $Ru(bpy)_3^{3+}$ in the presence of light. As the mole ratio titration proceeds some of the Ru(III) is reduced to Ru(II). As a result more Ce(IV) needs to be titrated to completely oxidize the Ru(II) resulting in the end-point occurring at a higher mole ratio.

For the photometric titrations there is not much difference in the end-point found between the titrations performed in the dark and those done in light. This could arise from the fact that the photometer probe passes white light through the solution and afterwards separates the desired wavelength for measurement. As a result light from the photometer is continuously promoting the reduction of Ru(III).

On the other hand, the spectrophotometer first passes the light through a monochromator so that only the light of the desired wavelength passes through the sample. As a result there is much less light intensity passing through the sample and less photo-reduction of Ru(III) will occur. For this reason the mole ratio titration performed with the spectrophotometer shows an end-point closer to the mole ratio 1.0 than titration performed with the photometer.

5.3 Photosensitive reduction of tris(2,2'-bipyridyl) ruthenium (III)

5.3.1 Introduction

One can see from the previous section that the rate of oxidation of $Ru(bpy)_3^{2+}$ with Ce(IV) depends on various factors and that light also plays a very important role in the oxidation reactions. In the presence of light, the regeneration of $Ru(bpy)_3^{2+}$ is likely to occur. In this section the kinetics of this regeneration of $Ru(bpy)_3^{2+}$ from oxidized $Ru(bpy)_3^{3+}$ was investigated.

5.3.2 Experimental procedure

Although photometer and spectrophotometer share the same working principle and each has their own advantages and disadvantages (see Chapter 2.1.12). In this section, both instruments were employed. The photometer was used to closely monitor the oxidation-reduction reactions of the species at 453 nm, while the spectrophotometer provided a perspective on the reactions in the full wavelength scale.

5.3.2.1 Photometric approach

The experimental setup was described in Chapter 2.1.3, the procedure is as follows: 25 ml of 5.540 x 10^{-5} M $Ru(bpy)_3^{2+}$ stock solution was transferred quantitatively into the reaction flask and the reaction temperature was carefully controlled for kinetic study purposes. The photometric data was recorded as soon as a measured volume of 1.250 x 10^{-3} M Ce(IV) was added. The volume of Ce(IV) added depended on the [Ce(IV)]/[Ru(II)] mole ratio required. The effect of light on the reaction solution obviously plays a crucial role in this experiment. The light source was kept at a fixed distance from the reaction vessel throughout the experiment.

5.3.2.2 Spectrophotometric approach

A similar procedure described in the previous section (Chapter 5.3.2.1) was followed. The only difference from the photometric approach is that after the oxidation of $Ru(bpy)_3^{2+}$ with excess Ce(IV), the reaction solution was immediately divided equally into two portions. The first portion was kept uncovered under the room light, and the other portion was covered with aluminium foil and kept in dark. The spectra of both solutions were recorded over time using a spectrophotometer.

5.3.3 Results and discussions

Upon the addition of Ce(IV) to $Ru(bpy)_3^{2+}$, the solution colour changes from yellow-orange to colourless, and with the presence of light, the resultant colourless solution slowly changes back to its original yellow-orange colour. Clearly, a reversible reaction occurs. The spectra changes were recorded and shown in the next section.

5.3.3.1 Photometric observations

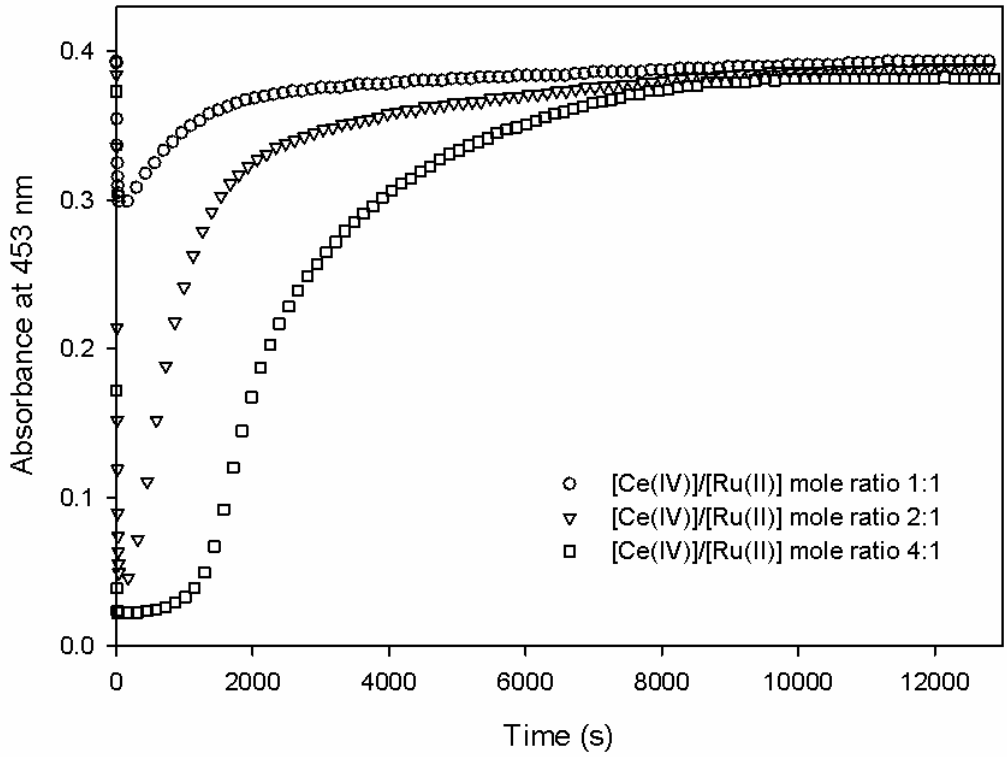

Figure 5.9: Progress curves demonstrating the rate of change of the absorbance at 453 nm at 293 K. Reagent concentrations: $[Ru(bpy)_3^{2+}]$ = 5.540 x 10^{-5} M; [Ce(IV)] = 1.250 x 10^{-3} M; [Ce(IV)]/[Ru(II)] mole ratios are denoted by the legend.

Figure 5.9 shows the progress curves of the oxidation-photoreduction reactions of $Ru(bpy)_3^{2+}$ with Ce(IV). The absorbance data was recorded at wavelength 453 nm over a period of 13000 s.

Figure 5.9 shows clearly that the absorbance at 453 nm initially decreased almost immediately, reached a plateau, and then gradually increased until leveling off. The initial steep drop of the absorbance is due to the addition of Ce(IV) to the $Ru(bpy)_3^{2+}$ solution, oxidation reaction between the two species occurred immediately. When more Ce(IV) is added the absorbance drops further until it reaches a minimum. For the mole ratio 4:1 solution the absorbance is maintained at this minimum for a period of about 1000 s until the absorbance starts to increase slowly. The excess Ce(IV) oxidizes any Ru(II) formed by the photo-reduction process maintaining this minimum absorbance. As soon as all the Ce(IV) is used up, Ru(II) starts to form and the absorbance gradually increases.

As time progressed, the absorbance readings came close to the ones recorded before the addition of Ce(IV). This indicates the $Ru(bpy)_3^{2+}$ was fully regenerated by the reduction of $Ru(bpy)_3^{3+}$ with light. The full spectra recorded before and after the photo-reduction are shown in the next section (Chapter 5.3.3.2).

Furthermore, Figure 5.10 (page 80) shows the effect of varying the temperatures on the rate of change of the absorbance at 453 nm with different Ce(IV) to Ru(II) mole ratios. Significant changes in absorbance readings can be observed from Figure 5.10 B. The slope of the progress curves becomes steeper indicating the increase in the rate of photo-reduction. At the same mole ratios, both the oxidation and photo-reduction occurred more rapidly as a result of the elevated temperatures. However at the Ce(IV) to Ru(II) mole ratio of 1.0, the data recorded are very similar irrespective of the temperature.

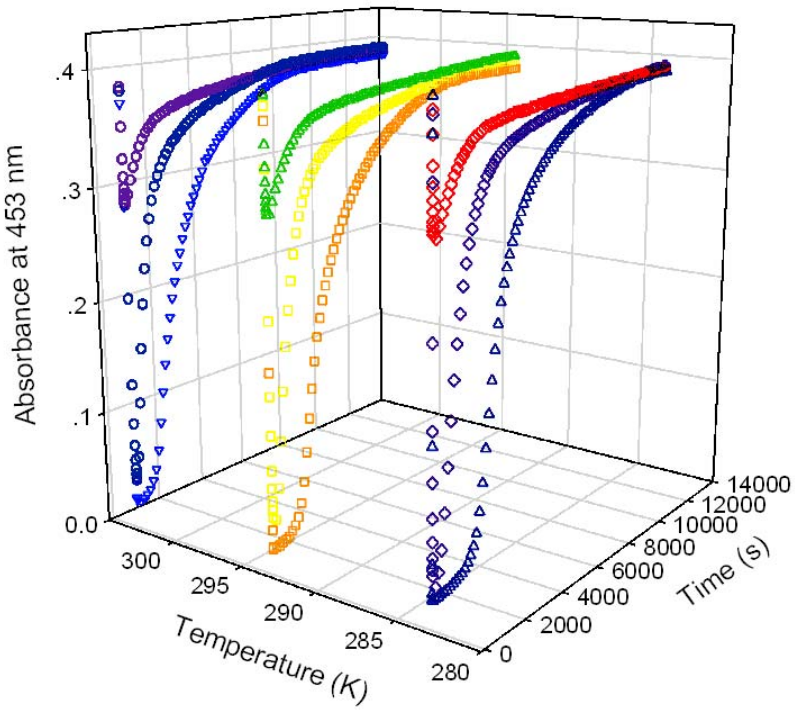

A

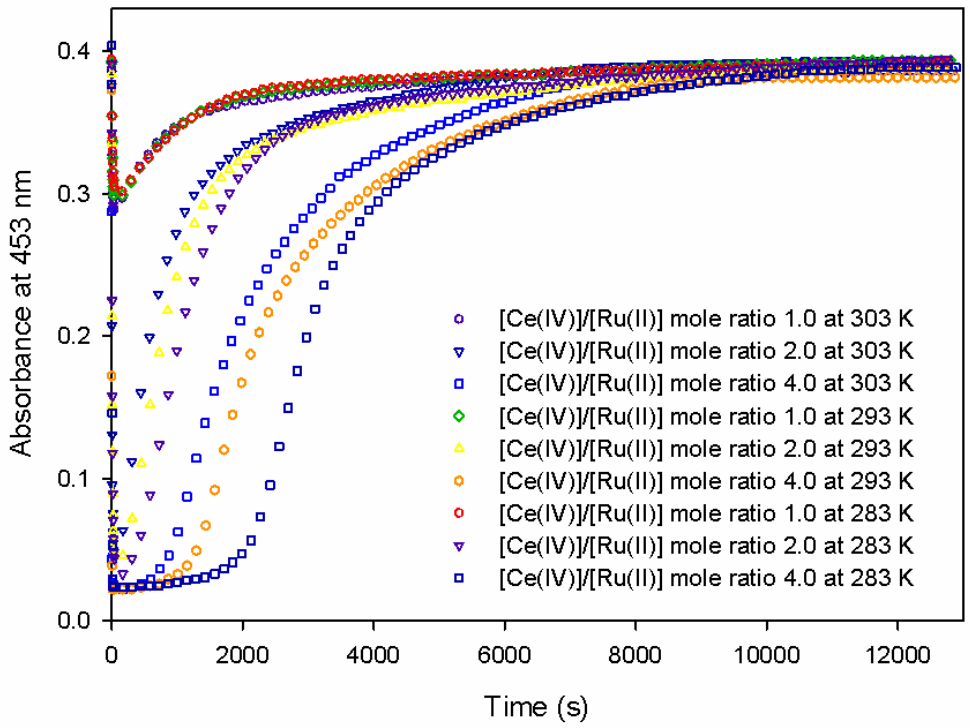

B

Figure 5.10 A and B: 3D and the overlay of the progress curves demonstrating the rate of change of the absorbance at 453 nm at different temperatures with different Ce(IV) to Ru(II) mole ratios. $[Ru(bpy)_3^{2+}]$ = 5.540 × 10^{-5} M; [Ce(IV)] = 1.250 x 10^{-3} M.

5.3.3.2 Spectrophotometric observations

In this section the kinetic absorbance changes were followed by recording the whole UV-Vis spectrum. The influence of room light was investigated by keeping one solution in the dark between spectrum recording, and another in room light between recordings as described in Section 5.3.2.2 (page 77).

Figure 5.11 (A) (page 82) depicts the changes in UV-Vis spectra of $Ru(bpy)_3^{2+}$ after oxidation by Ce(IV) in the presence of light. The solid arrows indicate the direction of absorbance changes with time. The presence of light causes the oxidized species peaks to increase at 286 and 453 nm, while the doublet at 304 and 313 nm decreases. Isosbestic points are obtained at the same wavelengths as for the titration of $Ru(bpy)_3^{2+}$ with Ce(IV). After more than 19 hours exposure to the room light, the final spectrum indicates the full recovery of $Ru(bpy)_3^{2+}$ from $Ru(bpy)_3^{3+}$.

The progress curve of Figure 5.11 (B) reveals the reduction of oxidized Ru(III) species by light at different wavelengths as mentioned above. Clearly, the absorbance decreases at 304 and 313 nm, while the 286 and 453 nm peaks increase.

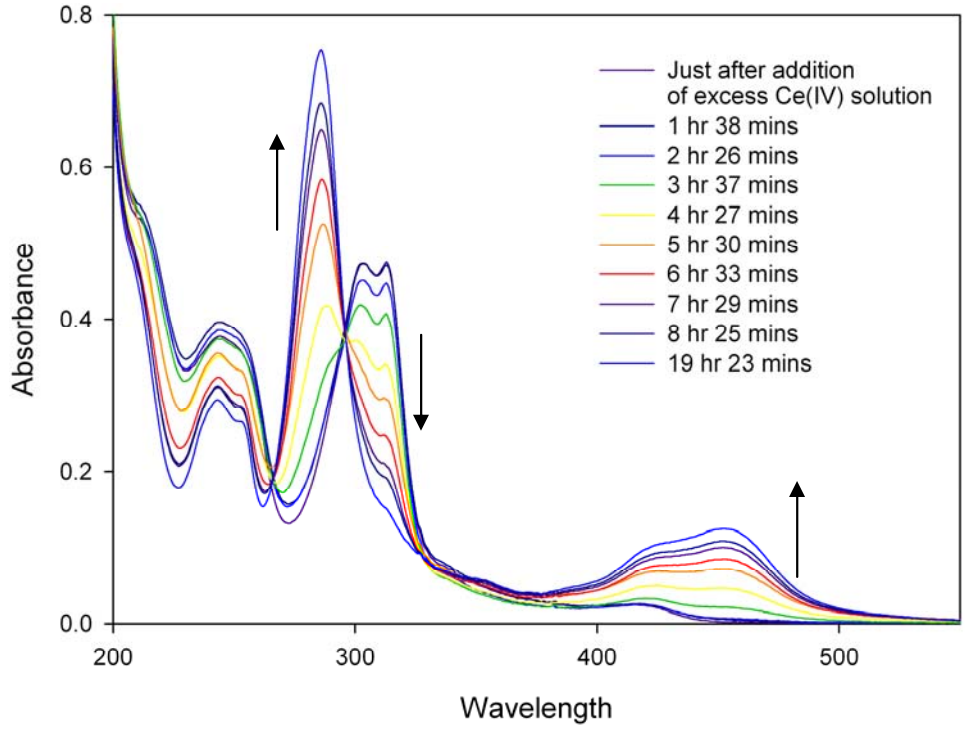

A

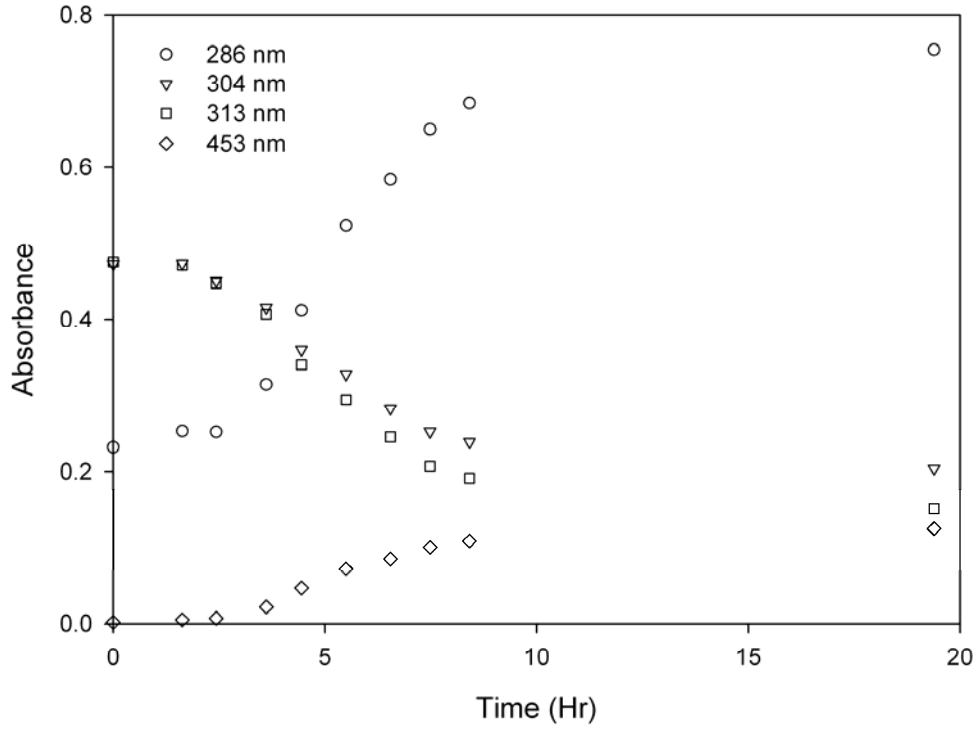

B

Figure 5.11 A and B: The UV-Vis spectra and progress curves showing the change of absorbance as a function of time. The reaction solution was kept uncovered under room light, and [Ce(IV)]/[Ru(II)] mole ratio 2.0. (A) The times at which these spectra were recorded are denoted in the legend. (B) Different wavelengths at which the progress curves constructed were indicated in the legend. $[Ru(bpy)_3^{2+}]$ = 1.108 x 10^{-5} M; [Ce(IV)] = 3.000 x 10^{-5} M.

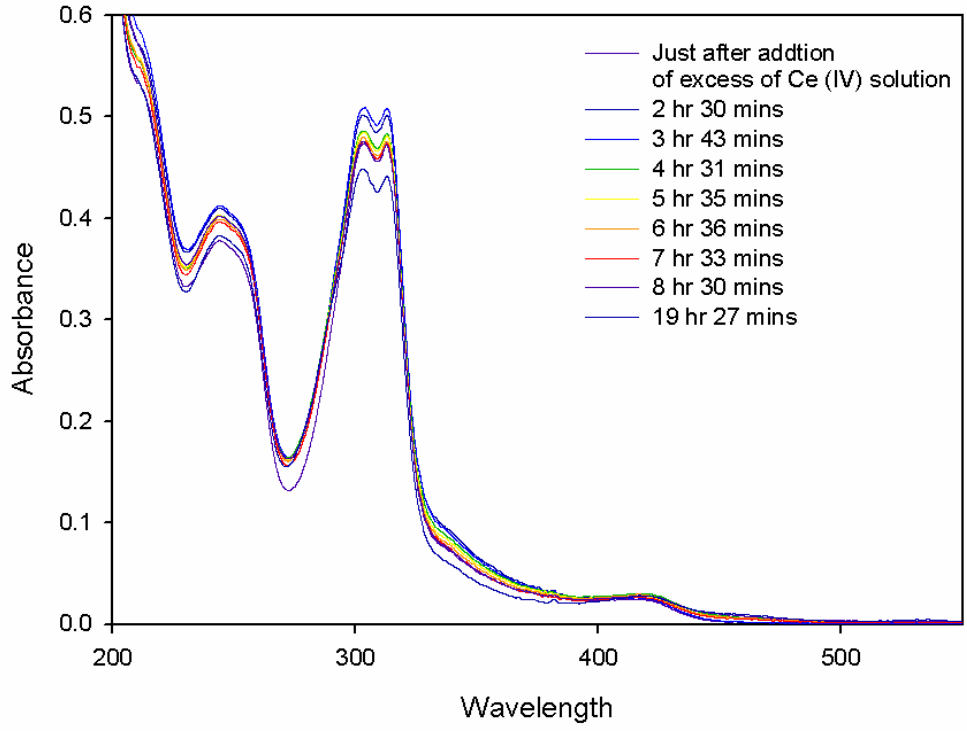

A

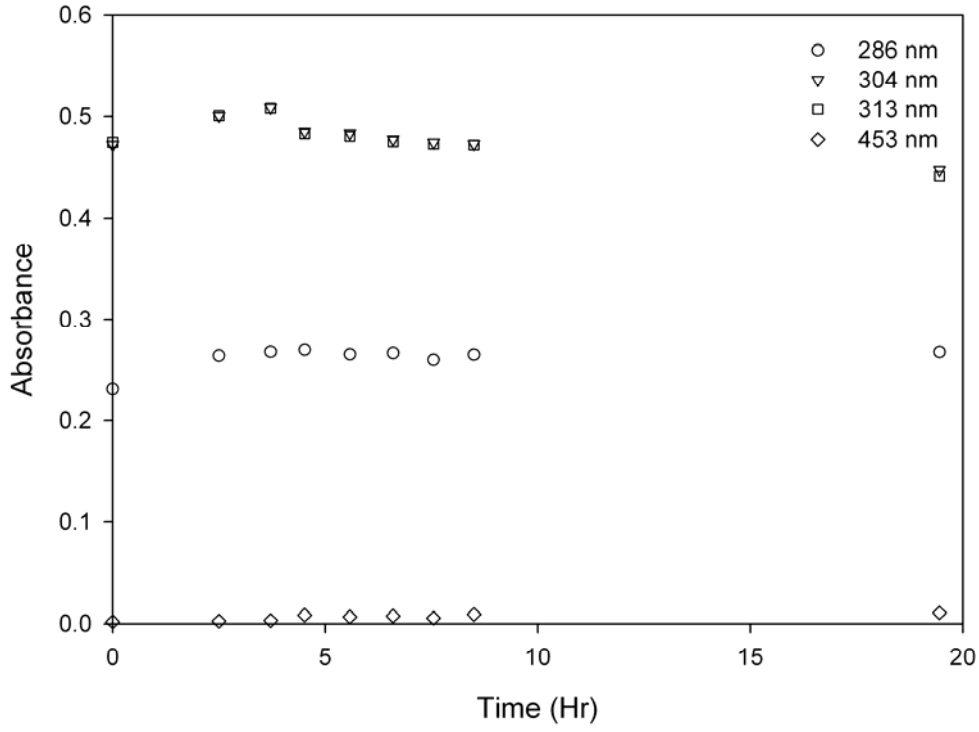

B

Figure 5.12 A and B: The UV-Vis spectra and progress curves showing the change of absorbance as a function of time. The reaction solution was covered and kept in dark, and [Ce(IV)]/[Ru(II)] mole ratio 2.0. (A) The times at which these spectra were recorded are denoted in the legend. (B) Different wavelengths at which the progress curves constructed were indicated in the legend. $[Ru(bpy)_3^{2+}]$ = 1.108 x 10^{-5} M; [Ce(IV)] = 3.000 x 10^{-5} M.

Figure 5.12 (A) illustrates the UV-Vis spectra for the reaction solution that was kept in the dark after oxidation by Ce(IV). If one compares Figure 5.11 (A) and 5.12 (A), it can clearly be seen that under dark condition the Ru(III) is not readily reduced back to Ru(II). This indicates the reduction is highly depending on the light conditions.

5.4 Determining the best reaction model

5.4.1 Introduction

This section describes the challenges in proposing an appropriate reaction model of the oxidation-light reduction reaction between $Ru(bpy)_3^{2+}$ and Ce(IV), which fits the experimental data within acceptable statistical error. A number of kinetic models were proposed, but only four models that best fit the experimental data are illustrated. A single theoretical model was chosen to represent the experimental data. Reasons for this choice will be provided.

5.4.2 Experimental

All spectra recorded in this chapter were obtained using a UV-Vis spectrophotometer at 25 ^{o}C, the procedure was performed as previously described in Chapter 2.5.

5.4.3 Computational software utilized for kinetic modeling

In order to determine how $Ru(bpy)_3^{2+}$ regenerates from $Ru(bpy)_3^{3+}$ with the presence of light, aqueous solutions of $Ru(bpy)_3^{2+}$ were first titrated with Ce(IV) solution of known concentration to form $Ru(bpy)_3^{3+}$, then the resultant solution was monitored for any spectral changes using a spectrophotometer . The data were analyzed using the DynaFit 3 [11] computer program. The program modeled the oxidation of $Ru(bpy)_3^{2+}$ by Ce(IV), and the regeneration of $Ru(bpy)_3^{2+}$ from the resultant $Ru(bpy)_3^{3+}$ solution. A screenshot of the program is shown in Figure 5.13.

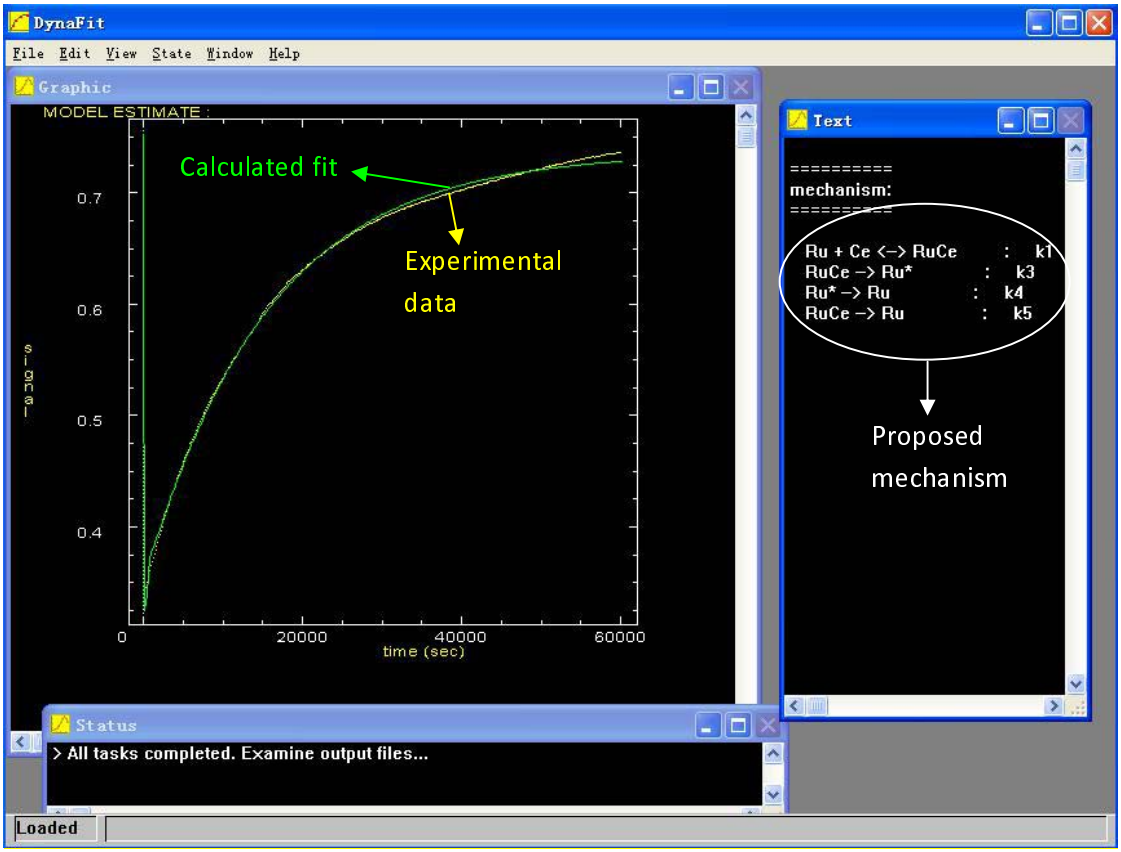

Figure 5.13: Program interface of DynaFit 3.

Figure 5.13 depicts the user interface of the program DynaFit 3 after the data have been imported as a tab delimited text file. The program requires the user to write a script file which contains the description of the proposed reaction mechanism, initial estimates of fitting parameters, and the location of experimental data on the disk [11]. Once the required data has been imported, the program uses the Gauss-Newton non-linear least square algorithm to calculate the best fit of the postulated theoretical model to the given experimental data. Furthermore, from the calculated total theoretical absorbance values and by comparing these with the experimental absorbance values certain constants can be determined, the results are shown in the next section.

5.4.4 Results and discussions

Models 1 to 4 in this section show the theoretical fit of the various models that were attempted. The black symbols indicate the experimental data and the red lines show the calculated absorbance curves obtained. The best fit for each model returned a set of molar extinction coefficients and rate constants. These parameters are, by definition, constants across the range of [Ce(IV)]/[Ru(II)] mole ratios. However,

because of experimental errors or because the theoretical model was not appropriate to the experimental data, the parameters varied from one [Ce(IV)]/[Ru(II)] mole ratio to another. Therefore, the best-fit constants were averaged over the whole [Ce(IV)]/[Ru(II)] mole ratio range.

Model 1

The first model is the simplest one which assumes that Ce(IV) oxidizes $Ru(bpy)_3^{2+}$ to form $Ru(bpy)_3^{3+}$. The resultant $Ru(bpy)_3^{3+}$ is unstable in the presence of light, and partial recovery of $Ru(bpy)_3^{2+}$ occurs. The regeneration of $Ru(bpy)_3^{2+}$ from $Ru(bpy)_3^{3+}$ is assumed to take place in a single step:

$$Ru(II) + Ce(IV) \xrightarrow{k_1} Ru(III)$$

$$Ru(III) \xrightarrow{k_2} Ru(II)$$

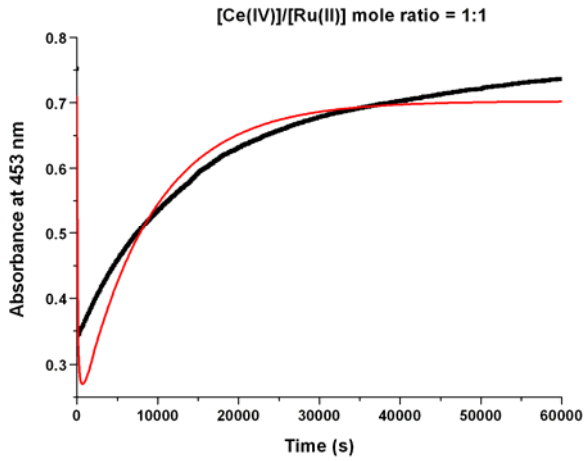

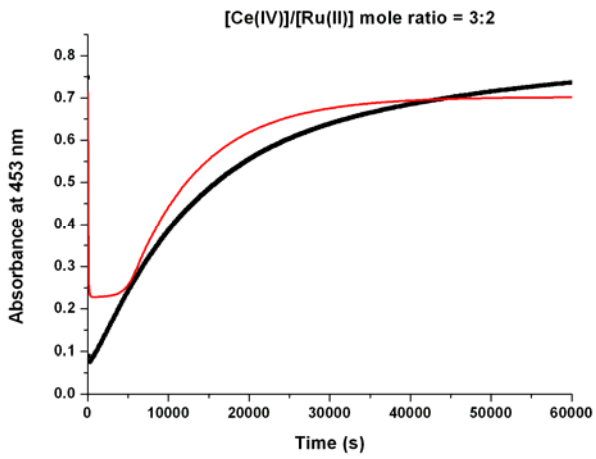

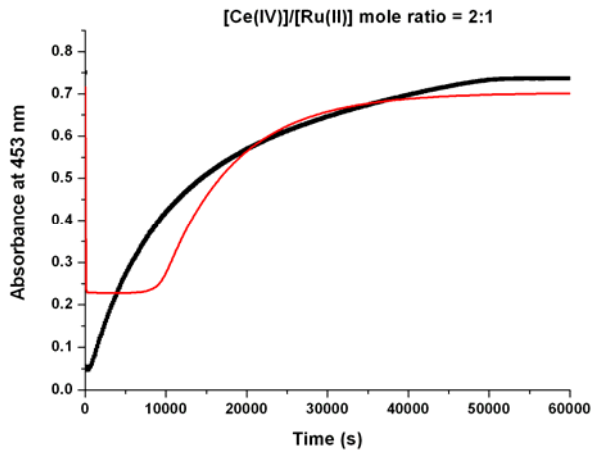

k_1	482.8
k_2	0.113×10^{-3}
$\varepsilon_{Ru(II)}$	13804
$\varepsilon_{Ce(IV)}$	127.6
$\varepsilon_{Ru(III)}$	4328.8

Model 2

This model assumes that the oxidation between $Ru(bpy)_3^{2+}$ and Ce(IV) occurs in the similar manner as described in Model 1, and the regeneration of $Ru(bpy)_3^{2+}$ from $Ru(bpy)_3^{3+}$ occurs involving the formation of an intermediate species Ru*. The oxidation state of this species remains unknown:

$$Ru(II) + Ce(IV) \xrightarrow{k_1} Ru(III)$$
$$Ru(III) \xrightarrow{k_2} Ru^*$$
$$Ru^* \xrightarrow{k_3} Ru(II)$$

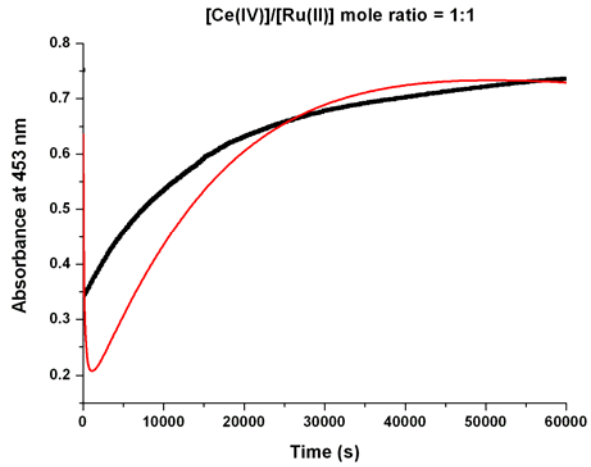

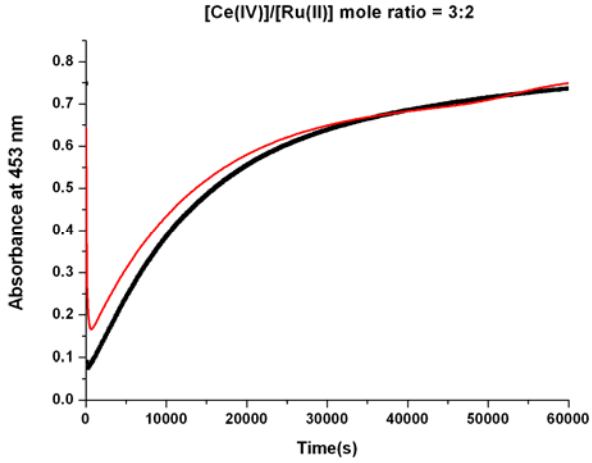

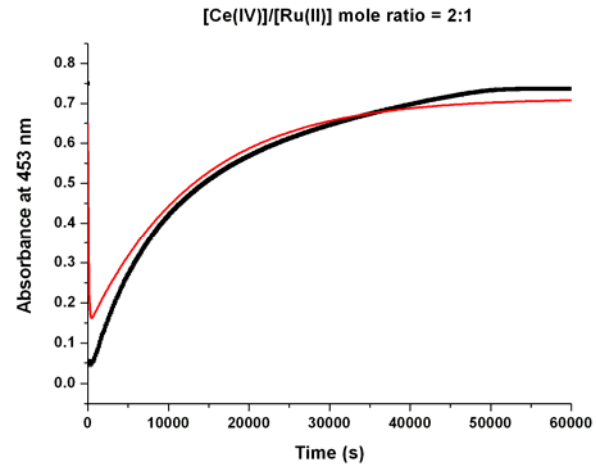

k_1	182.70
k_2	0.527×10^{-4}
k_3	0.204×10^{-4}
$\varepsilon_{Ru(II)}$	12195
$\varepsilon_{Ce(IV)}$	294
$\varepsilon_{Ru(III)}$	2507.9
ε_{Ru^*}	18379

Model 3

Model 3 assumes that the oxidation between $Ru(bpy)_3^{2+}$ and Ce(IV) occurs in the same manner as described in Model 2. However, the regeneration of $Ru(bpy)_3^{2+}$ from $Ru(bpy)_3^{3+}$ occurs via two routes simultaneously; one at which involves the formation of an intermediate species Ru*, the other route assumes the direct reduction from Ru(III):

$$Ru(II) + Ce(IV) \xrightarrow{k_1} Ru(III)$$

$$Ru(III) \xrightarrow{k_2} Ru(II)$$

$$Ru(III) \xrightarrow{k_3} Ru^*$$

$$Ru^* \xrightarrow{k_4} Ru(II)$$

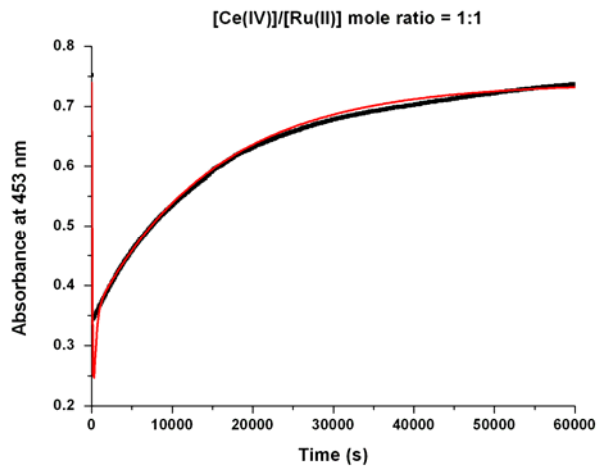

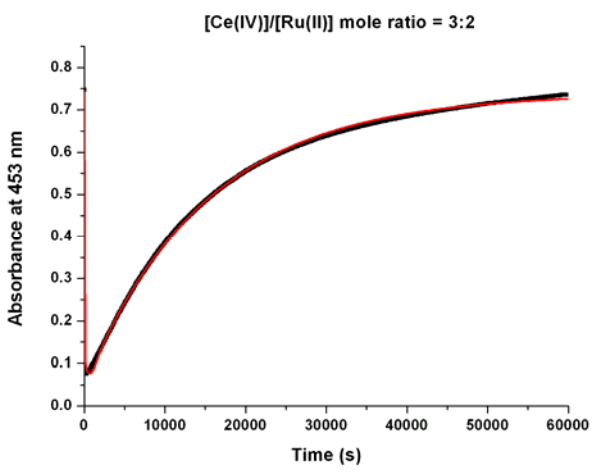

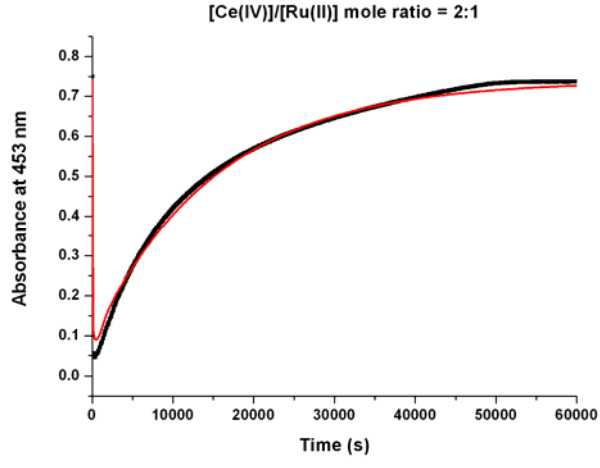

k_1	8604.6
k_2	0.680×10^{-4}
k_3	0.370×10^{-3}
k_4	0.643×10^{-4}
$\varepsilon_{Ru(II)}$	14369
$\varepsilon_{Ce(IV)}$	294
$\varepsilon_{Ru(III)}$	6582
ε_{Ru^*}	6914

Model 4

This model assumes a more complicated route for the regeneration of $Ru(bpy)_3^{2+}$ from $Ru(bpy)_3^{3+}$, which involves the reaction of Ru(III) and Ru(I) species:

$$Ru(II) + Ce(IV) \xrightarrow{k_1} Ru(III)$$
$$Ru(III) \xrightarrow{k_2} Ru(I)$$
$$Ru(III) + Ru(I) \xrightarrow{k_3} Ru^* + Ru(II)$$
$$Ru^* \xrightarrow{k_4} Ru(II)$$

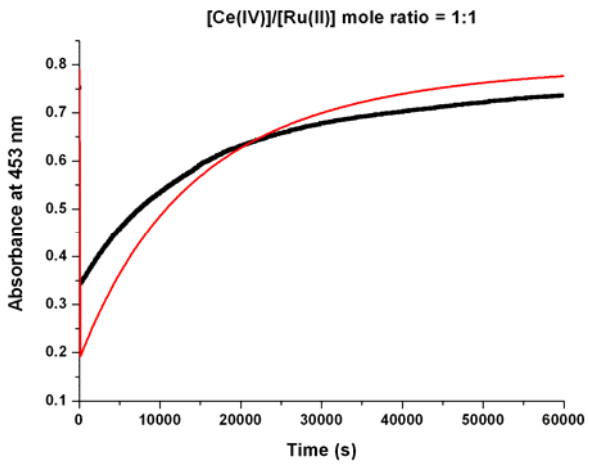

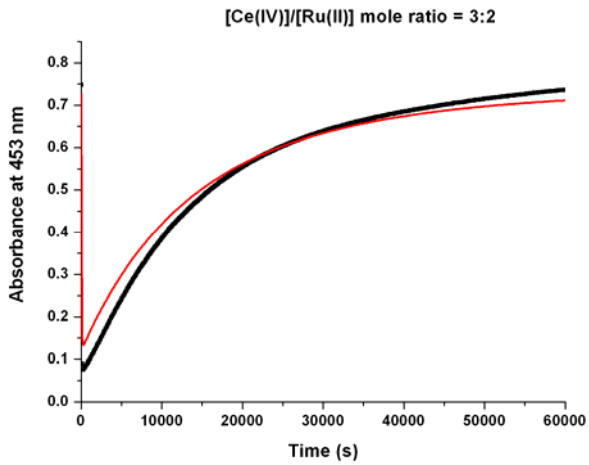

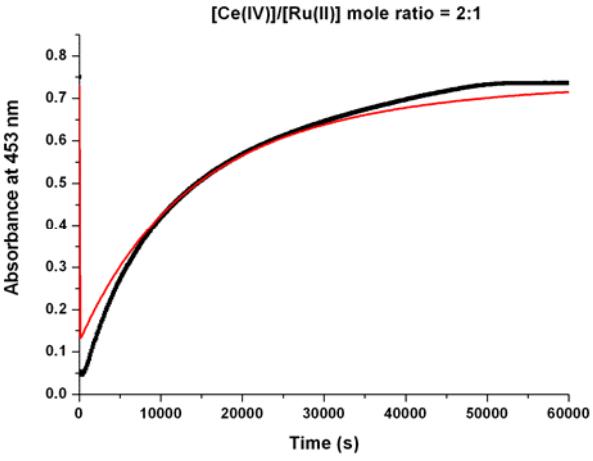

k_1	582
k_2	0.705×10^{-4}
k_3	0.2079
k_4	0.591×10^{-4}
$\varepsilon_{Ru(II)}$	14039
$\varepsilon_{Ce(IV)}$	150.4
$\varepsilon_{Ru(III)}$	2302.3
$\varepsilon_{Ru(I)}$	14248
ε_{Ru^*}	2285

The listed models represent the sum of the models fitted using the kinetic modeling software. Model 1 gives noticeably poor fits and may be discarded at once. Model 2 shows reasonable good fit at mole ratios 3:2 and 2:1, and compared with Model 1 it is apparently a better fit of the experimental data indicating an intermediate species forms. Both Models 3 and 4 gave fairly good fits at high mole ratios. It is important to stress that there are certain components resulting in uncertainties inherent in these reactions: for example, natural experimental error inherent in measurement and agitation of each solution. In addition, the time elapsed from initiation of the reaction to the first spectral recording also produces a relative error margin, since it leads to a loss of kinetic data during this time, especially if the oxidation between $Ru(bpy)_3^{2+}$ and Ce(IV) occurs very rapidly.

Based on the good theoretical fit obtained with Model 3, in addition to considering the calculated constants, Models 1, 2 and 4 were excluded and only Model 3 accepted. Model 3 is mechanistically reasonable, and simulations show perfect fits between the experimental data and calculated results at all [Ce(IV)]/[Ru(II)] mole ratios. Model 4 was first proposed by Rubinstein [29], however there are no spectral changes observed to provide evidence of the formation of Ru(I) species.

In conclusion, the light helps overcome the activation barrier of the regeneration reaction of $Ru(bpy)_3^{2+}$ by driving it via an intermediate. It is apparent from the simulation that photo-reduction is not a simple single step process.

5.4.5 Factors influencing the rate of reaction

Various factors can influence the rates of the reaction between $Ru(bpy)_3^{2+}$ and Ce(IV). In this section, the effect of temperature and light was investigated.

5.4.5.1 Experimental

Each reaction was prepared in a 1-cm quartz cuvette. Distilled water and $Ru(bpy)_3^{2+}$ was first added into the cuvette. This brought the reaction to the desired concentration in Ru(II). The spectrum of the initial solution was then recorded in the range of 650 nm to 200 nm. For scans in the visible region only, the range of 650 nm to 400 nm was chosen. Thereafter, the oxidizing agent Ce(IV) was added at time equals zero seconds. The progress of the reaction was followed. Reactions were also performed at different temperatures. This was accomplished by placing all

reagent vessels in a water-bath. The water from the water-bath was also circulating through an outer sleeve surrounding the cuvette holder, which kept the cuvette at desired temperatures.

5.4.5.2 Varying the temperature

Figures 5.14 to 5.16 show the progress curves for the regeneration of $Ru(bpy)_3^{2+}$ from $Ru(bpy)_3^{3+}$ at various temperatures and mole ratios. It is clear to see that the rates of the reactions increase with increasing temperature.

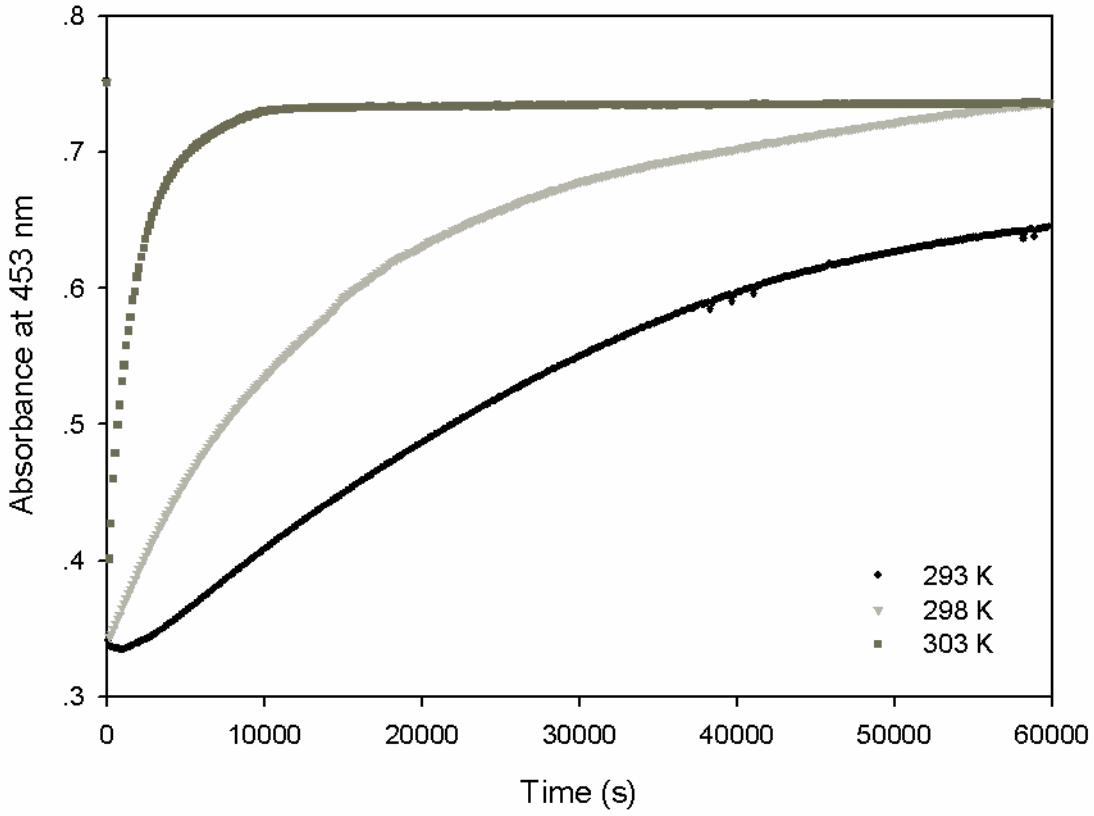

Figure 5.14: Progress curves of the regeneration of $Ru(bpy)_3^{2+}$ from $Ru(bpy)_3^{3+}$ at various temperatures. [Ce(IV)]/[$Ru(bpy)_3^{2+}$] mole ratio at 1:1. Reagent concentrations: [$Ru(bpy)_3^{2+}$] = 5.540 x 10^{-5} M; [Ce(IV)] = 1.250 x 10^{-3} M.

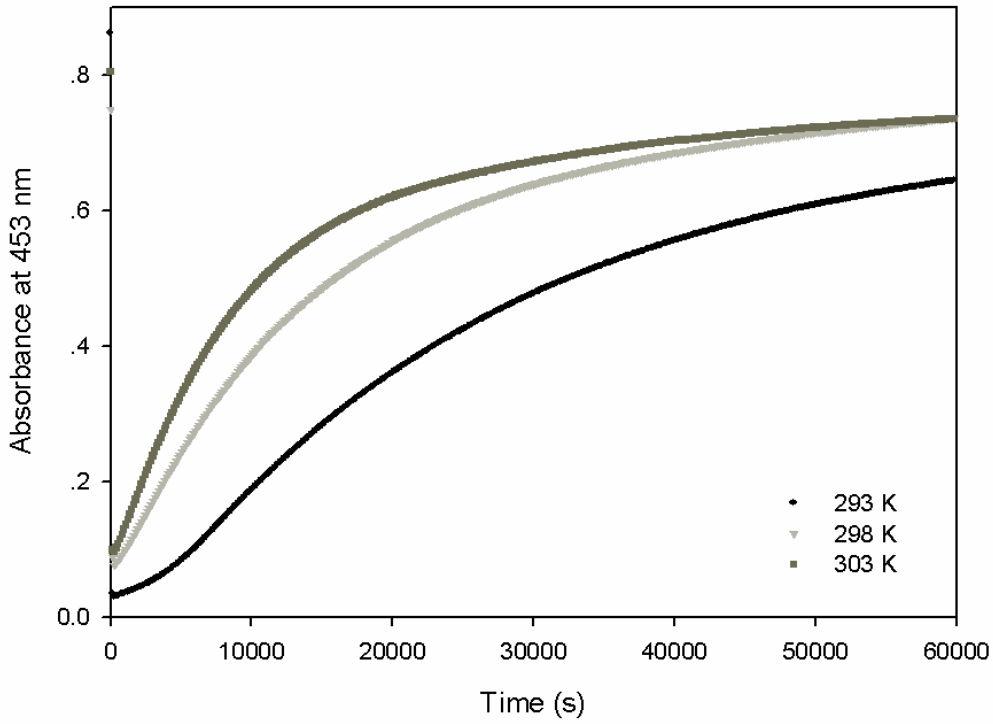

Figure 5.15: Progress curves of the regeneration of $Ru(bpy)_3^{2+}$ from $Ru(bpy)_3^{3+}$ at various temperatures. [Ce(IV)]/[$Ru(bpy)_3^{2+}$] mole ratio at 3:2. Reagent concentrations: [$Ru(bpy)_3^{2+}$] = 5.540 x 10^{-5} M; [Ce(IV)] = 1.250 x 10^{-3} M.

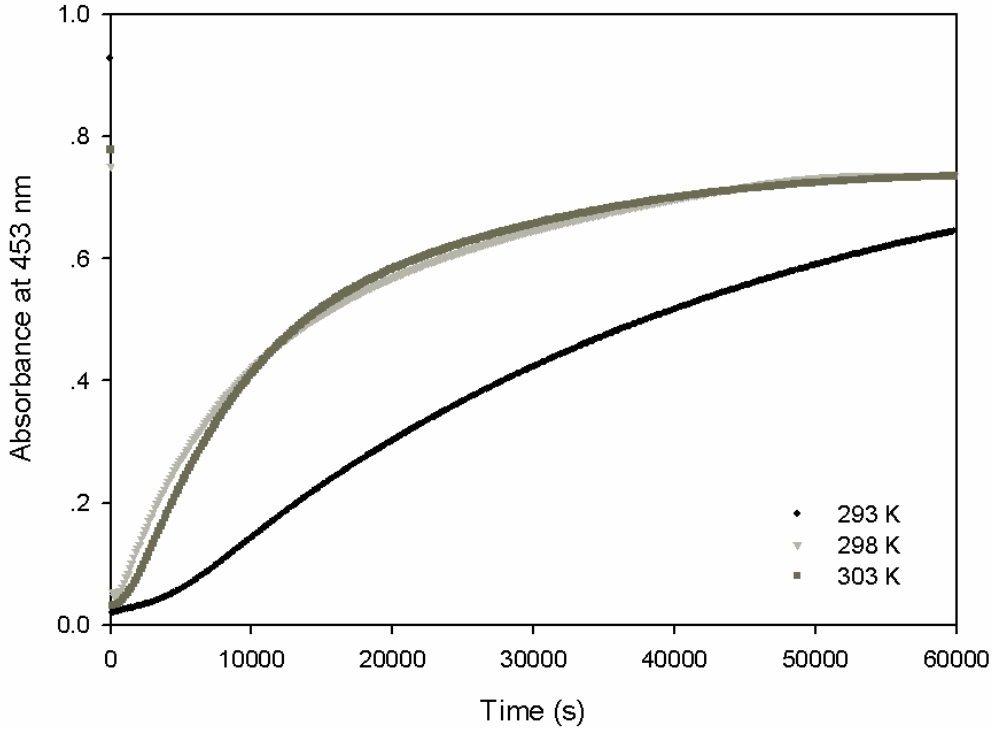

Figure 5.16: Progress curves of the regeneration of $Ru(bpy)_3^{2+}$ from $Ru(bpy)_3^{3+}$ at various temperatures. [Ce(IV)]/[$Ru(bpy)_3^{2+}$] mole ratio at 2:1. Reagent concentrations: [$Ru(bpy)_3^{2+}$] = 5.540 x 10^{-5} M; [Ce(IV)] = 1.250 x 10^{-3} M.

By keeping the [Ce(IV)]/[Ru(II)] mole ratio constant and the light source fixed, and varying the temperature the following observations were made:

(1) The reaction rate increases with temperature across the [Ce(IV)]/[Ru(II)] mole ratios investigated. At 293 K the regeneration of $Ru(bpy)_3^{2+}$ takes much longer time to compete while at 298 K or higher temperature the reaction is over in the time period investigated. The rate of the reaction is temperature dependent.

(2) At higher [Ce(IV)]/[Ru(II)] mole ratios, it appears that the temperature plays a less important role than at lower mole ratios when temperature is above 293 K.

5.4.5.3 Varying the light source

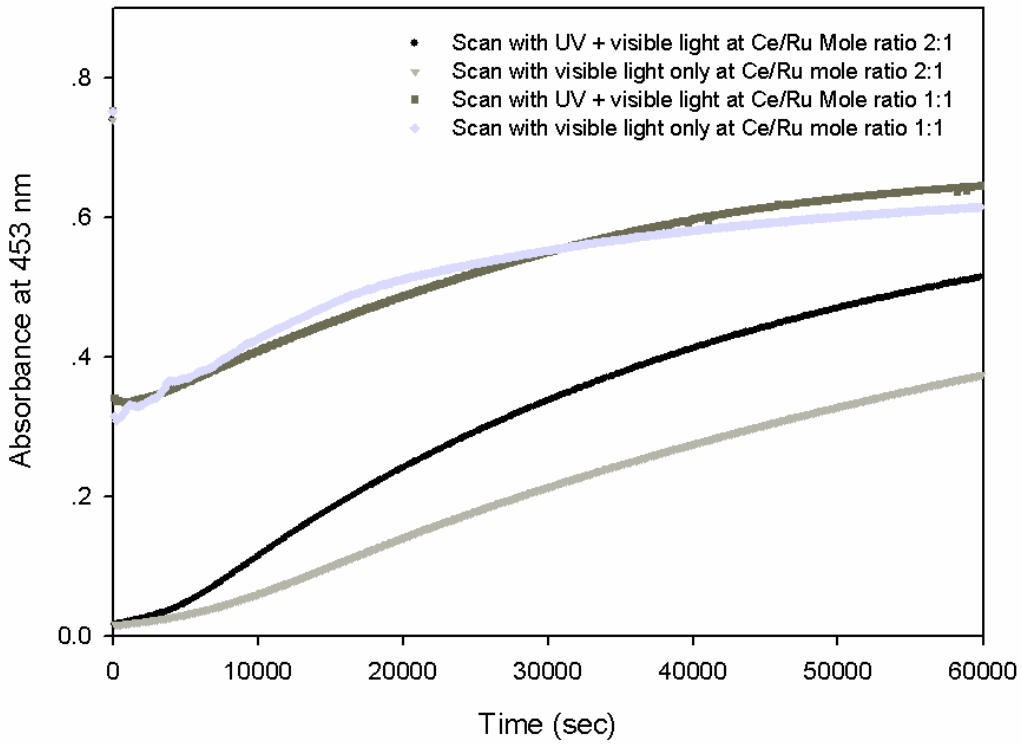

Figure 5.17: Progress curves of the regeneration of $Ru(bpy)_3^{2+}$ from $Ru(bpy)_3^{3+}$ upon varying the light source during a scan. The [Ce(IV)]/[$Ru(bpy)_3^{2+}$] mole ratios are indicated in the legend. Reagent concentrations: [$Ru(bpy)_3^{2+}$] = 5.540 x 10^{-5} M; [Ce(IV)] = 1.250 x 10^{-3} M.

Figure 5.17 shows the progress curves of the regeneration of $Ru(bpy)_3^{2+}$ from $Ru(bpy)_3^{3+}$ upon varying the light source during a scan. By keeping the [Ce(IV)]/[Ru(II)] mole ratio and temperature constant at 298 K, the effect of light on the reaction could be observed.

(1) At [Ce(IV)]/[Ru(II)] mole ratio 2:1, it appears that the reaction rate increases with UV lamp switch on during a scan. The UV light helps to overcome the activation barrier of the regeneration of $Ru(bpy)_3^{2+}$.

(2) Interestingly, there is minimum change of the rate of reaction at [Ce(IV)]/[Ru(II)] mole ratio 1:1, the UV light has less of an effect on the rate of the reaction.

5.5 Conclusions

In this chapter the oxidation reaction of $Ru(bpy)_3^{2+}$ with Ce(IV) was investigated. A discrepancy of [Ce(IV)]/[Ru(II)] mole ratio at the end-point was found between the titrations recorded using spectrophotometer and photometer. Further study shows the regeneration of $Ru(bpy)_3^{2+}$ from $Ru(bpy)_3^{3+}$ could be the reason for this discrepancy. In addition, kinetic modelling software was used to simulate the reaction mechanisms from the experimental data, which shows the regeneration of $Ru(bpy)_3^{2+}$ from $Ru(bpy)_3^{3+}$ is not a simple one step reaction, an intermediate species was involved. However, assignment of charges to this intermediate remains uncertain. Furthermore, it has been shown that the recovery of $Ru(bpy)_3^{2+}$ is temperature and light dependent.

Chapter 6

Conclusion

6.1 Characterization of ruthenium (II) polypyridine complexes

The electronic absorption-and emission-spectra of $Ru(bpy)_3^{2+}$ in acetonitrile showed that the metal-to-ligand charge transfer (MLCT) transition takes place at 453 nm, and upon excitation at 453 nm, the complex luminescences intensely with the emission maximum at about 600 nm, which is characteristic MLCT luminescence from the triplet MLCT Ru(dπ) to ligand (π*) state. In addition, the electron-transfer quencher, phenothiazine is shown to be a very efficient electron acceptor for quenching the excited state of $Ru(bpy)_3^{2+}$. The Stern-Volmer analysis yielded a quenching rate constant (k_q) of 2.503 x 10^9 $M^{-1}s^{-1}$, which describes the extremely rapid reaction process of phenothiazine with $Ru(bpy)_3^{2+}$, the results are in good agreement with the reports in the literature.

The cyclic voltammogram shows an $E_{1/2}$ value of 0.963 V for the Ru(II)/Ru(III) redox couple with respect to the internal reference ferrocene. The diffusion coefficient of $Ru(bpy)_3^{2+}$ in acetonitrile at 298 K was determined to be 1.02 x 10^{-5} cm^2/s, which value correlates very well with the coefficients reported of the same compound in different solvents at 298 K. The estimation of the heterogeneous electron transfer rate constant (k_s) leads to an average value of 0.0127 cm/s, which is confirmed with k_s reported for the quasi-reversible reaction.

6.2 Reactions of tris(2,2'-bipyridyl) ruthenium (II) with acids and bases

The $Ru(bpy)_3^{2+}$ stability studies were conducted in a non-aqueous medium with the presence of acids and a base. $Ru(bpy)_3^{2+}$ is very stable in non-aqueous media at room temperature and does not easily react with strong organic acids and base. This is confirmed by the spectra of the MLCT band that remained relatively constant under the various reaction conditions.

6.3 Reactions of tris(2,2'-bipyridyl) ruthenium (II) with oxidants

Photometric titrations of $Ru(bpy)_3^{2+}$ with oxidants showed that persulphate and lead dioxide could easily oxidize $Ru(bpy)_3^{2+}$ to $Ru(bpy)_3^{3+}$ in the presence of heat and H_2SO_4 respectively. However, with the oxidation reaction of $Ru(bpy)_3^{2+}$ with cerium (IV) it was found that the resultant $Ru(bpy)_3^{3+}$ gradually reverts back to $Ru(bpy)_3^{2+}$ when stored under room light. The regeneration of $Ru(bpy)_3^{2+}$ was investigated by observing the spectral changes of the reaction solution. Kinetic modeling software was used to fit several theoretical models to the experimentally obtained kinetic data, which shows the regeneration of $Ru(bpy)_3^{2+}$ from $Ru(bpy)_3^{3+}$ is not a simple one step reaction, and an intermediate species is involved. However, assignment of charges to this intermediate remains uncertain. The model that produced the best theoretical fit was given by:

$$\mathrm{Ru(II) + Ce(IV)} \xrightarrow{k_1} \mathrm{Ru(III)}$$

$$\mathrm{Ru(III)} \xrightarrow{k_2} \mathrm{Ru(II)}$$

$$\mathrm{Ru(III)} \xrightarrow{k_3} \mathrm{Ru^*}$$

$$\mathrm{Ru^*} \xrightarrow{k_4} \mathrm{Ru(II)}$$

In this model which is mechanistically feasible, the regeneration of $Ru(bpy)_3^{2+}$ from $Ru(bpy)_3^{3+}$ occurs via two routes simultaneously; one which involves the formation of an intermediate species Ru*, the other route assumes the direct reduction from Ru(III). The rates of the above reactions were calculated.

6.4 Suggestions for future studies

The photosensitive reduction of the $Ru(bpy)_3^{3+}$ could be examined further: more kinetic data should be obtained, and with the aid of other computational simulation software, investigations could be made to determine the exact intermediate species, regarding its oxidation states and properties.

The study should also be extended to the photochemical domain, where the light intensity should be measured by chemical means, and to use it to measure the photochemical quantum yield. The photochemical reactivity of the complex could then be determined.

References

1. The Department of Mineral and Energy, *Platinum-group metal mines in South Africa 2007,* Republic of South Africa, 2007, Internet Website: http://www.dme.gov.za/pdfs/minerals/D6%202007.pdf
2. Kalyanasundaram, K.; Gratzel, M.; *Coordination Chemistry Reviews*, 1998, **177**, (i) 363, (ii) 375.
3. Vermaak, C.F.; *The platinum group metals - A global perspective*, 1995, MINTEK. Randburg, South Africa.
4. Griffith, W.P.; *The chemistry of the rare platinum metals (Os, Ru, Ir and Rh)*, 1967, Interscience Publishers.
5. Cotton, F.A.; Wilkinson, G.; *Advanced Inorganic Chemistry - A comprehensive text*, Fourth edition, 1980, John Wiley & Sons Publisher, New York.
6. Wikipedia on-line webpage:
   (i) http://en.wikipedia.org/wiki/polypyridine_complex
   (ii) http://en.wikipedia.org/wiki/P-Toluenesulfonic_acid
   (iii) http://en.wikipedia.org/wiki/Oxalic_acid
   (iv) http://en.wikipedia.org/wiki/Trifluoroacetic_acid
   (v) http://en.wikipedia.org/wiki/Tert-Butanol
7. Juris, A.; Campagna, S.; Balzani, V.; Gremaud, G.; von Zelewsky, A.; *Inorg. Chem.*, 1988, **27**, 3652.
8. Borgström, M.; Johansson, O.; Lomoth, R.; Berglund-Baudin, H.; Wallin, S.; Sun, L.; Åkermark, B.; Hammarström, L.; *Inorg. Chem*., 2003, **42**, 5173-5184.
9. Bioanalytical Systems, *Instruction manual for BAS epsilon for electrochemistry*, Version 1.30, 2002, 64.
10. Hosten, E.C.; *Complexing Interactions with Arsenazo III*, PhD dissertation, 1996, University of Port Elizabeth, Port Elizabeth.
11. Kuzmic, P.; *Program DYNAFIT for the analysis of enzyme kinetic data: Application to HIV proteinase*, *Anal. Biochem.,* 1996, **237**, 260–273.
12. http://chemistry.binghamton.edu/chem445/Ru(bipy)3/Ru(bipy)3.htm
13. Evans, I. P.; Spencer, A.; Wilkinson, G. J.; *J. Chem. Soc.*, *Dalton. Trans*., *1973*, 204-209.
14. DeArmond, M. K.; Carlin, C. M.; *Coord. Chem. Rev*., 1981, **36**, 325.
15. Kalyanasundaram, K.; *Coord. Chem. Rev*., 1982, **46**, 159.

16. http://www.lasalle.edu/~gentry/C301/Lab%208.%20Quenching.%20V3.pdf
17. Kaneko, M.; Hou, X.; Yamada, A.; *Bull. Chem. Soc. Jpn*., 1987, **60**, 2525-2526.
18. Jones, W. E. Jr.; Fox, M. A.; *J. phys. Chem*., 1994, **98**, 5095.
19. http://Joi.jlc.jst.go.jp/jst.journalarchive/cl1972/16.2355
20. Stripin, D. R.; Moss, J. A.; Chen, P.; Erickson, B. W.; Meyer, T. J.; *J. Am. Chem. Soc*., 1998, **120**, 4885.
21. Kaneko, M.; Awaya, N.; Yamada, A.; *The Chemical Society of Japan*, 1982, 619.
22. Mueller, T. R.; Adams, R. N.; *Anal. Chim. Acta*., 1961, **25**, 482.
23. Mabbott, G. A.; *Journal of Chemical education*, 1983, **60**, 698.
24. Kissinger, P. T.; Heineman, W. R.; *Journal of Chemical Education*, 1983, **60**, 704.
25. Baldwin, R. P.; Ravichandran, K.; Johnson, R. K.; *Journal of Chemical Education*, 1984, **61**, 820.
26. http://www.asdlib.org/onlineArticles/ecourseware/Kelly_Potentiometry/PDF-4-Reversibility.pdf
27. Wei, S.; Zhao, L.; Cheng, X.; Lin, J.; *Anal. Chim. Acta*., 2005, **545**, 65-73.
28. Gerardi, R. D.; Barnett, N. W.; Jones, P.; *Anal. Chim. Acta*., 1999, **388**, 1-10.
29. Rubinstein, I.; Bard, A. J.; *J. Am. Chem. Soc*., 1981, **103**, 512-516.
30. Hercules, D. M.; Lytle, F. E.; *J. Am. Chem. Soc*., 1966, **88**, 4745.
31. http://chemprof.tripod.com/redtable.htm
32. http://redox-tech.com/persulfate1.htm
33. Burstall, F. H.; *J. Chem. Soc*., 1936, 173.
34. López-Cornejo, P.; Mozo, J. D.; Roldán, E.; Domínguez, M.; Sánchez, F.; *Chemical Physics Letters*, 2002, **352**, 33-38.
35. Balcerzak, M.; Swiecicka, E.; *Anal. Chim. Acta*., 1997, **349**, 53-57.
36. Savvin, S. B.; *Russ. Chem. Rev*., 1963, **32** (2), 93-107.
37. Savvin, S. B.; *Talanta*, 1961, **8**, 673-685.
38. Savvin, S. B.; *Talanta*, 1964, **11**, 1-6.
39. Savvin, S. B.; *Talanta*, 1964, **11**, 7-19.
40. Khan, M. M. T.; Ramachandraiah, G.; Rao, A. P.; *Inorg. Chem*., 1986, **25**, 665-670.
41. Cady, H. H.; Connick, R. E.; *J. Am. Chem. Soc*., 1960, **80**, 2646-2652.
42. Cady, H. H.; Connick, R. E.; *J. Am. Chem. Soc*., 1960, **80**, 4187-4191.
43. Concepcion, J. J.; Jurss, J. W.; Templeton, J. L.; Meyer, T. J.; *J. Am. Chem. Soc.*, 2008, **130** (49), 16462–16463.